Supernova Simulations

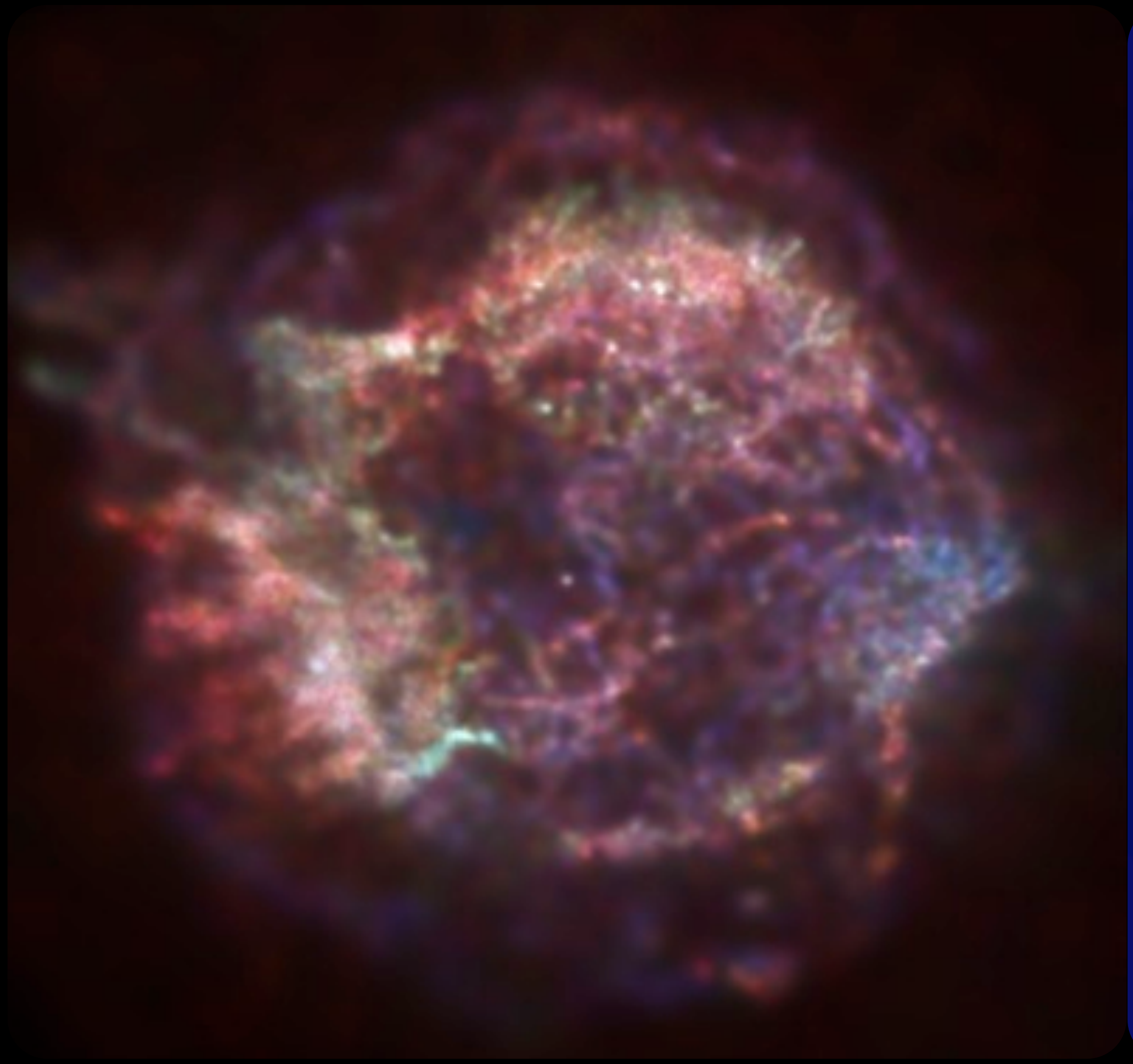

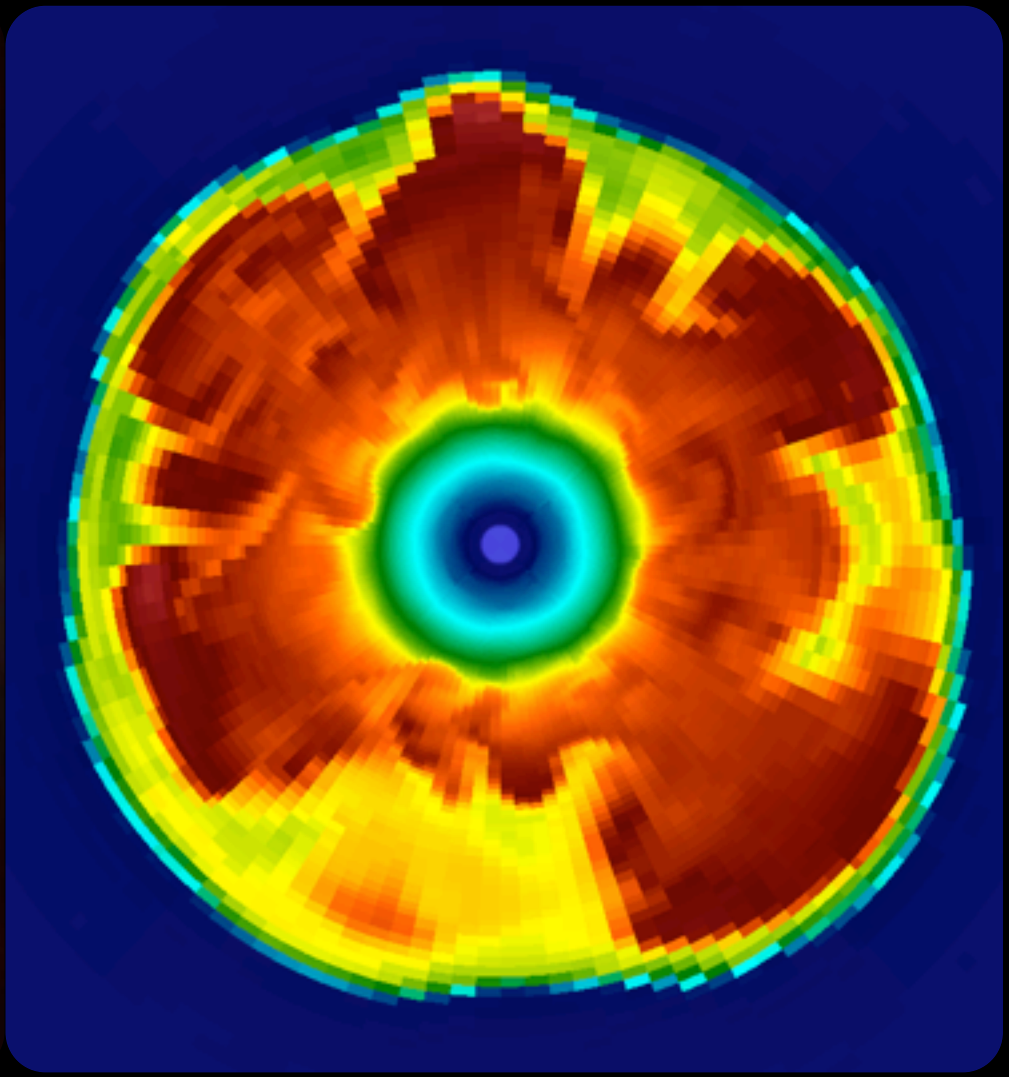

with CHIMERA

Blondin, Bruenn, *Budiardja*, *Chertkow*, Endeve, *Harris*, Hix, *Lee*, Lentz, Marronetti, *Mauney*, Messer, Mezzacappa & *Yakunin* (Florida Atlantic U., North Carolina State U., ORNL/U. Tenn.)

Textbook Supernova

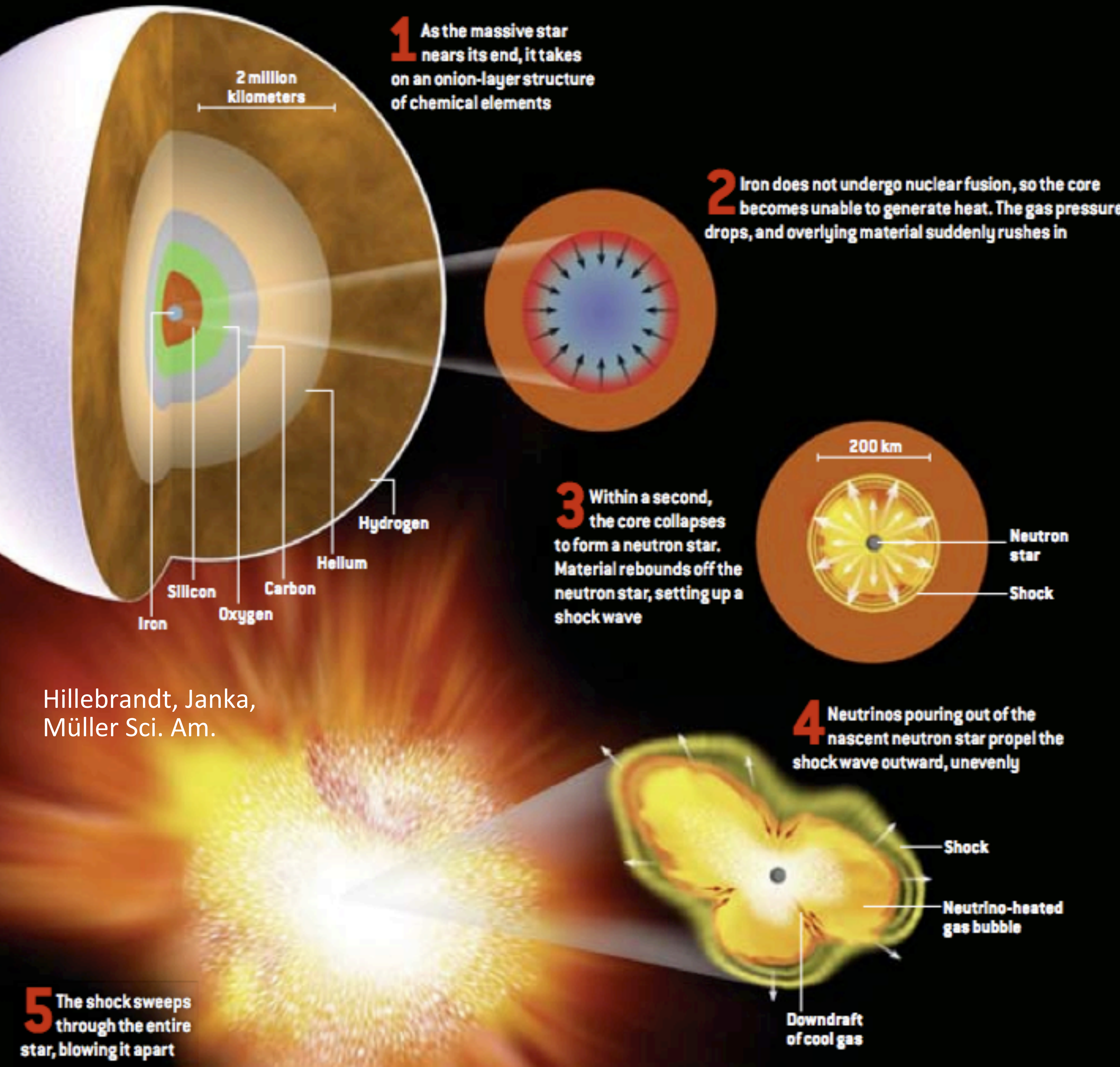

Hillebrandt, Janka, Müller Sci. Am.

A Core-Collapse Supernova is the inevitable death knell of a massive star (~10+ $M_{\odot}$).

The explosion enriches the interstellar medium with elements from Oxygen to Nickel and potentially the r-process elements as well.

CHIMERA

CHIMERA

CHIMERA has 3 “heads”

- Spectral Neutrino Transport (MGFLD-TRANS, Bruenn) in Ray-by-Ray Approximation
- Shock-capturing Hydrodynamics (VH1, Blondin)
- Nuclear Kinetics (XNet, Hix & Thielemann)

CHIMERA

CHIMERA has 3 “heads”

- Spectral Neutrino Transport (MGFLD-TRANS, Bruenn) in Ray-by-Ray Approximation
- Shock-capturing Hydrodynamics (VH1, Blondin)
- Nuclear Kinetics (XNet, Hix & Thielemann)

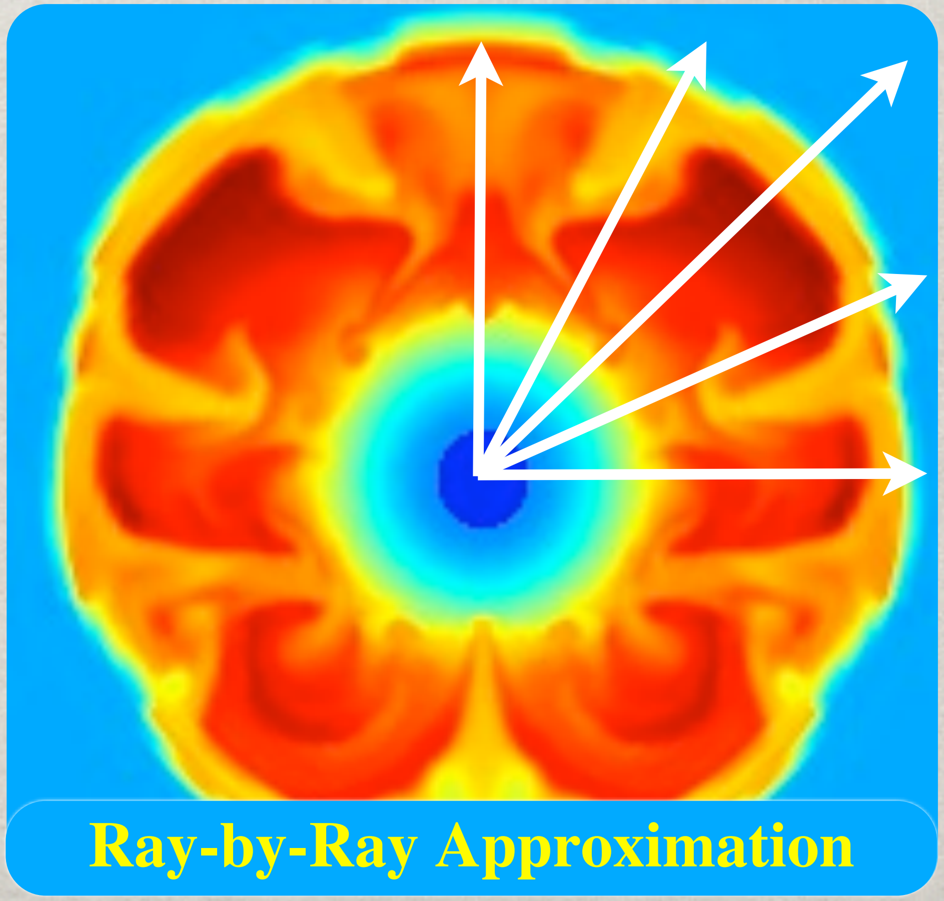

CHIMERA

CHIMERA has 3 "heads"

* Spectral Neutrino Transport (MGFLD-TRANS, Bruenn) in Ray-by-Ray Approximation
* Shock-capturing Hydrodynamics (VH1, Blondin)
* Nuclear Kinetics (XNet, Hix & Thielemann)

Plus Realistic Equations of State, Newtonian Gravity with Spherical GR Corrections.

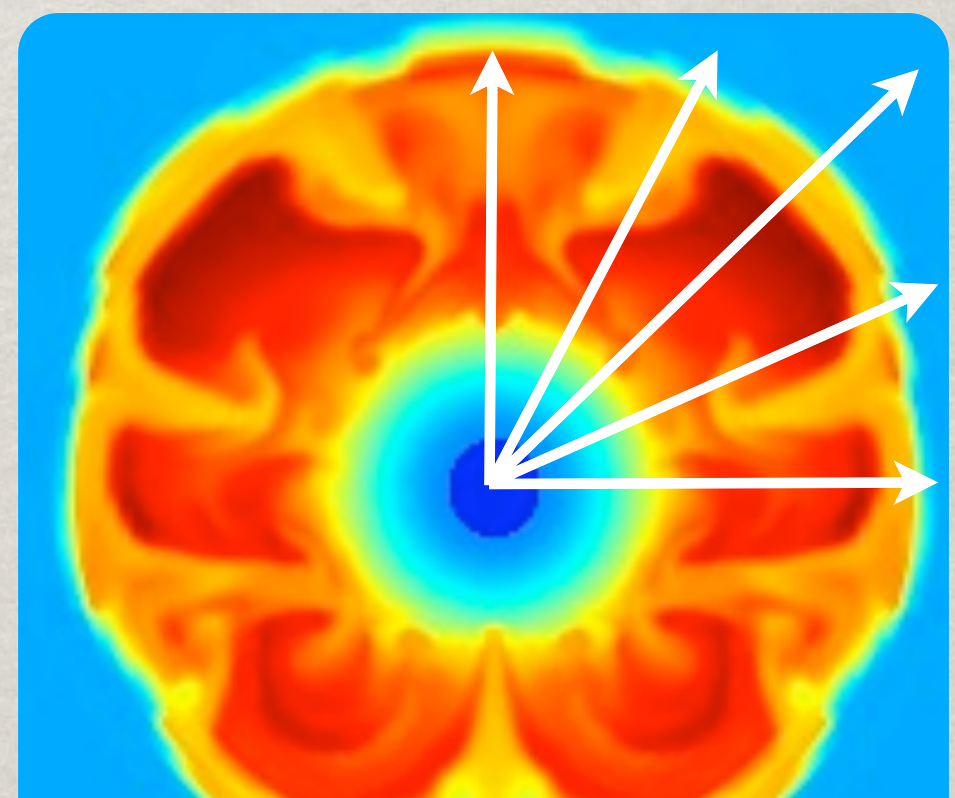

Ray-by-Ray Approximation

CHIMERA

CHIMERA has 3 "heads"

- Spectral Neutrino Transport (MGFLD-TRANS, Bruenn) in Ray-by-Ray Approximation
- Shock-capturing Hydrodynamics (VH1, Blondin)
- Nuclear Kinetics (XNet, Hix & Thielemann)

  Plus Realistic Equations of State, Newtonian Gravity with Spherical GR Corrections.

Advantages compared to models of the 1990s include

  Spectral neutrino transport

  Run for postbounce times > 400 ms.

  Run on a 180 degree grid.

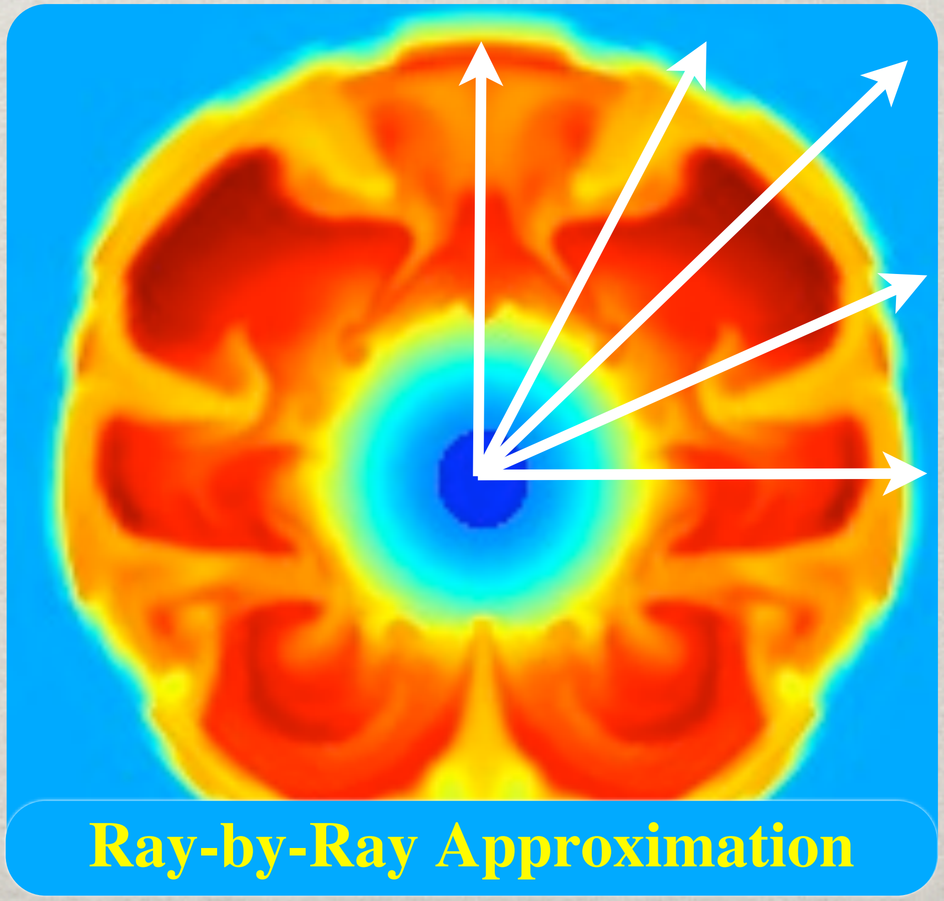

Newest models

Since March 2012, we have been running a family of axisymmetric (2D) models using 12, 15, 20 & 25 $M_\odot$ progenitors from Woosley & Heger (2007).

Newest models

Since March 2012, we have been running a family of axisymmetric (2D) models using 12, 15, 20 & 25 $M_{\odot}$ progenitors from Woosley & Heger (2007).

This is not our first set of 2D models, most notably a set with the same 4 progenitors in 2009 reached as late as 1 second after bounce. However, the ongoing accumulation of corrections and improvements within CHIMERA has prompted us to revisit these models.

Newest models

Since March 2012, we have been running a family of axisymmetric (2D) models using 12, 15, 20 & 25 $M_\odot$ progenitors from Woosley & Heger (2007).

This is not our first set of 2D models, most notably a set with the same 4 progenitors in 2009 reached as late as 1 second after bounce. However, the ongoing accumulation of corrections and improvements within CHIMERA has prompted us to revisit these models.

Current 2012 models include
1) Improvement in radial resolution to 512 zones.
2) Improved NSE-nonNSE transition, including detailed EoS composition at low density with NSE.
3) Lattimer-Swesty EoS with K=220 MeV.
4) Numerical corrections.

Newest models

Since March 2012, we have been running a family of axisymmetric (2D) models using 12, 15, 20 & 25 $M_\odot$ progenitors from Woosley & Heger (2007).

This is not our first set of 2D models, most notably a set with the same 4 progenitors in 2009 reached as late as 1 second after bounce. However, the ongoing accumulation of corrections and improvements within CHIMERA has prompted us to revisit these models.

Current 2012 models include
1) Improvement in radial resolution to 512 zones.
2) Improved NSE-nonNSE transition, including detailed EoS composition at low density with NSE.
3) Lattimer-Swesty EoS with K=220 MeV.
4) Numerical corrections.

At present, the 4 models are still running, though the mean shock radius of each has passed 6000 km.

The Early Phase

For the first ~100 ms after bounce, the supernova shock is essentially spherical, with 1D models identical to 2D models.

Once the Standing Accretion Shock Instability (SASI) and neutrino-driven convection begin, the shock deforms and gradually progresses outward in radius.

We find that the ν-driven convection precedes the development of the SASI at low mass (12 $M_\odot$) and trails the SASI at high mass (25 $M_\odot$).

One notable feature is the considerable delay in launching an explosion, 150-200 ms slower compared to older models.

The Early Phase

For the first ~100 ms after bounce, the supernova shock is essentially spherical, with 1D models identical to 2D models.

Once the Standing Accretion Shock Instability (SASI) and neutrino-driven convection begin, the shock deforms and gradually progresses outward in radius.

We find that the ν-driven convection precedes the development of the SASI at low mass ($12\ M_\odot$) and trails the SASI at high mass ($25\ M_\odot$).

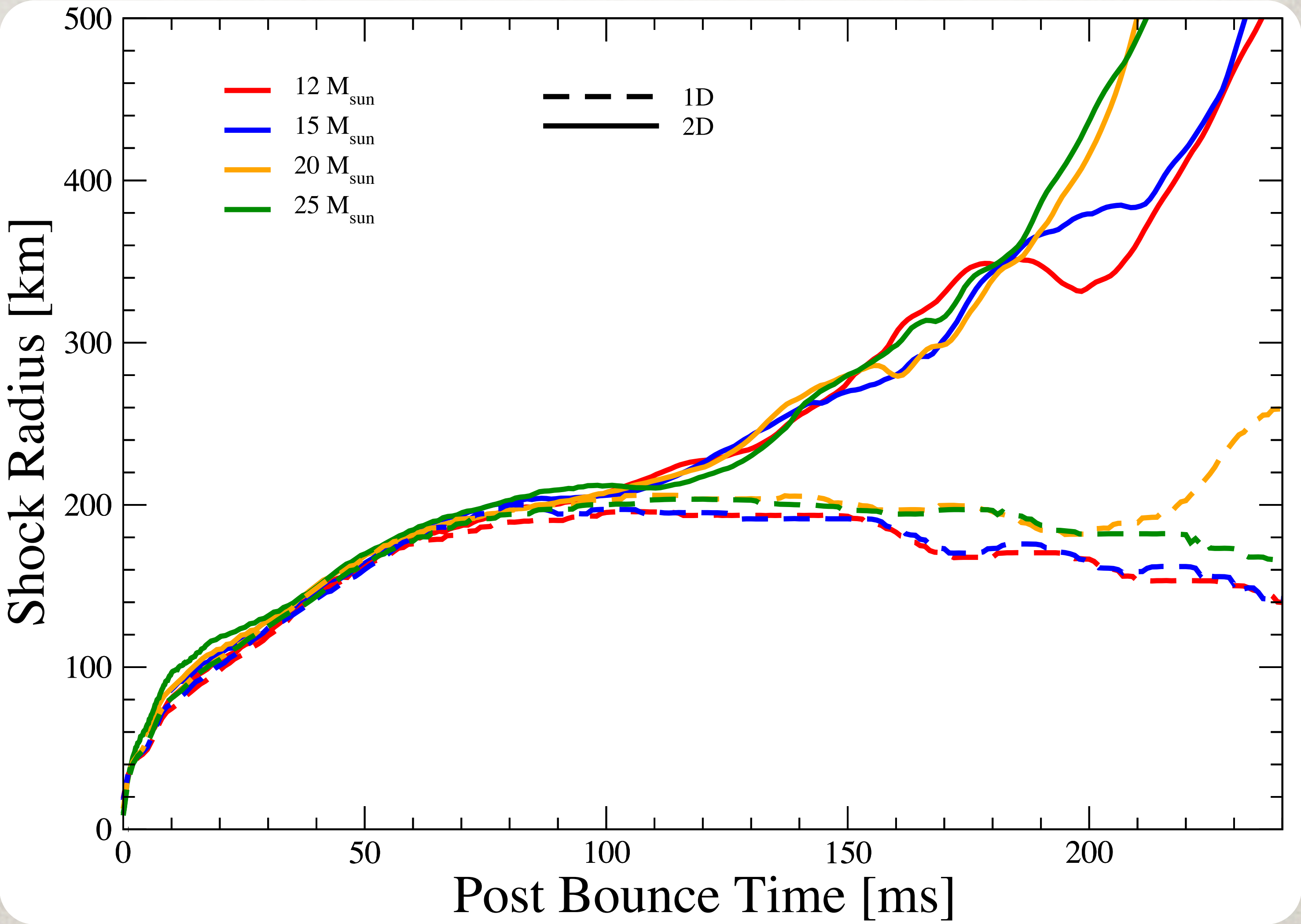

One notable feature is the considerable delay in launching an explosion, 150-200 ms slower compared to older models.

The Early Phase

For the first ~100 ms after bounce, the supernova shock is essentially spherical, with 1D models identical to 2D models.

Once the Standing Accretion Shock Instability (SASI) and neutrino-driven convection begin, the shock deforms and gradually progresses outward in radius.

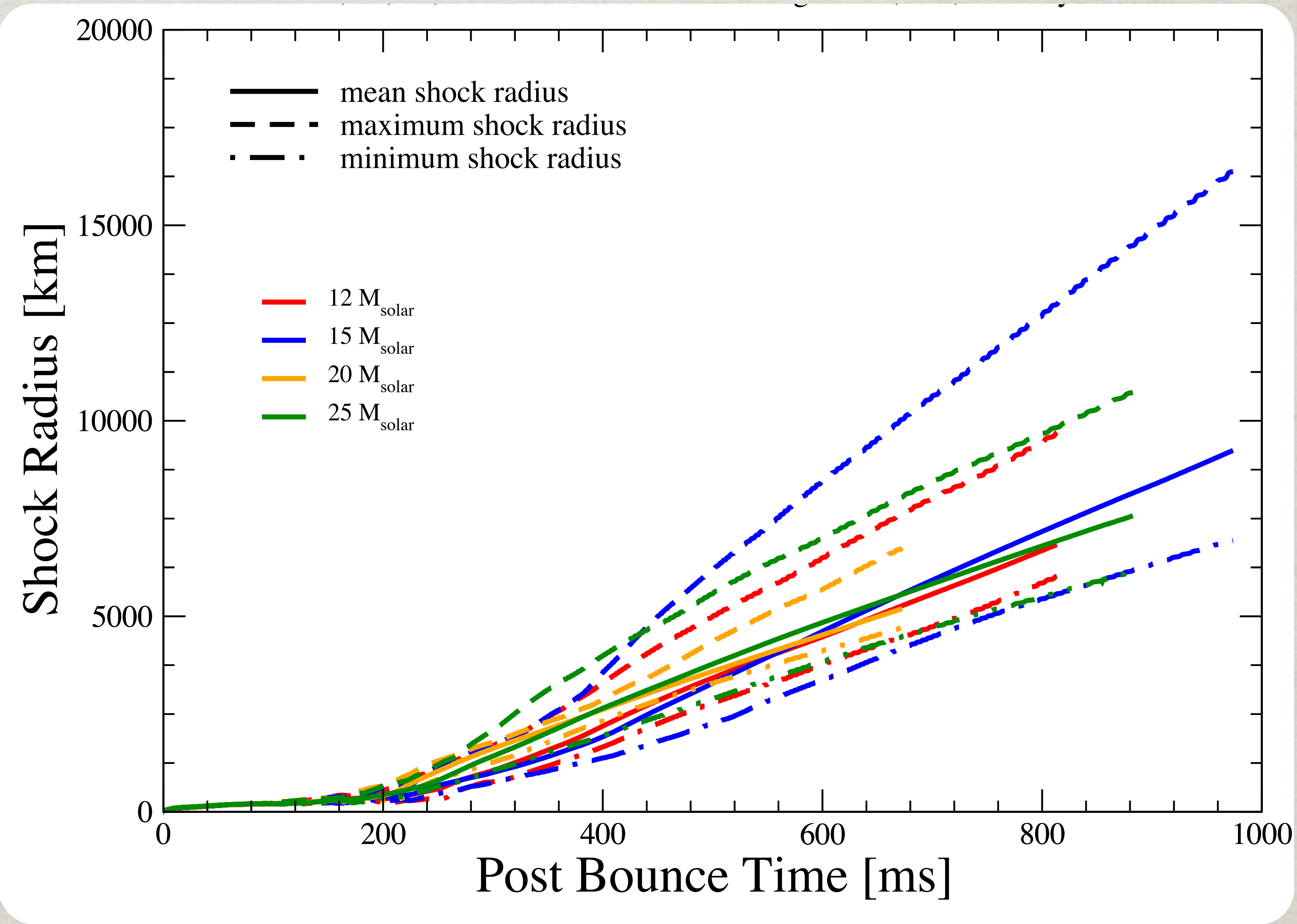

The Early Phase

For the first ~100 ms after bounce, the supernova shock is essentially spherical, with 1D models identical to 2D models.

Once the Standing Accretion Shock Instability (SASI) and neutrino-driven convection begin, the shock deforms and gradually progresses outward in radius.

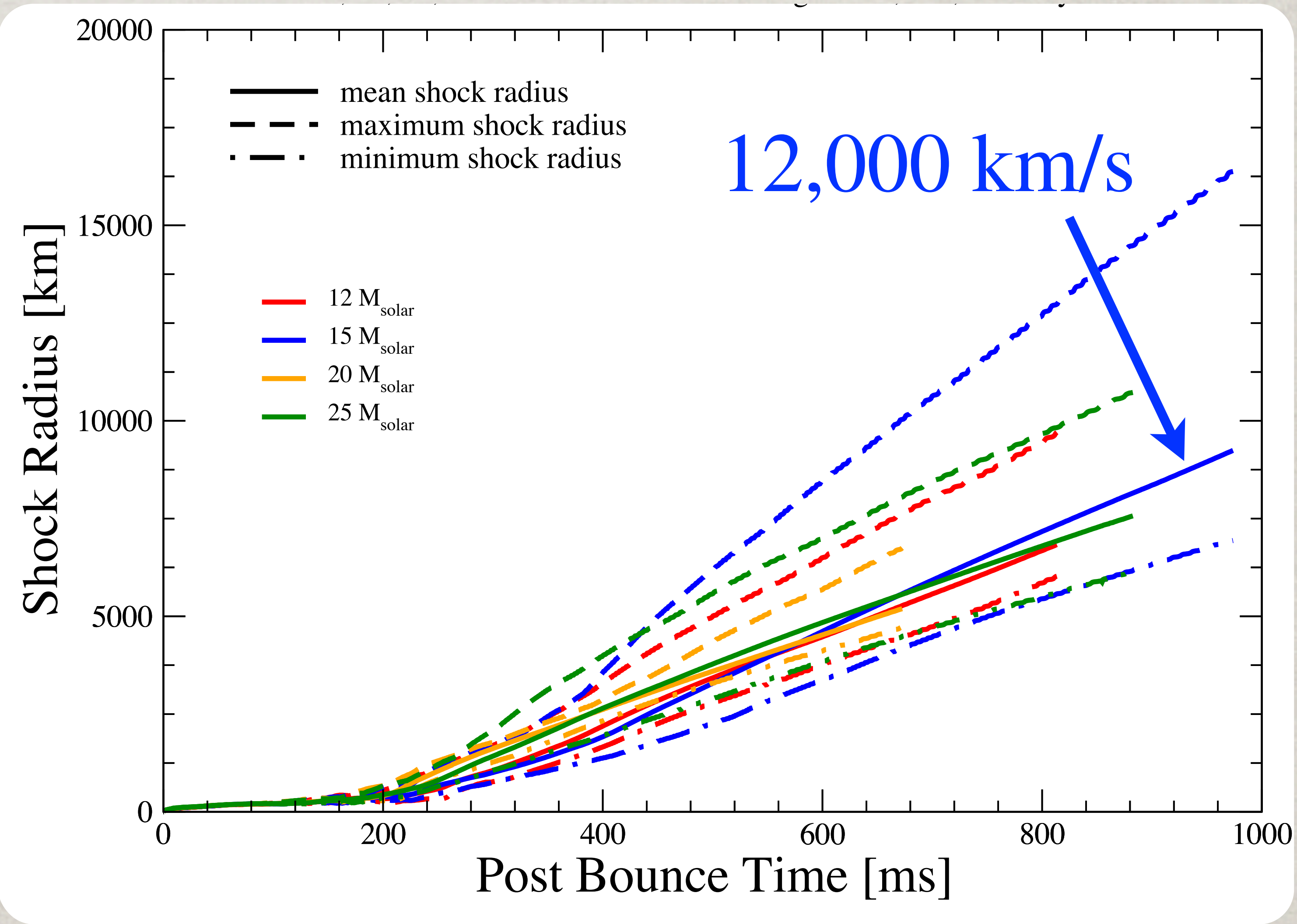

The Early Phase

For the first ~100 ms after bounce, the supernova shock is essentially spherical, with 1D models identical to 2D models.

Once the Standing Accretion Shock Instability (SASI) and neutrino-driven convection begin, the shock deforms and gradually progresses outward in radius.

We find that the ν-driven convection precedes the development of the SASI at low mass (12 $M_\odot$) and trails the SASI at high mass (25 $M_\odot$).

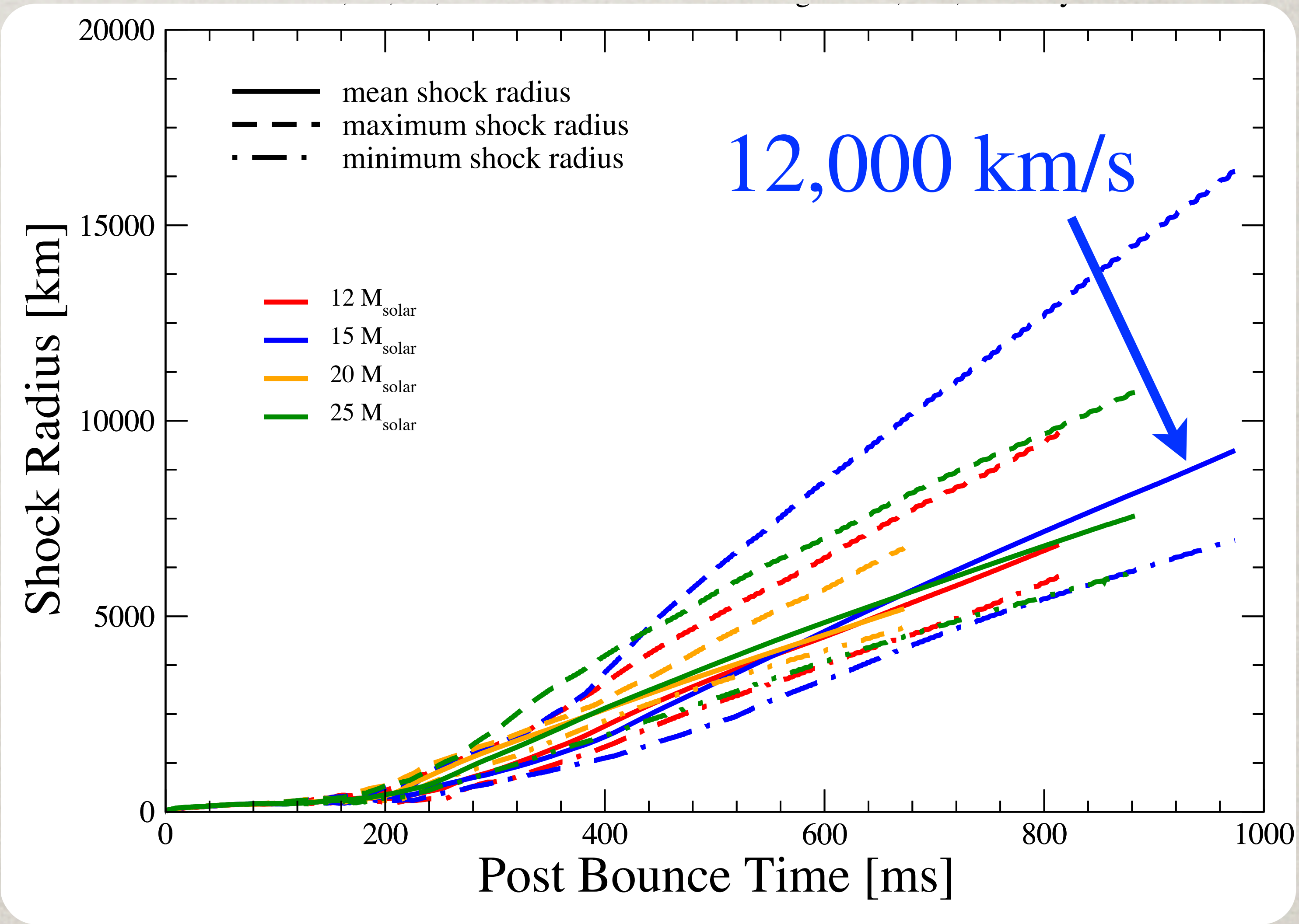

The Early Phase

For the first ~100 ms after bounce, the supernova shock is essentially spherical, with 1D models identical to 2D models.

Once the Standing Accretion Shock Instability (SASI) and neutrino-driven convection begin, the shock deforms and gradually progresses outward in radius.

We find that the ν-driven convection precedes the development of the SASI at low mass ($12\ M_\odot$) and trails the SASI at high mass ($25\ M_\odot$).

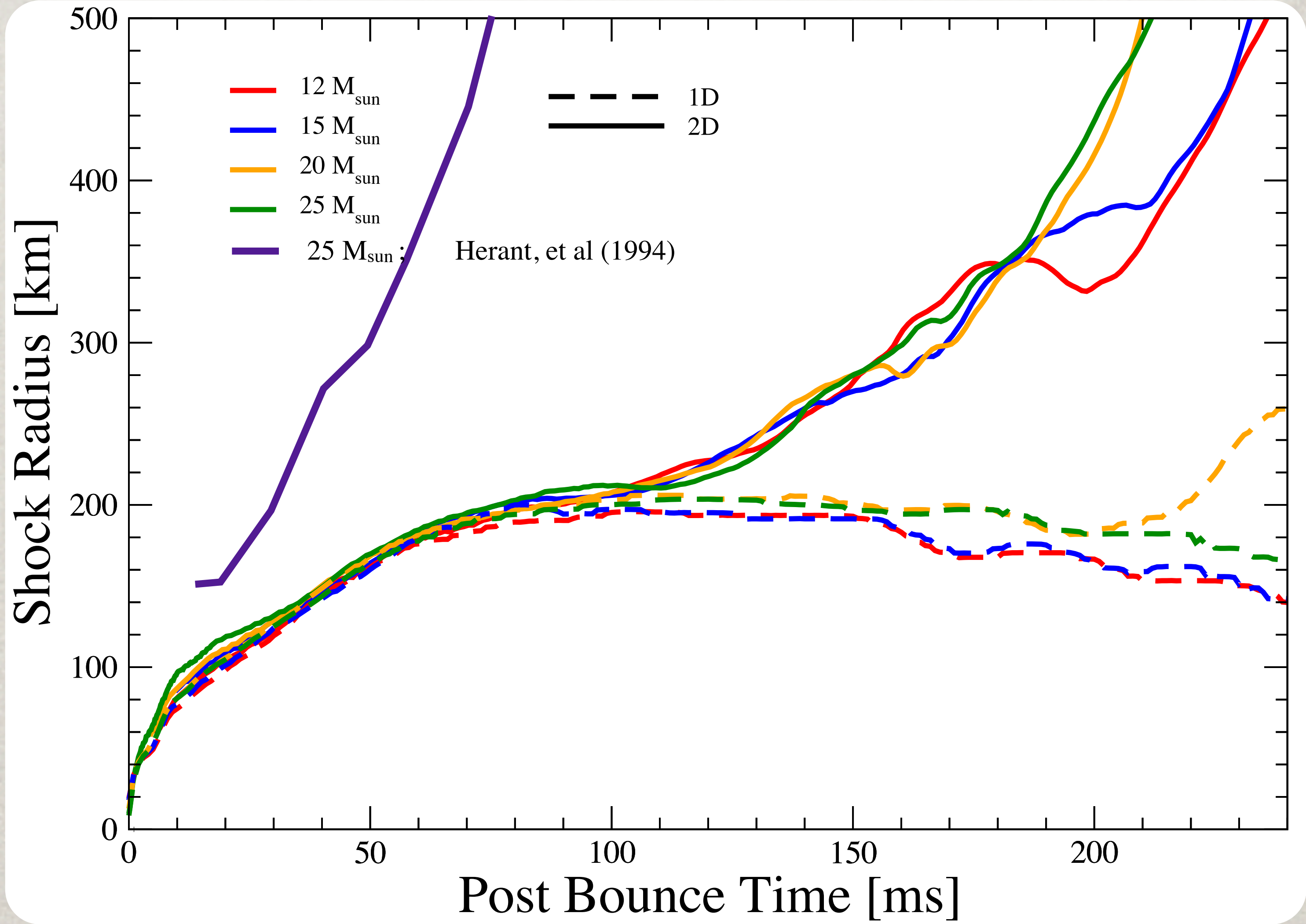

One notable feature is the considerable delay in launching an explosion, 150-200 ms slower compared to older models.

Shock Stagnation

The early behavior of the stalled shock, prior to multi-dimensional effects, is a balance between the ram pressure of the accreting matter and the post-shock pressure created as the shock-heated matter emits neutrinos and gradually settles onto the proto-neutron star.

Shock Stagnation

The early behavior of the stalled shock, prior to multi-dimensional effects, is a balance between the ram pressure of the accreting matter and the post-shock pressure created as the shock-heated matter emits neutrinos and gradually settles onto the proto-neutron star.

An analytic relation for the radius of the stalled shock can be derived (see Janka (2012; ARNPS 62 407).

$$R_s \propto \frac{R_{NS}^{8/3}(k_B T_\nu)^{8/3}}{\dot{M}^{2/3} M_{NS}^{1/3}}$$

Shock Stagnation

The early behavior of the stalled shock, prior to multi-dimensional effects, is a balance between the ram pressure of the accreting matter and the post-shock pressure created as the shock-heated matter emits neutrinos and gradually settles onto the proto-neutron star.

An analytic relation for the radius of the stalled shock can be derived (see Janka (2012; ARNPS 62 407).

$$R_s \propto \frac{R_{NS}^{8/3}(k_B T_\nu)^{8/3}}{\dot{M}^{2/3} M_{NS}^{1/3}}$$

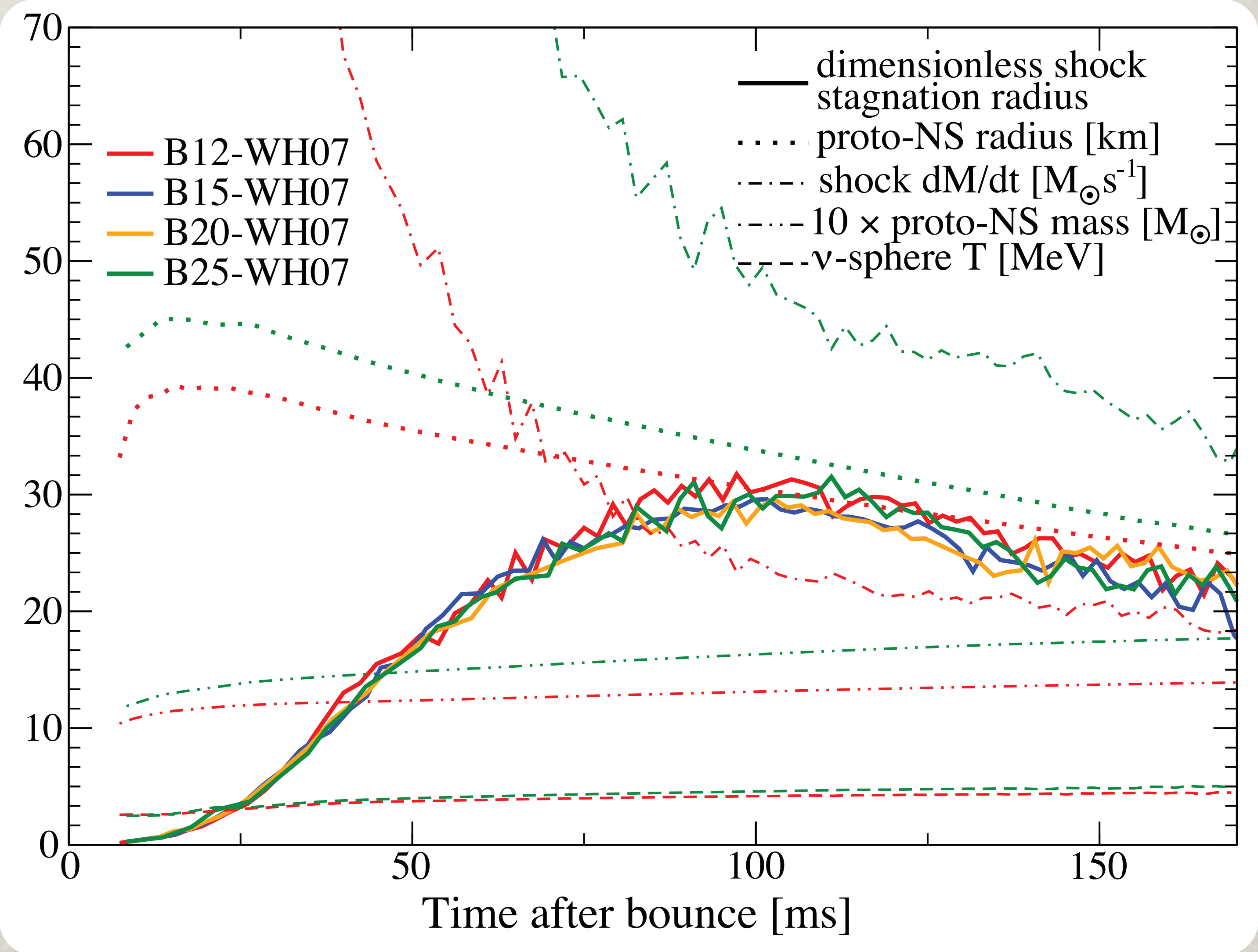

In our B-series models, the larger R_{NS} and T_ν with increasing mass balance the larger M_{NS} and $\dot{M}$, causing R_s to be similar from 12-25 $M_\odot$.

Supernova: the Movie

Bruenn, Mezzacappa, Hix, … (2013)

Supernova: the Movie

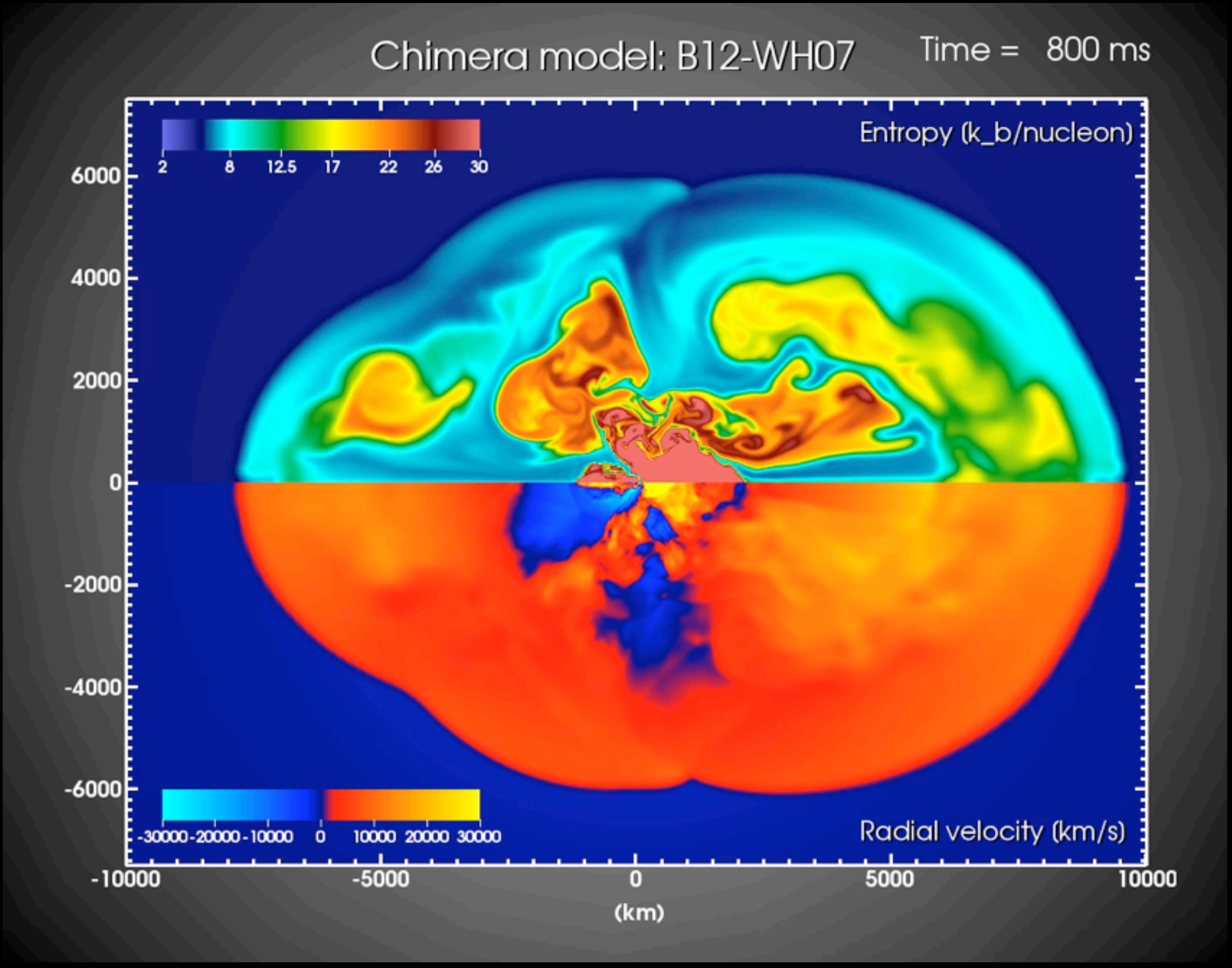

Supernova: the Movie

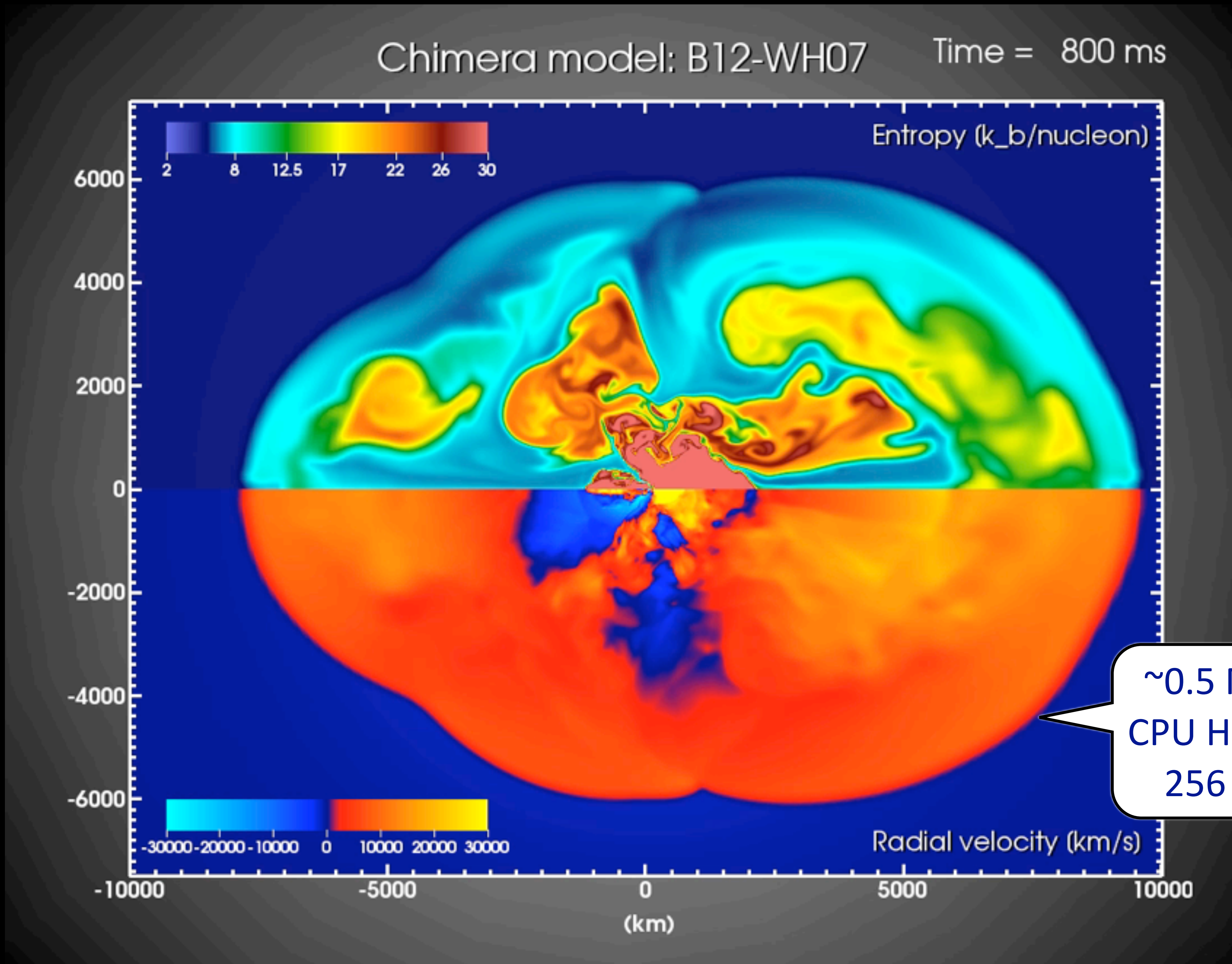

~0.5 Million CPU Hours on 256 proc.

Supernova: the Movie

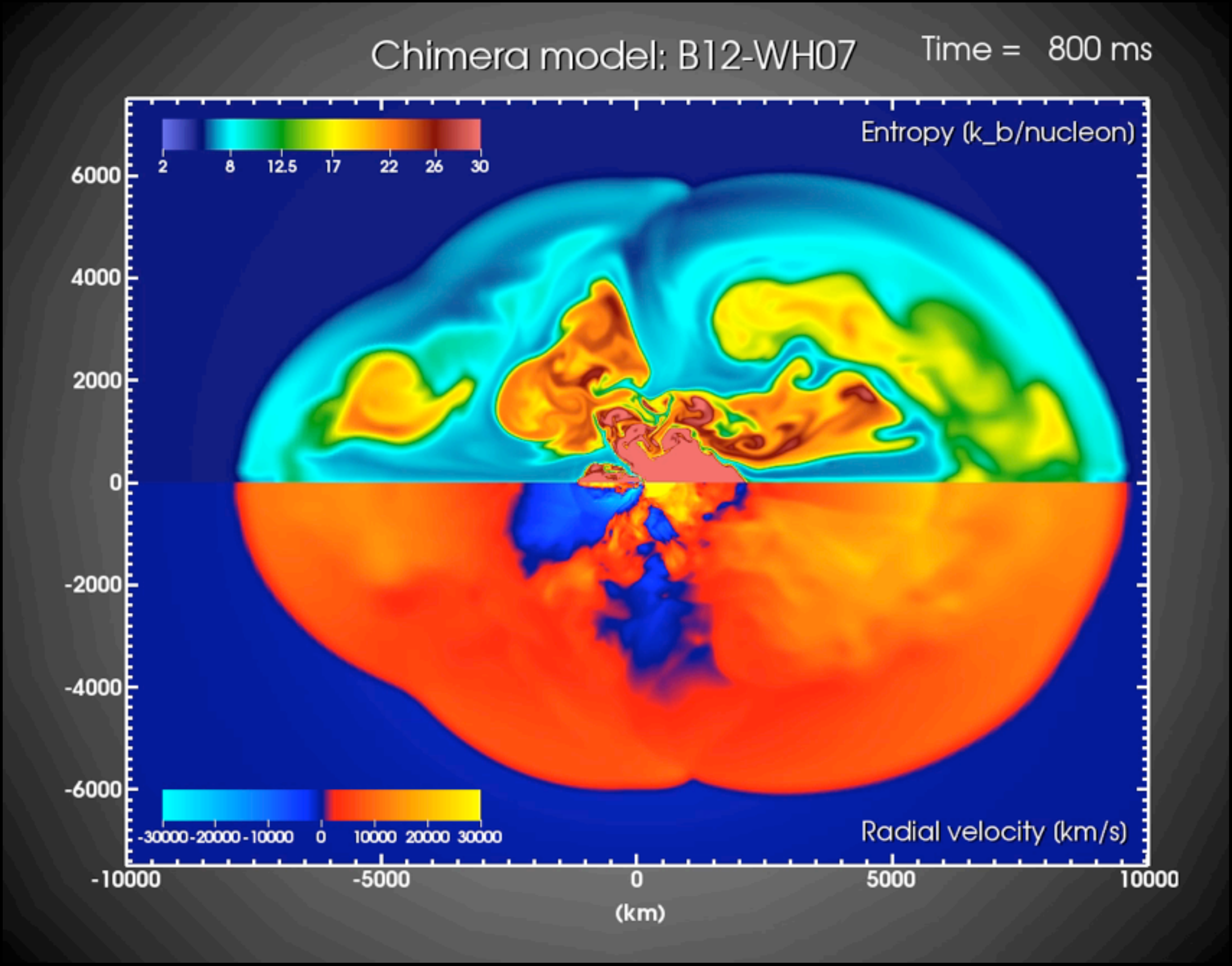

How to make an explosion

SASI gradually pushes the shock outward, increasing the size of the heating region until heating timescale ($\tau_{heating}$) is smaller than advection timescale ($\tau_{advection}$).

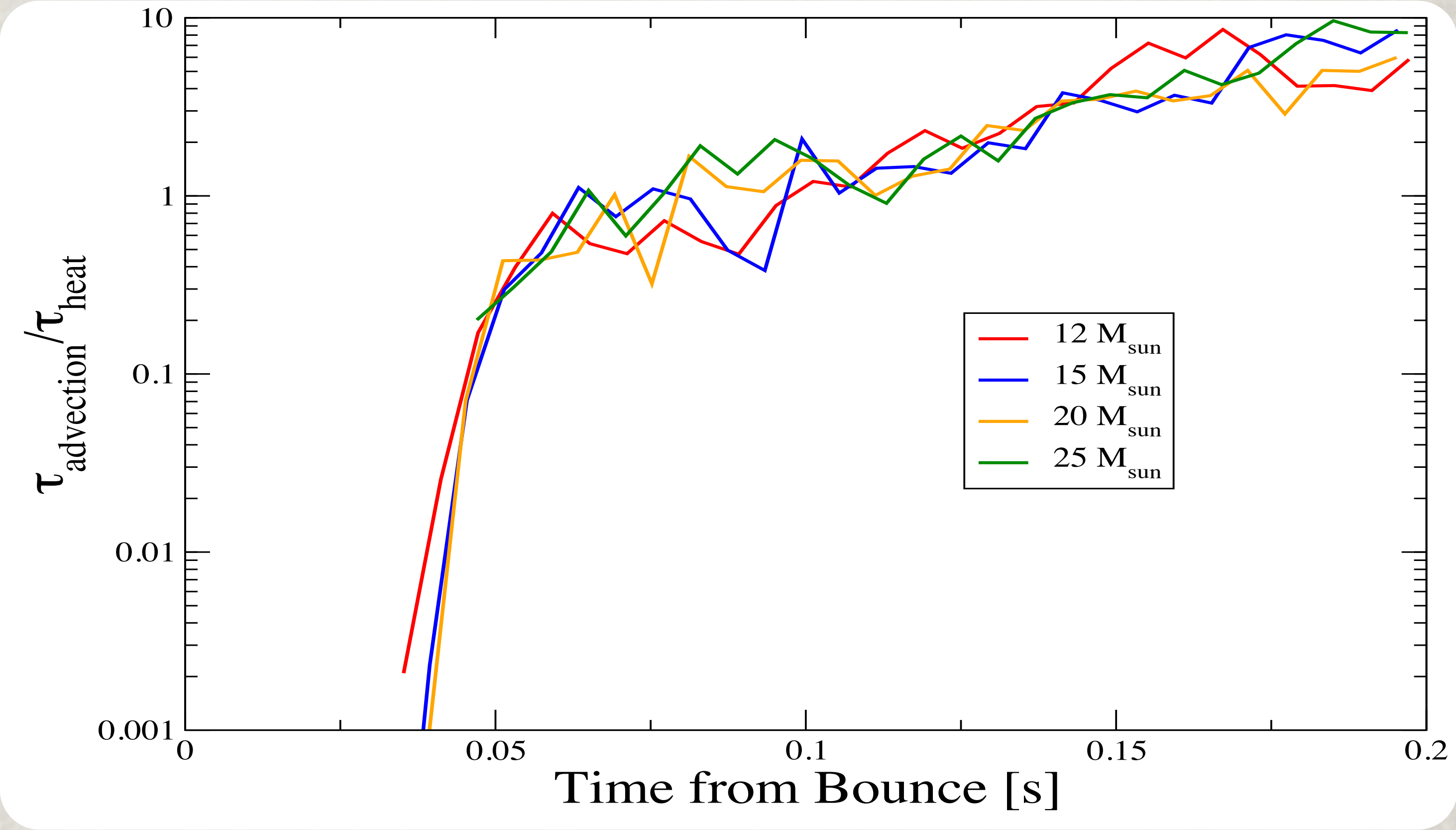

How to make an explosion

SASI gradually pushes the shock outward, increasing the size of the heating region until heating timescale ($\tau_{heating}$) is smaller than advection timescale ($\tau_{advection}$).

Much of the explosion energy comes from the neutrino heating region, below the ejecta, in the form of PdV work and advected internal energy.

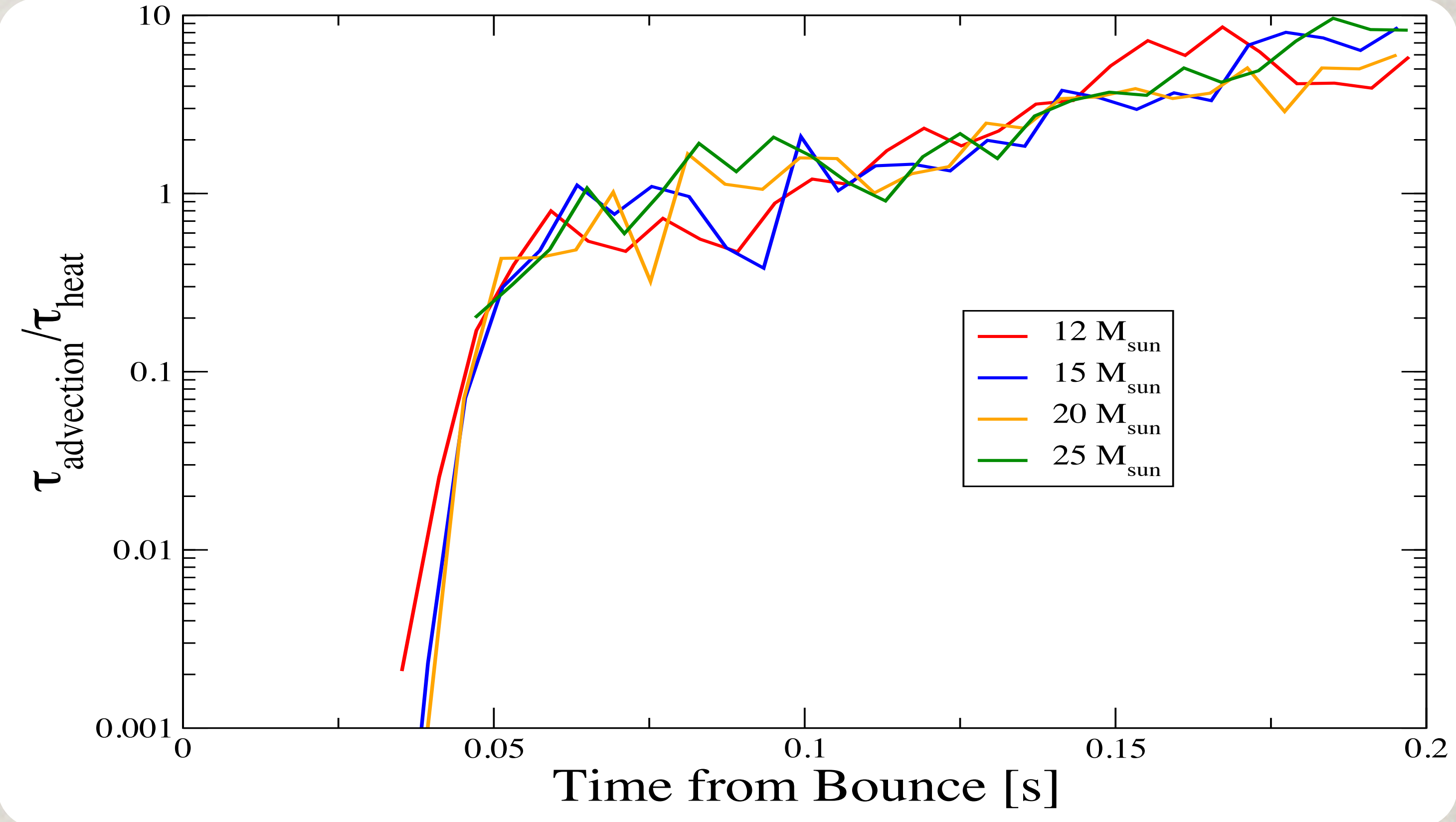

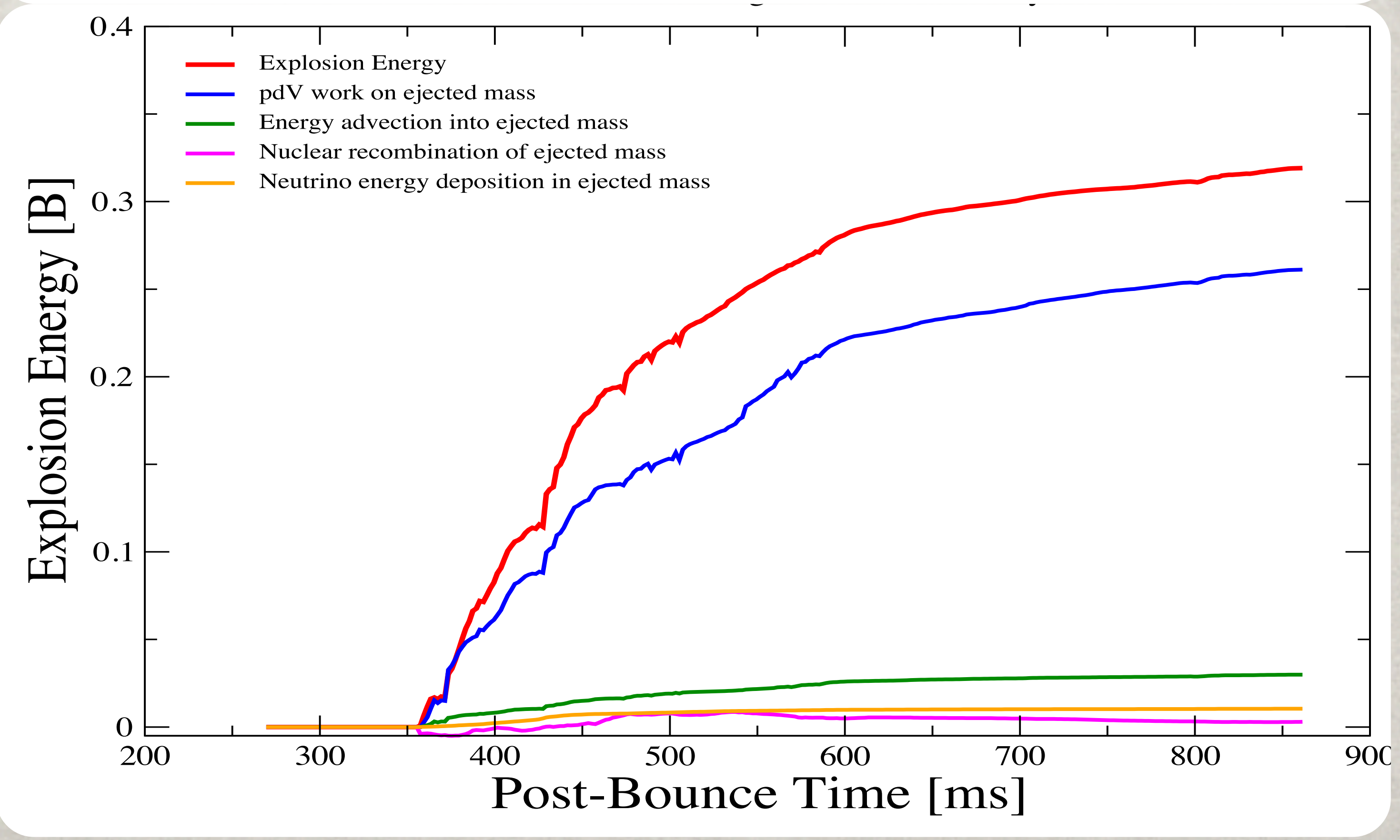

Working Neutrinos

The initially spherical gain surface between the cooling and heating regions begins to distort ~70 ms after bounce.

Beginning ~120 ms, the heating region is marked by low entropy downflows, with the strongest heating at their base.

Working Neutrinos

The initially spherical gain surface between the cooling and heating regions begins to distort ~70 ms after bounce.

Beginning ~120 ms, the heating region is marked by low entropy downflows, with the strongest heating at their base.

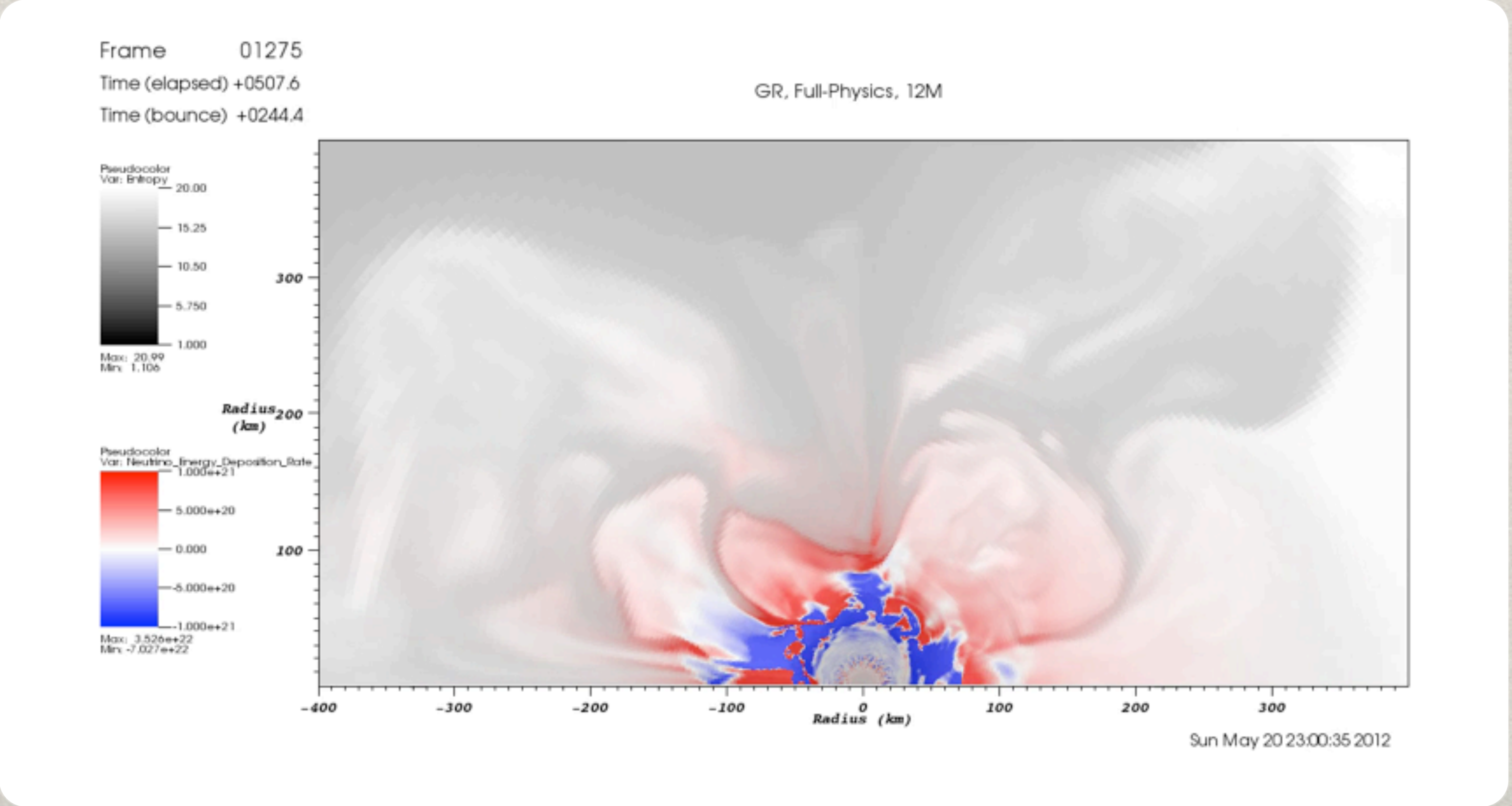

Working Neutrinos

The initially spherical gain surface between the cooling and heating regions begins to distort ~70 ms after bounce.

Beginning ~120 ms, the heating region is marked by low entropy downflows, with the strongest heating at their base.

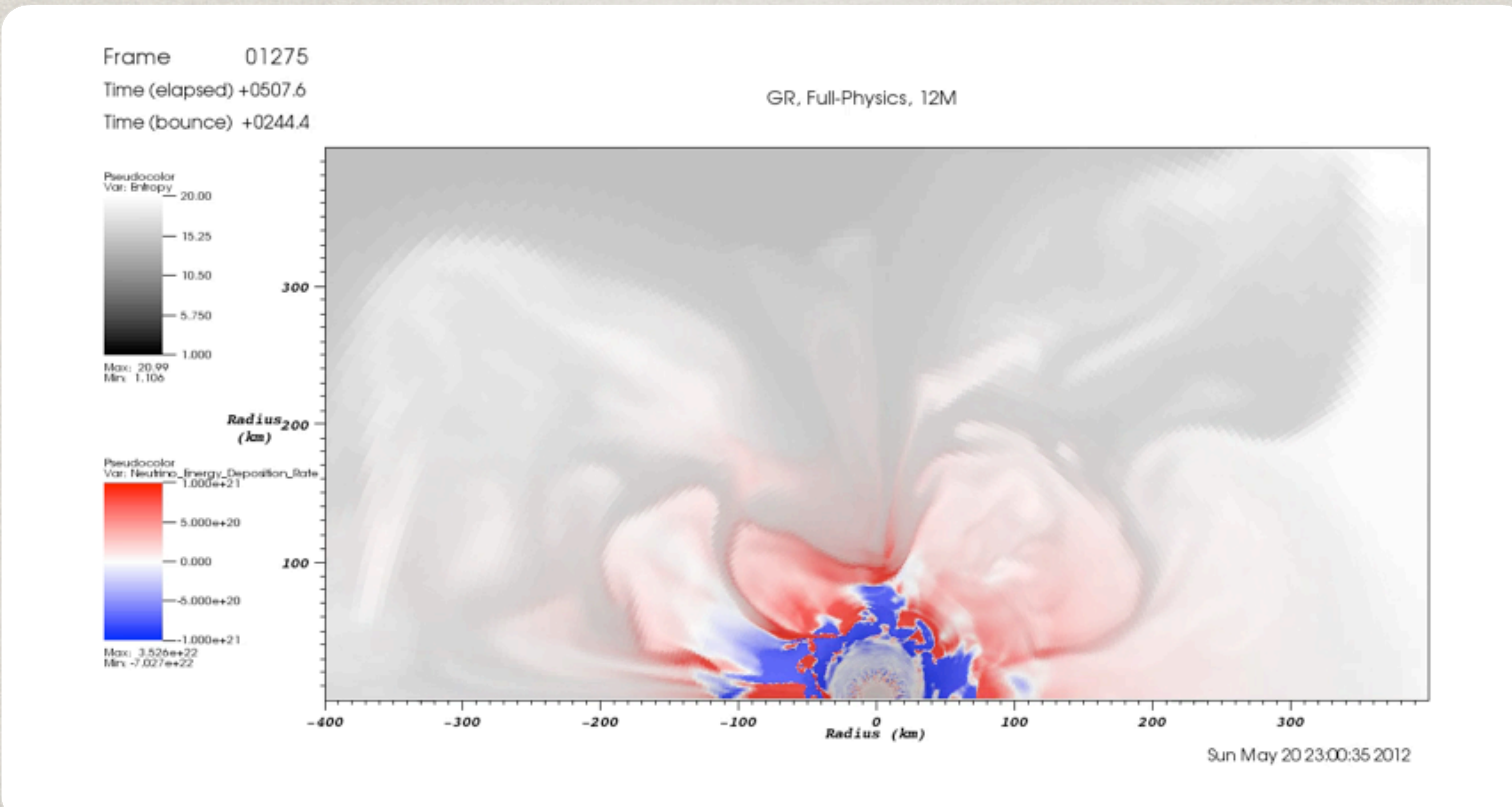

Shock Shape

The shape of the shock is determined by the interplay between convection and the SASI, with large individual plumes producing strongly prolate to mildly oblate shocks, depending on the plume's orientation.

Overall, trend is toward prolate explosions along the axis of symmetry, likely a result of the imposed axisymmetry.

Shock Shape

The shape of the shock is determined by the interplay between convection and the SASI, with large individual plumes producing strongly prolate to mildly oblate shocks, depending on the plume's orientation.

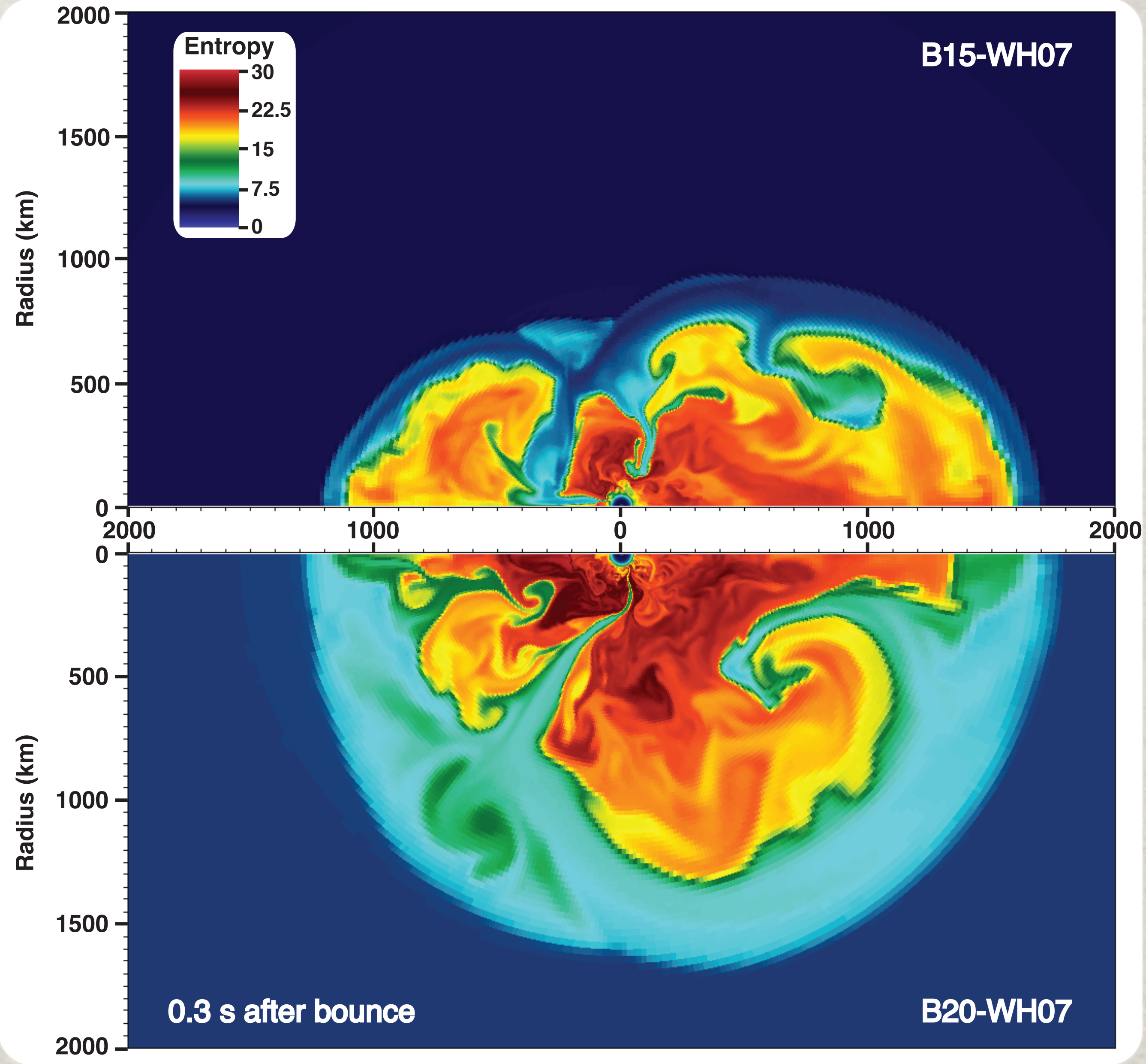

Overall, trend is toward prolate explosions along the axis of symmetry, likely a result of the imposed axisymmetry.

Shock Shape

The shape of the shock is determined by the interplay between convection and the SASI, with large individual plumes producing strongly prolate to mildly oblate shocks, depending on the plume's orientation.

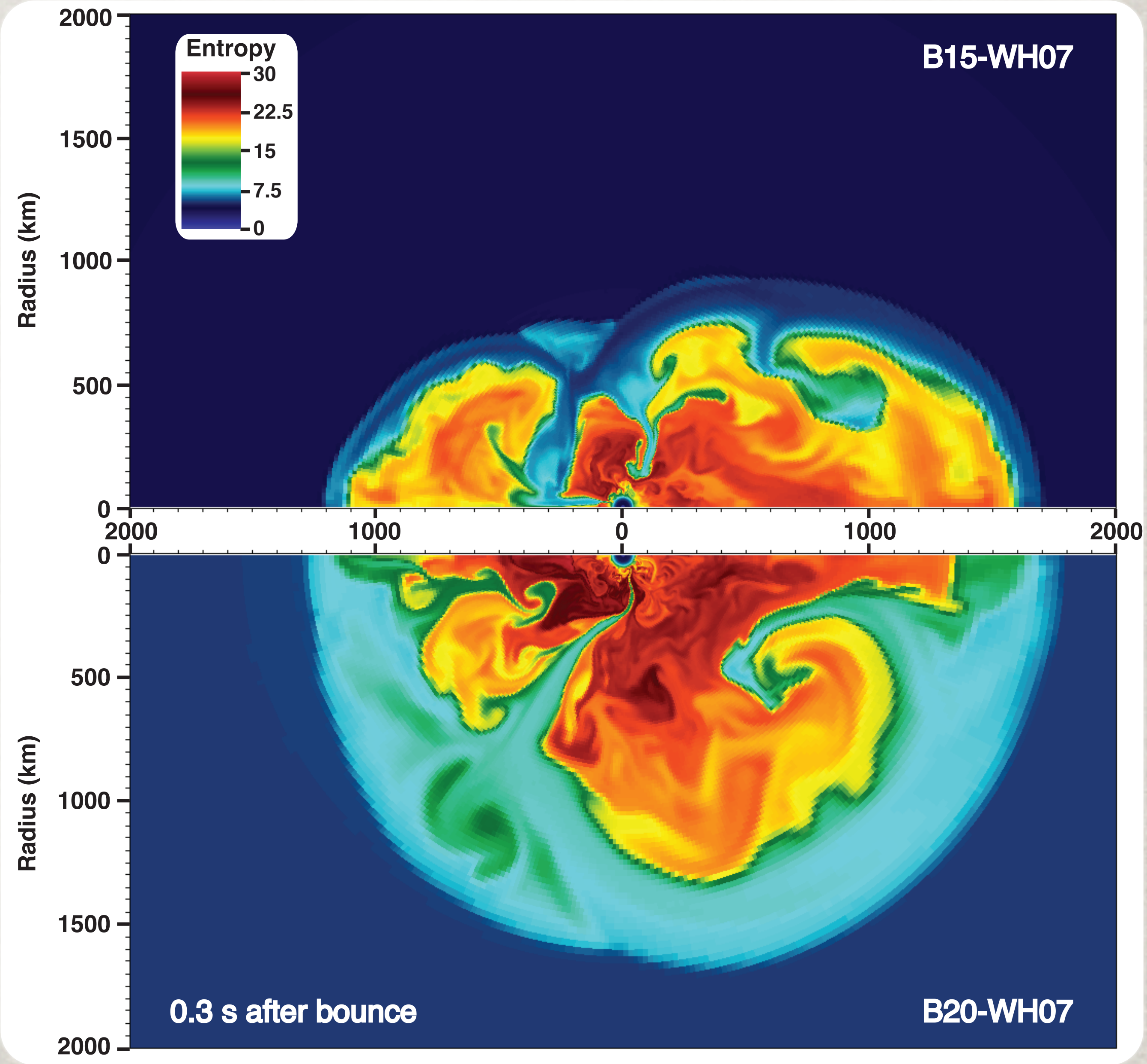

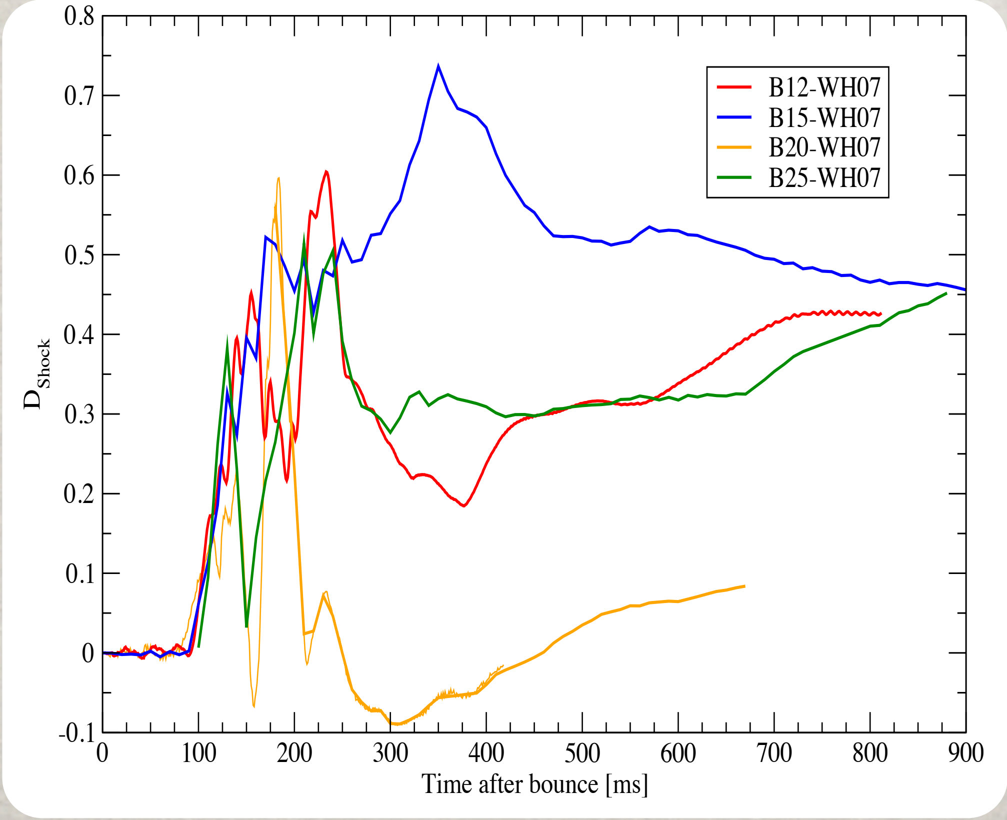

Overall, trend is toward prolate explosions along the axis of symmetry, likely a result of the imposed axisymmetry.

Explosion Energies

Once we achieve the most basic observable, an explosion, we can begin to compare to the myriad of other potential observations.

Explosion Energies

Once we achieve the most basic observable, an explosion, we can begin to compare to the myriad of other potential observations. Foremost is the kinetic energy of the explosion.

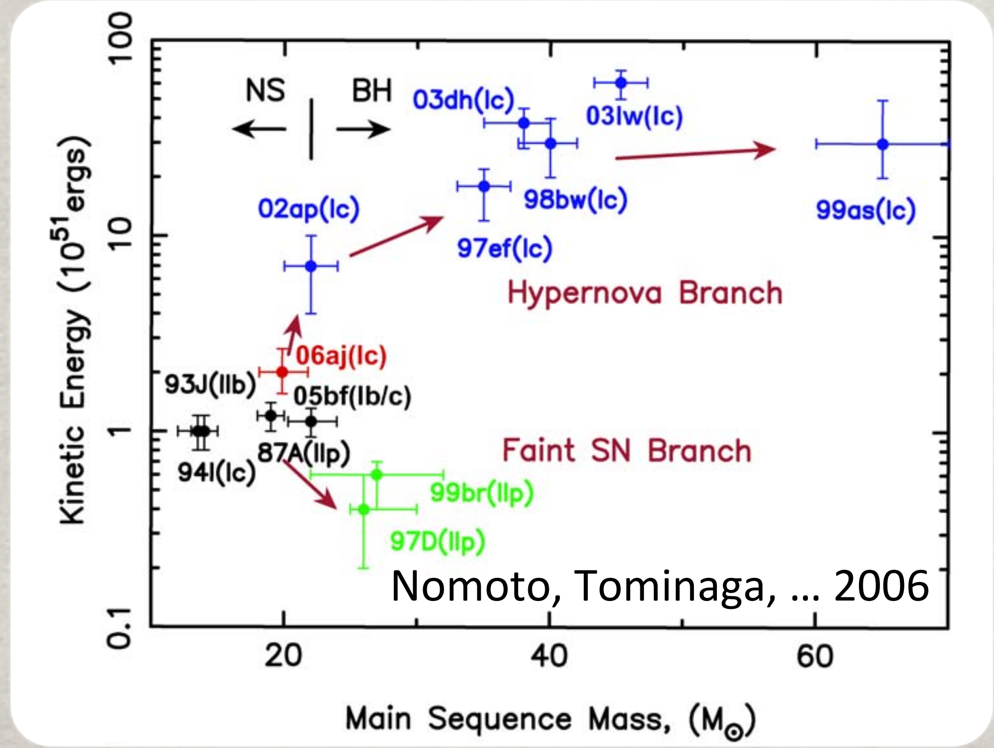

Explosion Energies

Once we achieve the most basic observable, an explosion, we can begin to compare to the myriad of other potential observations.

Foremost is the kinetic energy of the explosion.

Unfortunately, models are still in the stage where internal energy dominates, so we must estimate the explosion energy by assuming efficient conversion of $E_i \Rightarrow E_k$.

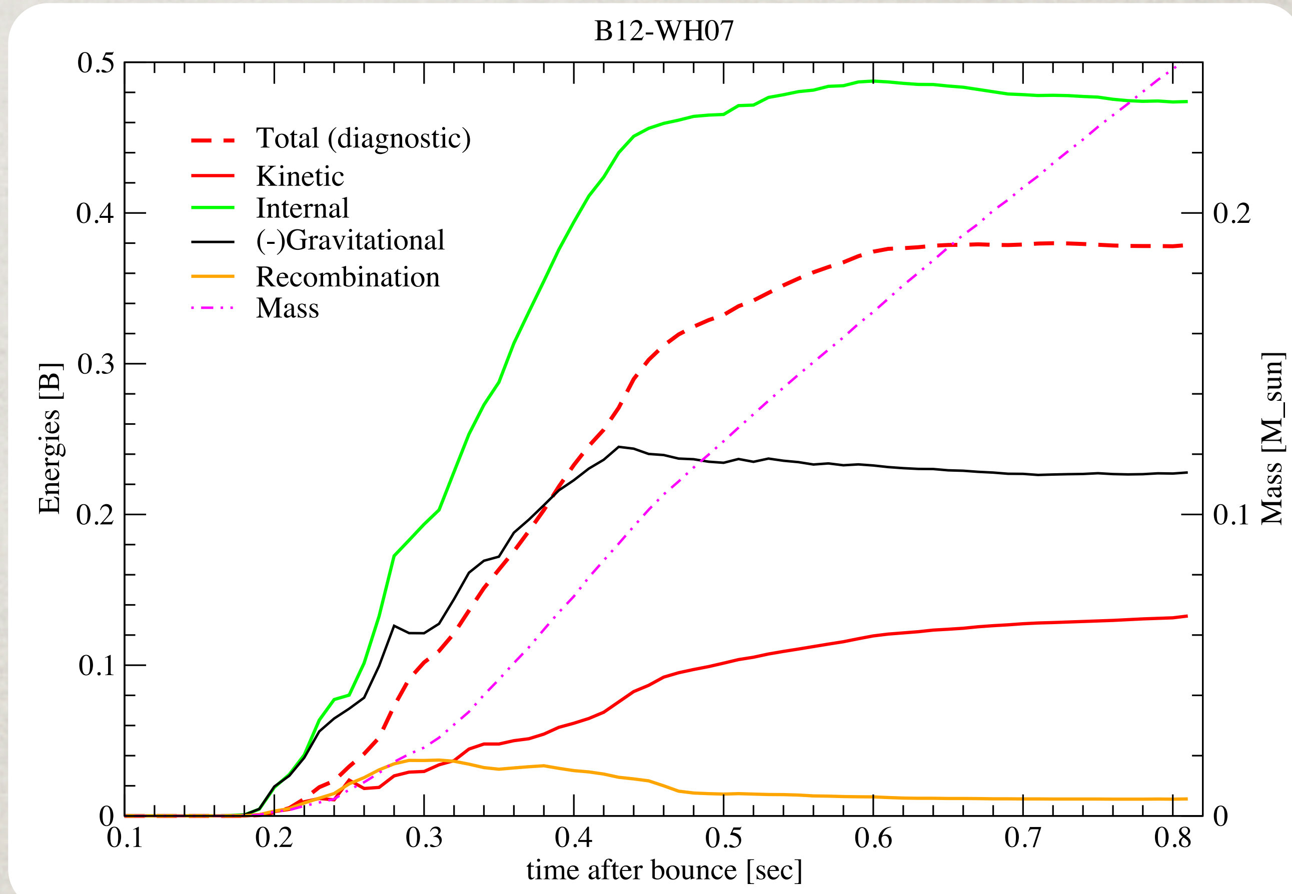

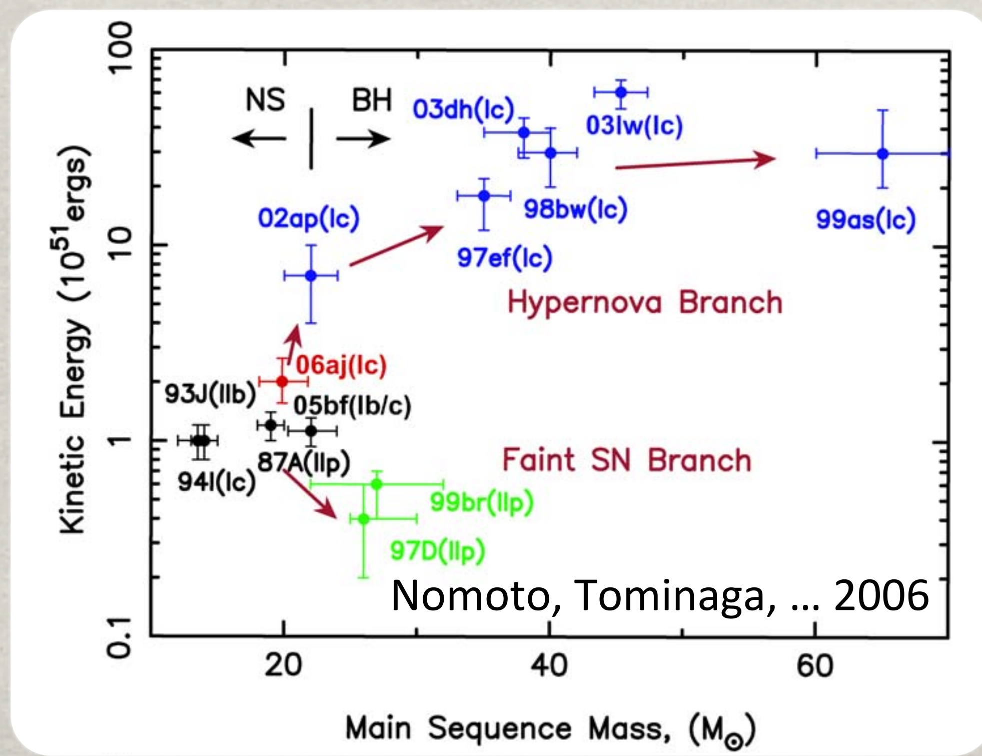

Nomoto, Tominaga, … 2006

Explosion Energies

Once we achieve the most basic observable, an explosion, we can begin to compare to the myriad of other potential observations.

Foremost is the kinetic energy of the explosion.

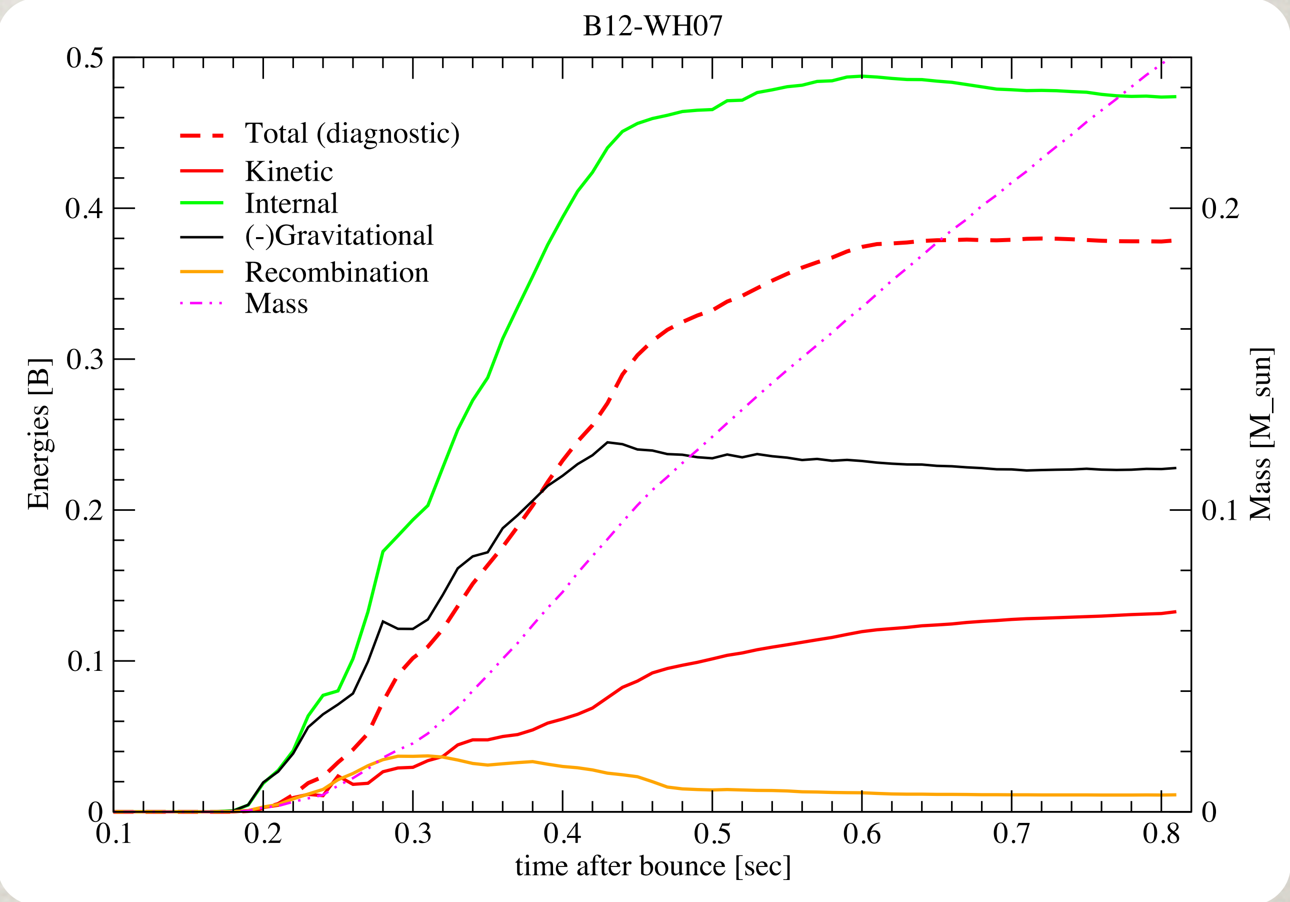

Unfortunately, models are still in the stage where internal energy dominates, so we must estimate the explosion energy by assuming efficient conversion of $E_i \Rightarrow E_k$.

One can construct a "diagnostic" energy, $E^+ = E_i + E_g + E_k$, summed over zones where $E^+ > 0$.

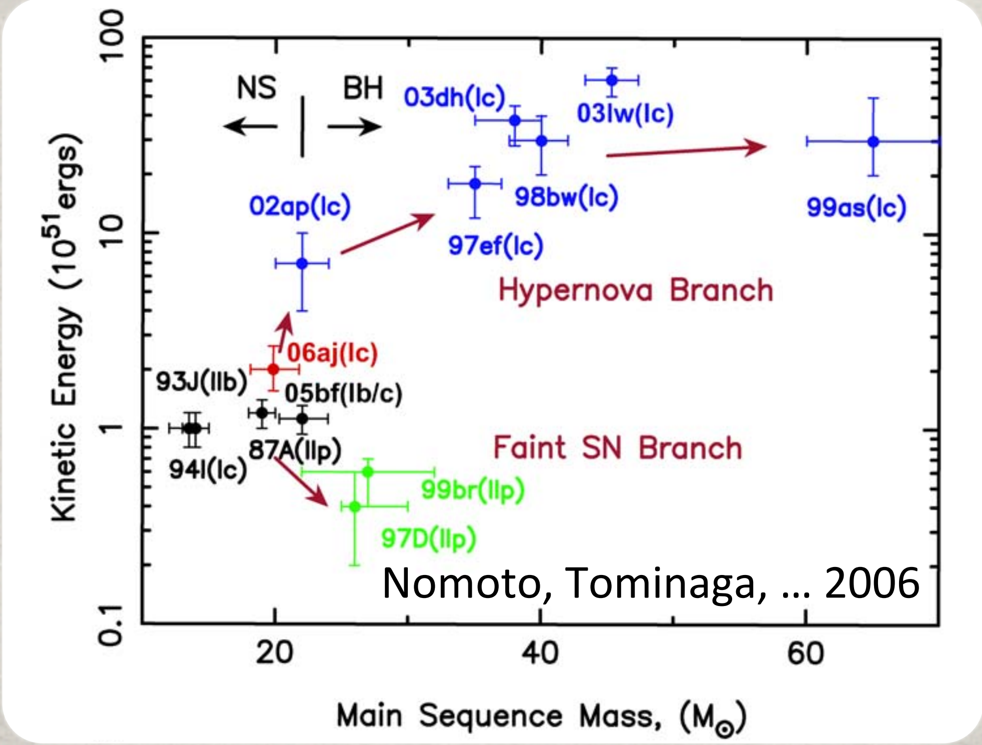

Explosion Energies

Once we achieve the most basic observable, an explosion, we can begin to compare to the myriad of other potential observations.

Foremost is the kinetic energy of the explosion.

Unfortunately, models are still in the stage where internal energy dominates, so we must estimate the explosion energy by assuming efficient conversion of $E_i \Rightarrow E_k$.

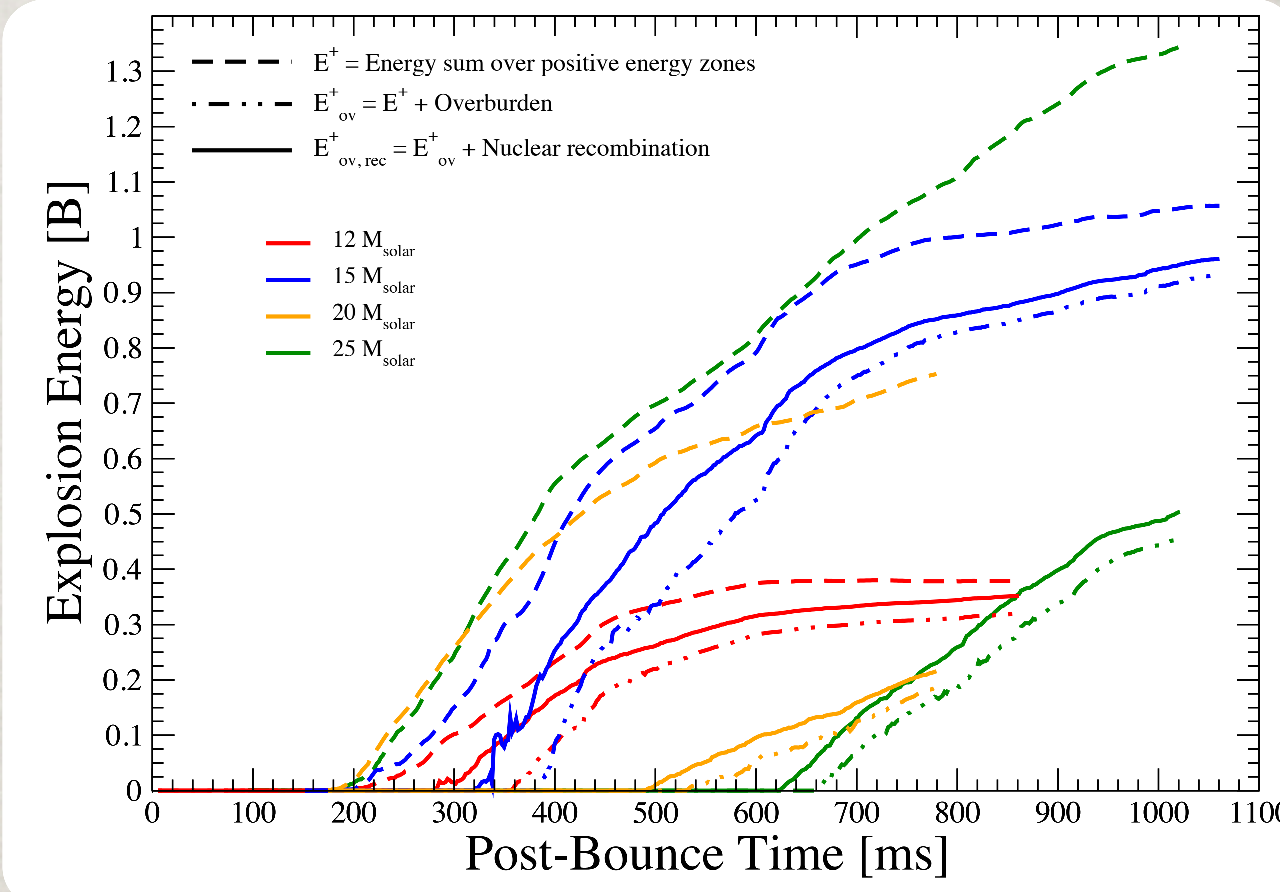

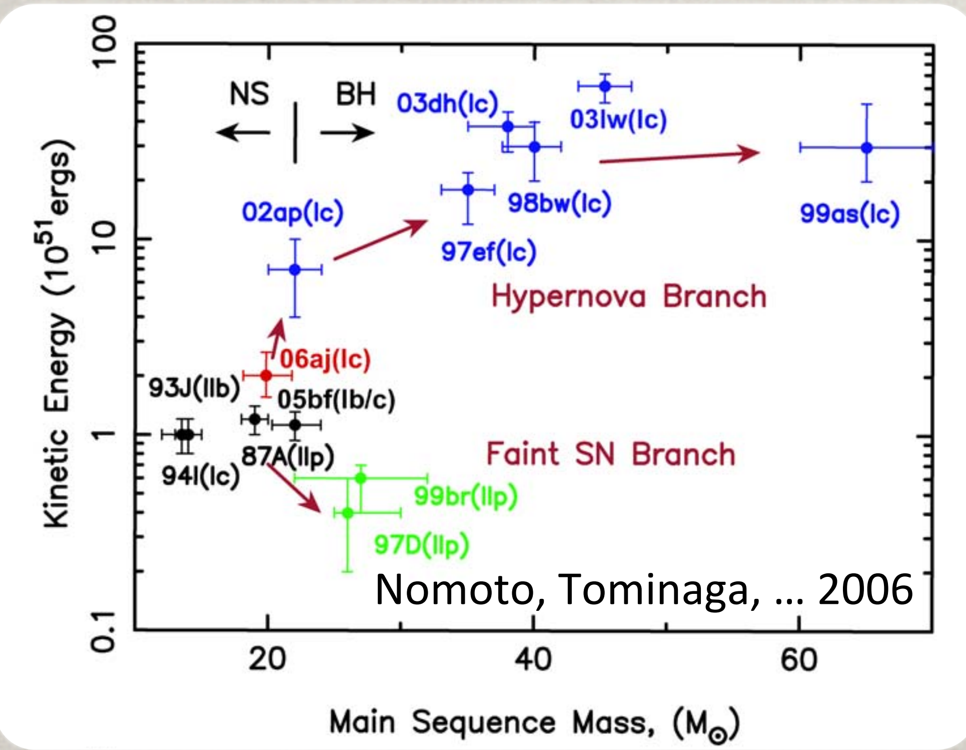

One can construct a "diagnostic" energy, $E^+ = E_i + E_g + E_k$, summed over zones where $E^+ > 0$.

To this we add contributions from nuclear recombination and removing the envelope.

Explosion Energies

Once we achieve the most basic observable, an explosion, we can begin to compare to the myriad of other potential observations.

Foremost is the kinetic energy of the explosion.

Unfortunately, models are still in the stage where internal energy dominates, so we must estimate the explosion energy by assuming efficient conversion of $E_i \Rightarrow E_k$.

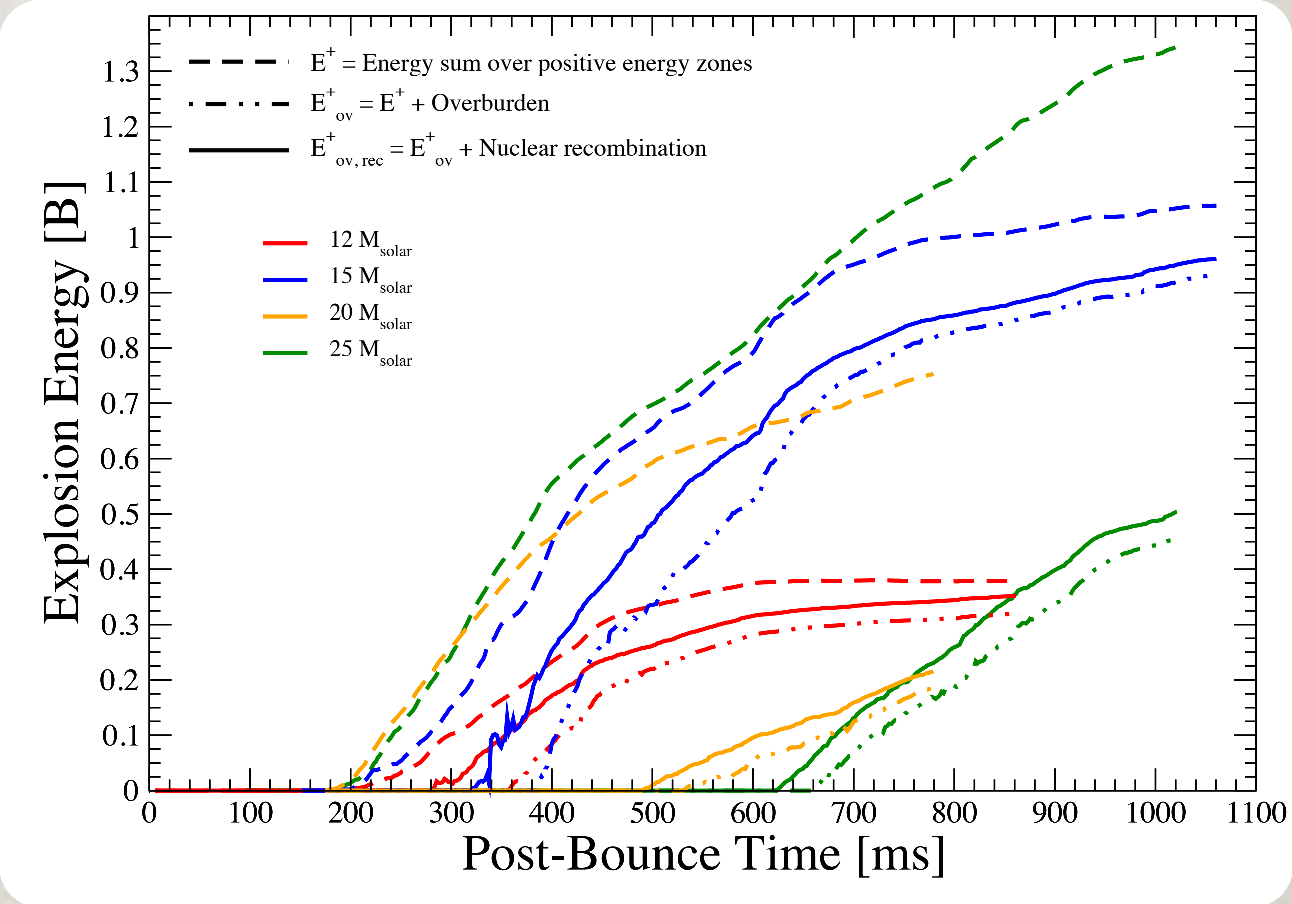

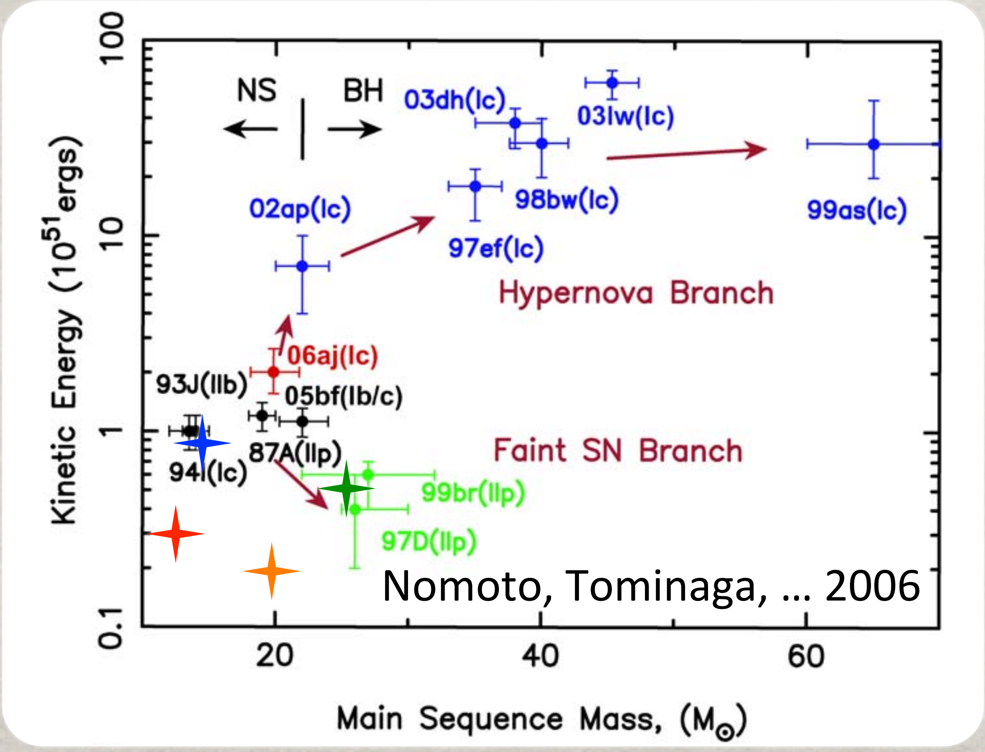

One can construct a "diagnostic" energy, $E^{+} = E_i + E_g + E_k$, summed over zones where $E^{+} > 0$.

To this we add contributions from nuclear recombination and removing the envelope.

Counterpoint

Self-consistent models using the MPA VERTEX code also produce successful neutrino-driven explosions.

Counterpoint

Self-consistent models using the MPA VERTEX code also produce successful neutrino-driven explosions.

However, explosions are even more delayed with significantly smaller explosion energies.

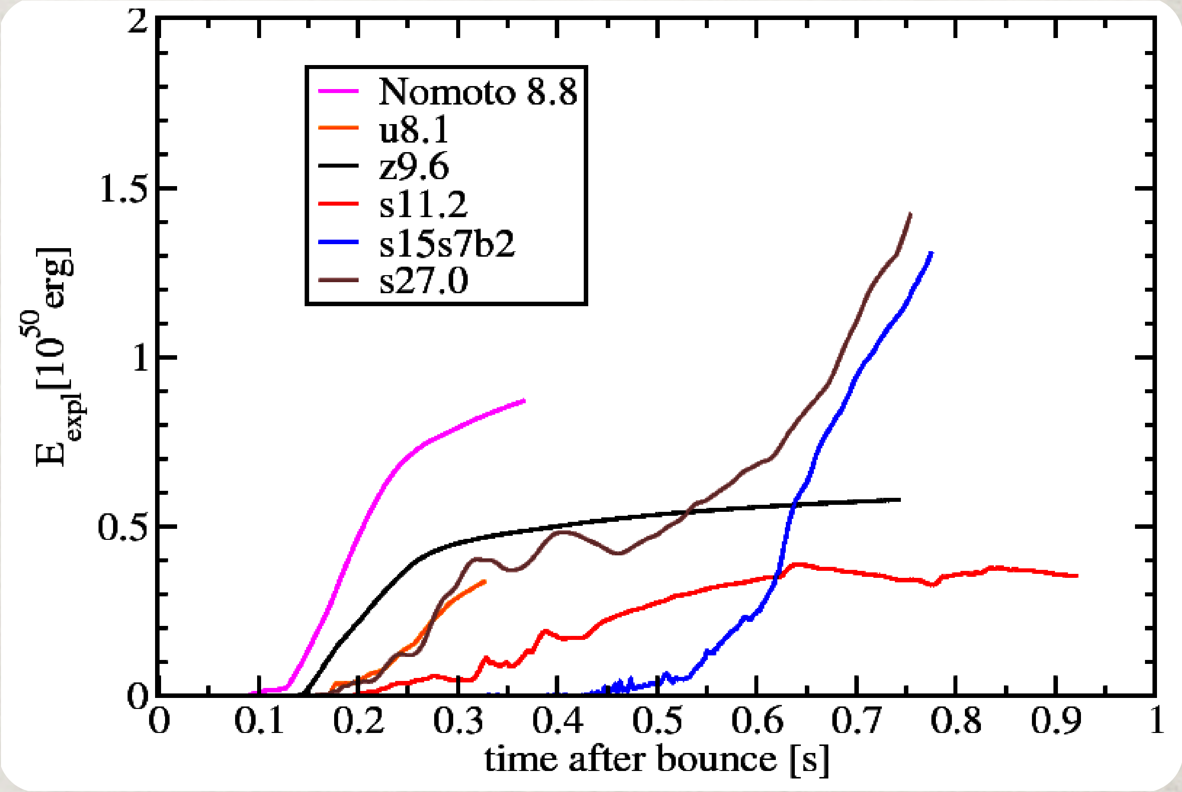

Counterpoint

Self-consistent models using the MPA VERTEX code also produce successful neutrino-driven explosions.

However, explosions are even more delayed with significantly smaller explosion energies.

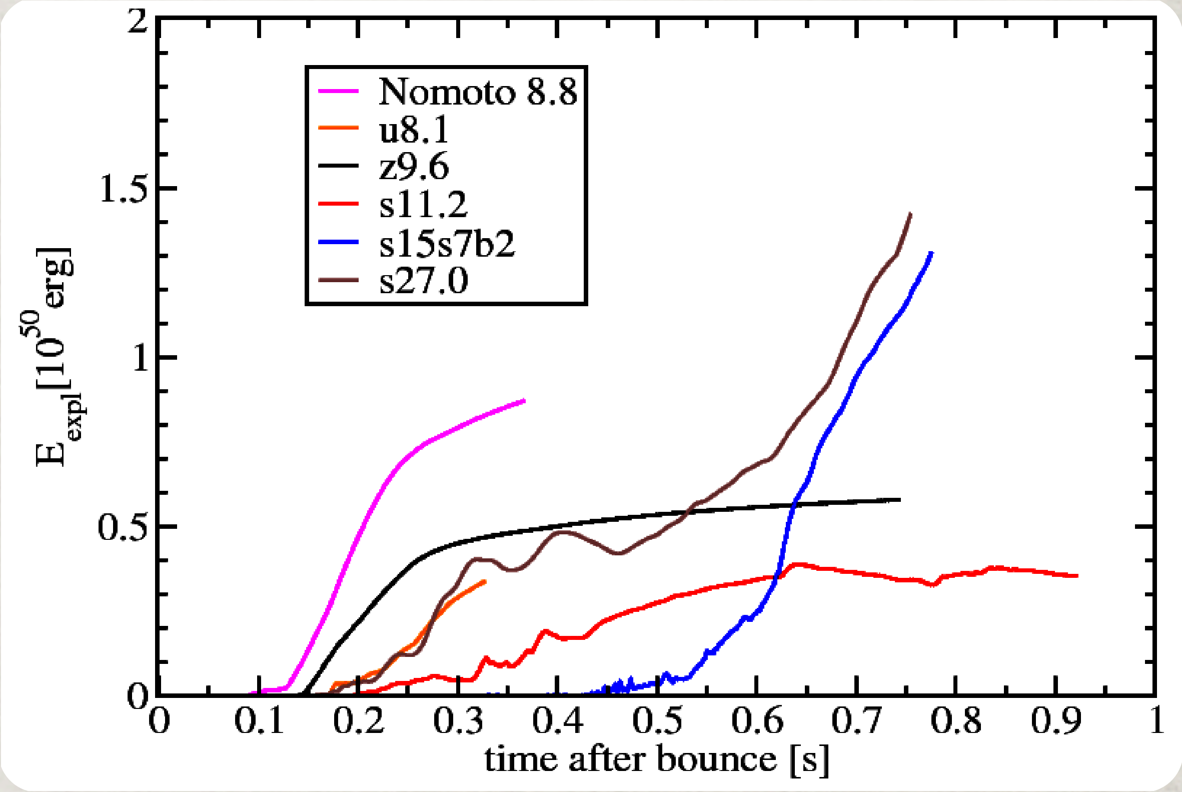

Some of the differences can be attributed to different progenitors.

Counterpoint

Self-consistent models using the MPA VERTEX code also produce successful neutrino-driven explosions.

However, explosions are even more delayed with significantly smaller explosion energies.

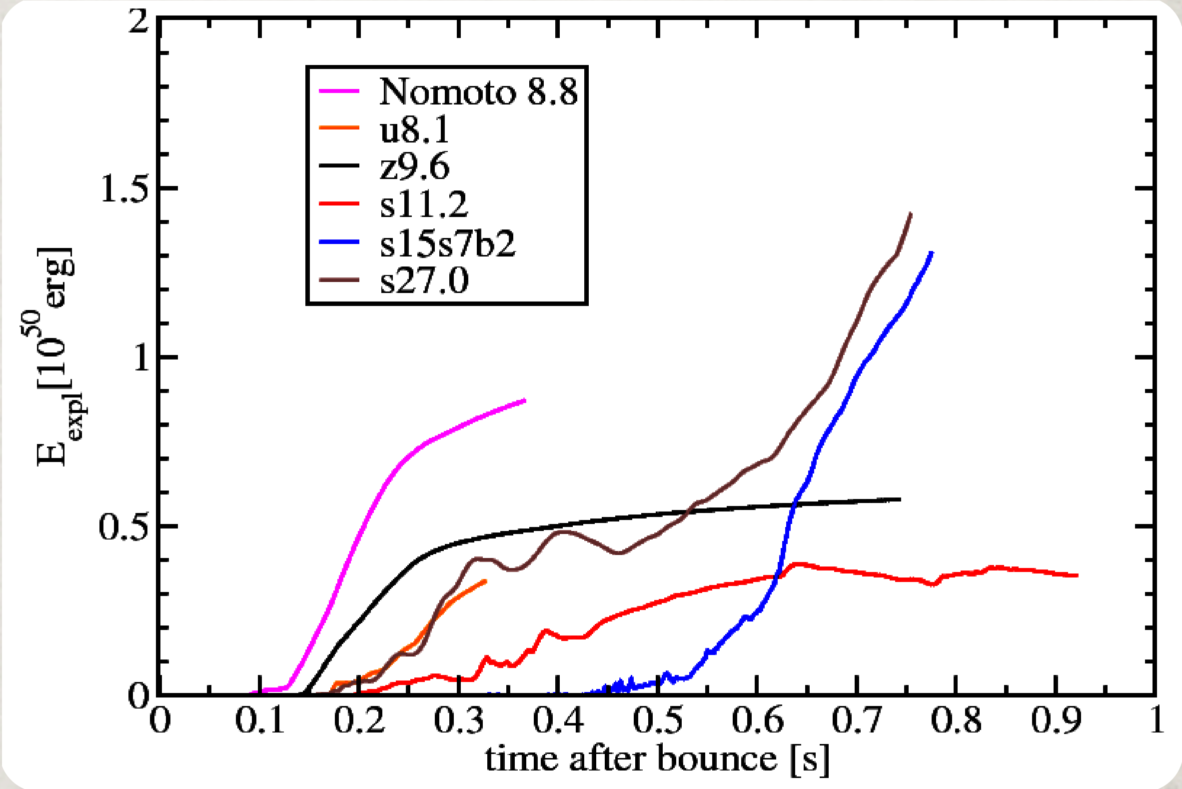

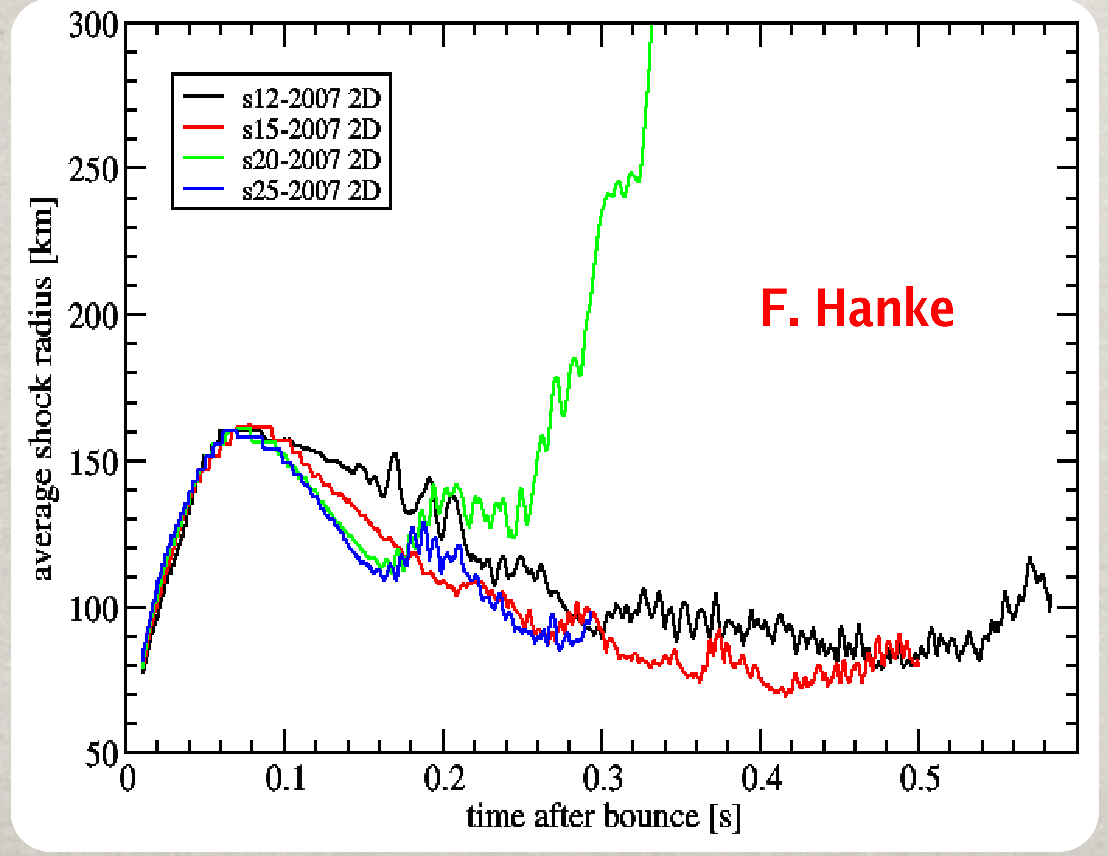

Some of the differences can be attributed to different progenitors.

In recent VERTEX models using Woosley & Heger (2007) progenitors, only the 20 solar mass model exhibits an explosion over first 0.5 seconds.

Nickel Mass

Another important observable, related to the explosion energy and very relevant to the nucleosynthesis is the mass of ^{56}Ni.

Only in the 12 $M_\odot$ case is the ^{56}Ni mass saturated.

Mass of other iron-peak species is comparable to ^{56}Ni.

Results are reasonable, though fallback over longer timescales is uncertain. Recent studies are finding differing results on fallback.

Nickel Mass

Another important observable, related to the explosion energy and very relevant to the nucleosynthesis is the mass of ^{56}Ni.

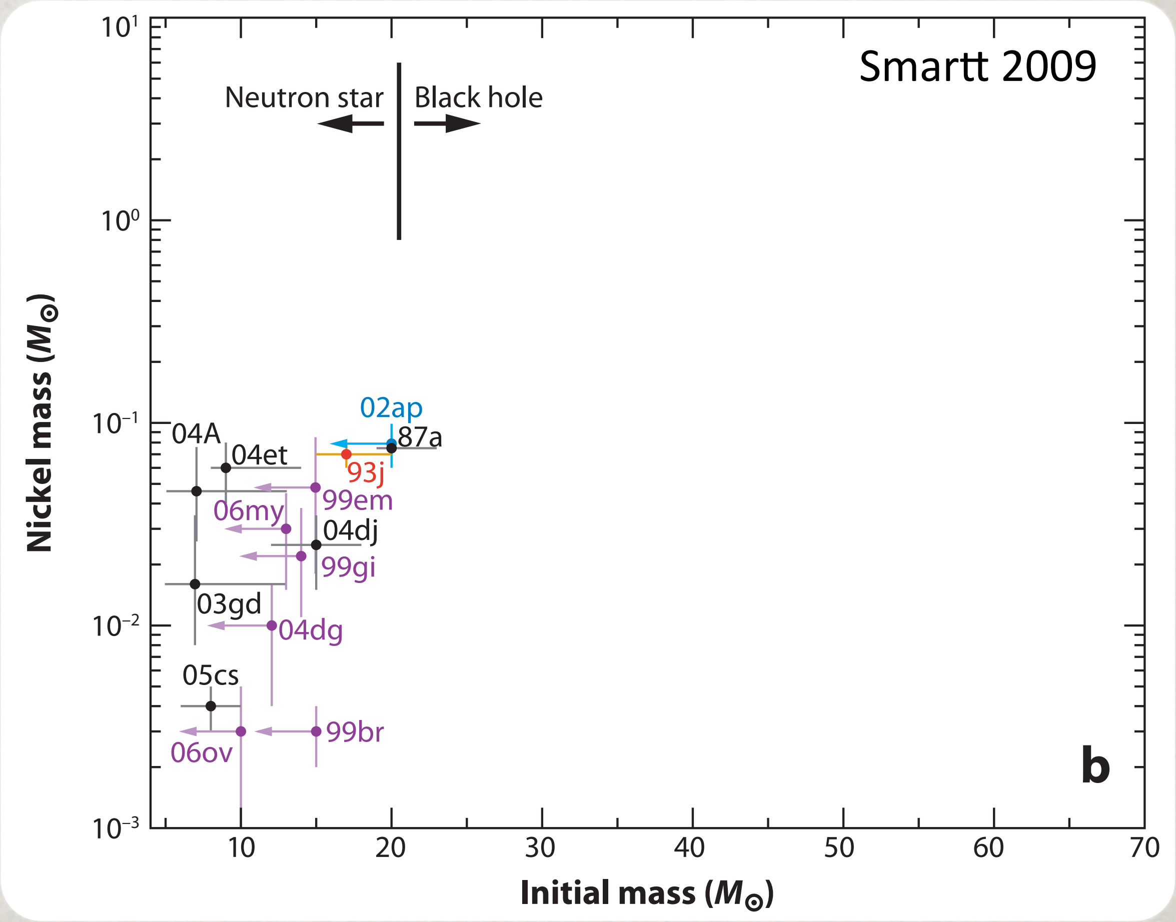

Only in the 12 $M_\odot$ case is the ^{56}Ni mass saturated.

Mass of other iron-peak species is comparable to ^{56}Ni.

Results are reasonable, though fallback over longer timescales is uncertain. Recent studies are finding differing results on fallback.

Nickel Mass

Another important observable, related to the explosion energy and very relevant to the nucleosynthesis is the mass of ^{56}Ni.

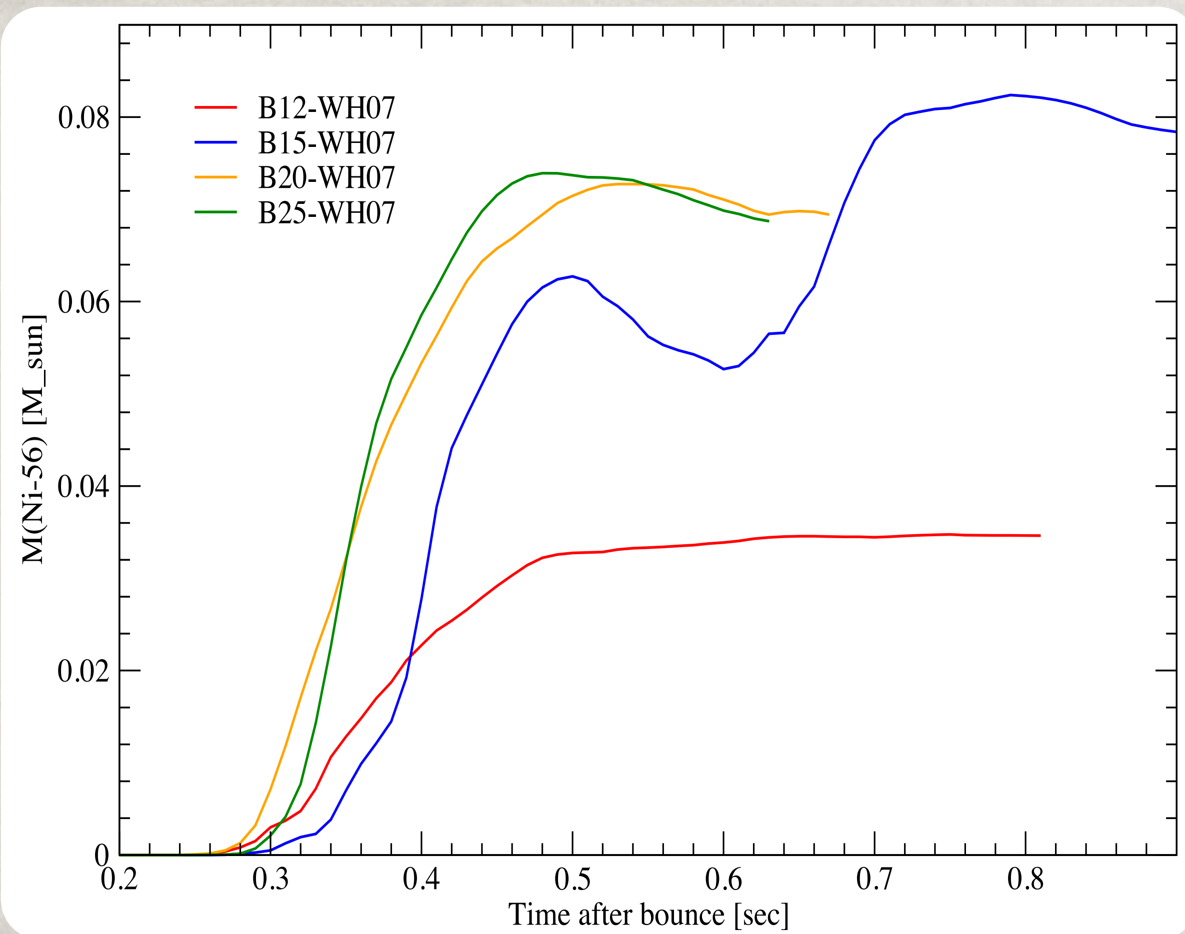

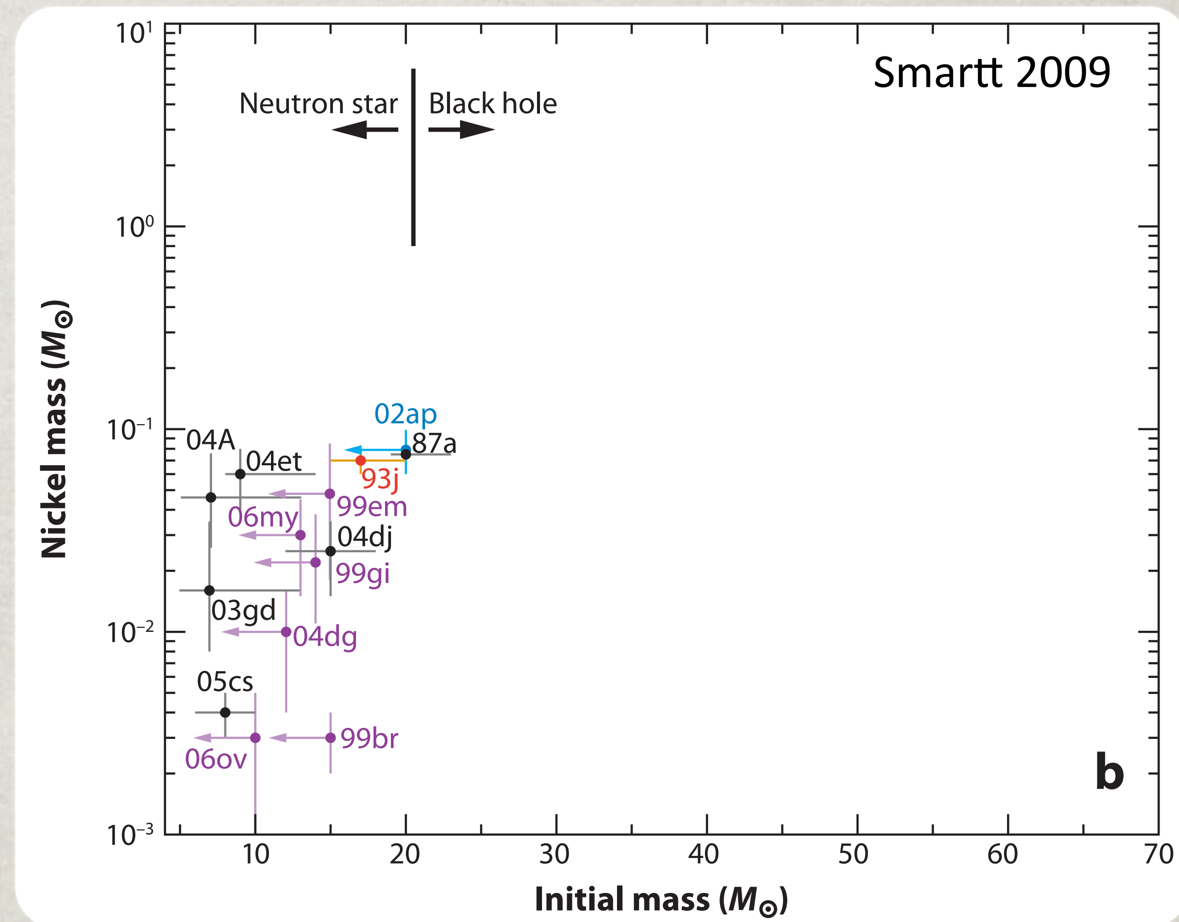

Only in the 12 $M_\odot$ case is the ^{56}Ni mass saturated.

Nickel Mass

Another important observable, related to the explosion energy and very relevant to the nucleosynthesis is the mass of ^{56}Ni.

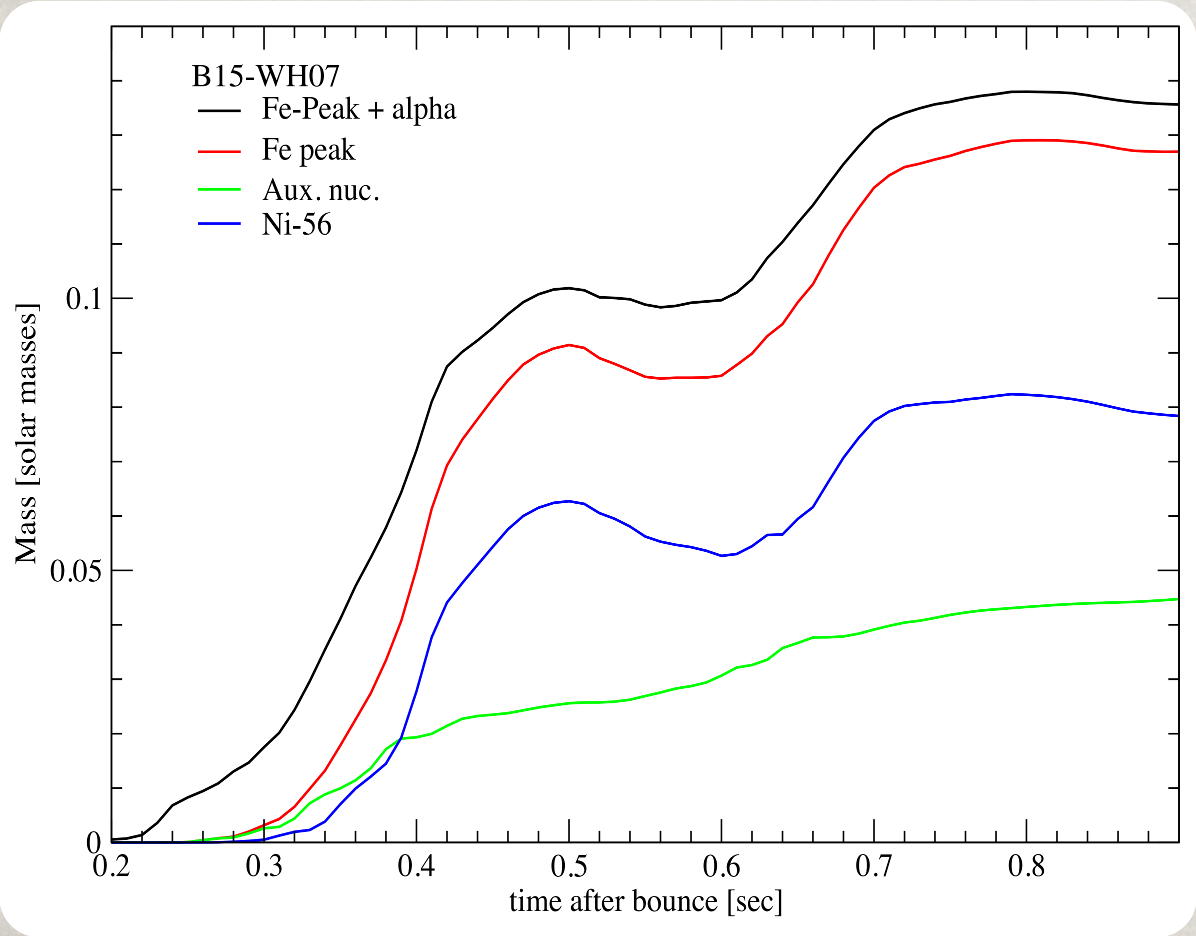

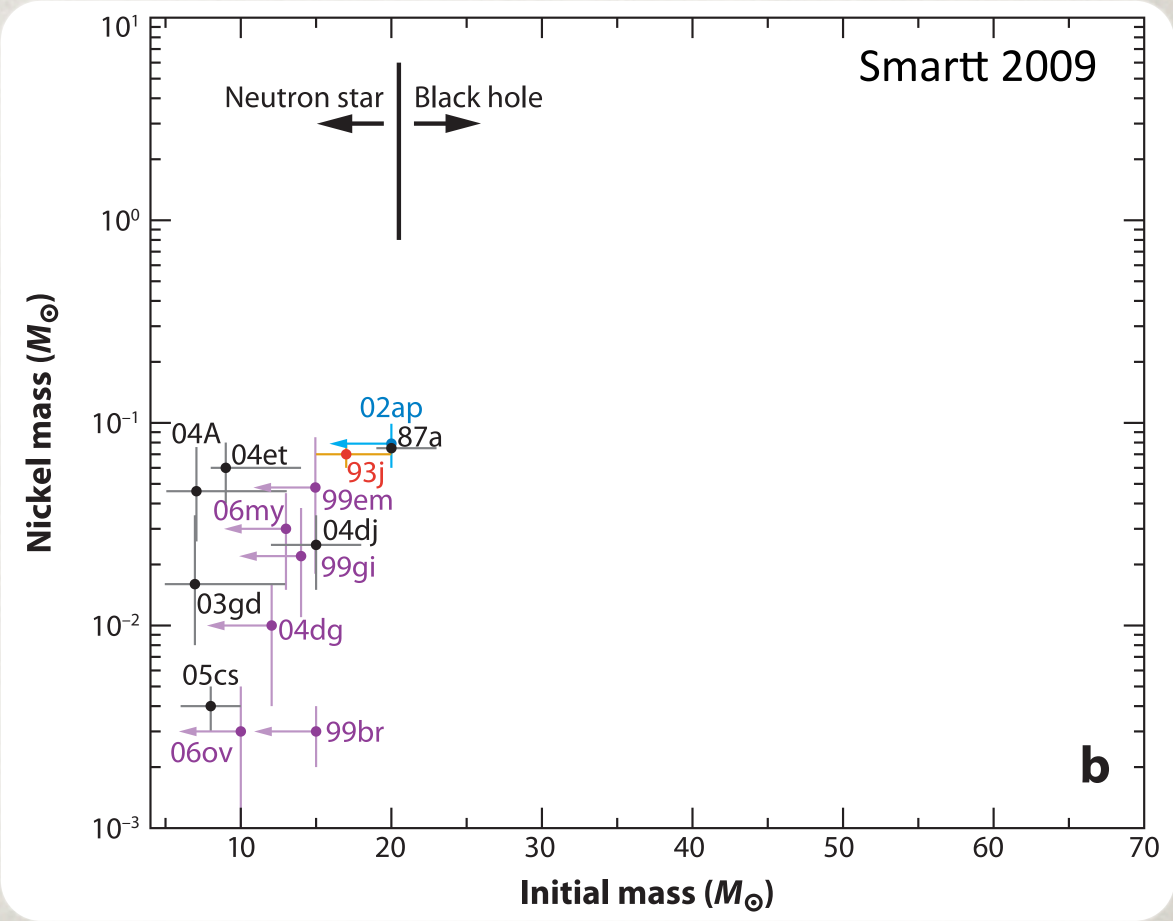

Only in the 12 $M_\odot$ case is the ^{56}Ni mass saturated.

Mass of other iron-peak species is comparable to ^{56}Ni.

Nickel Mass

Another important observable, related to the explosion energy and very relevant to the nucleosynthesis is the mass of ^{56}Ni.

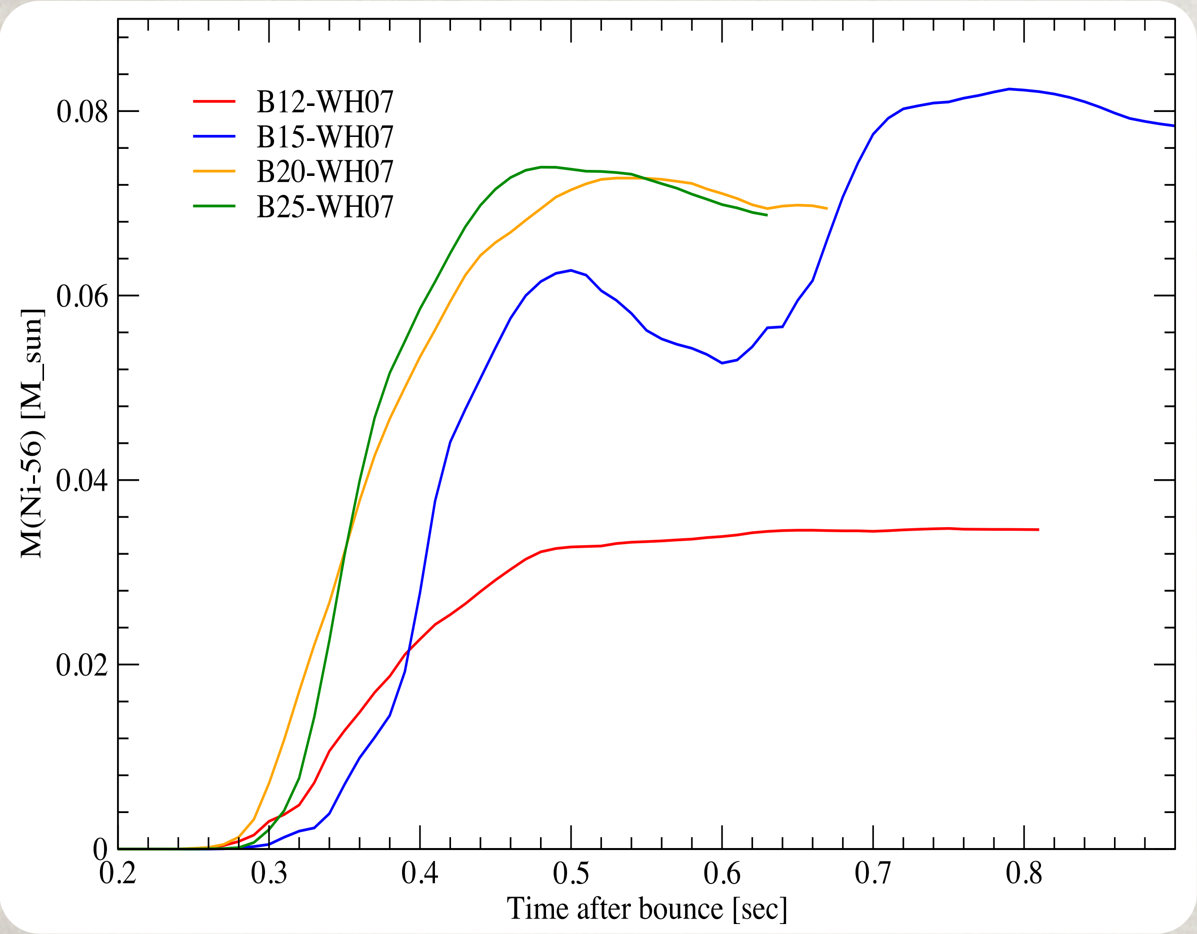

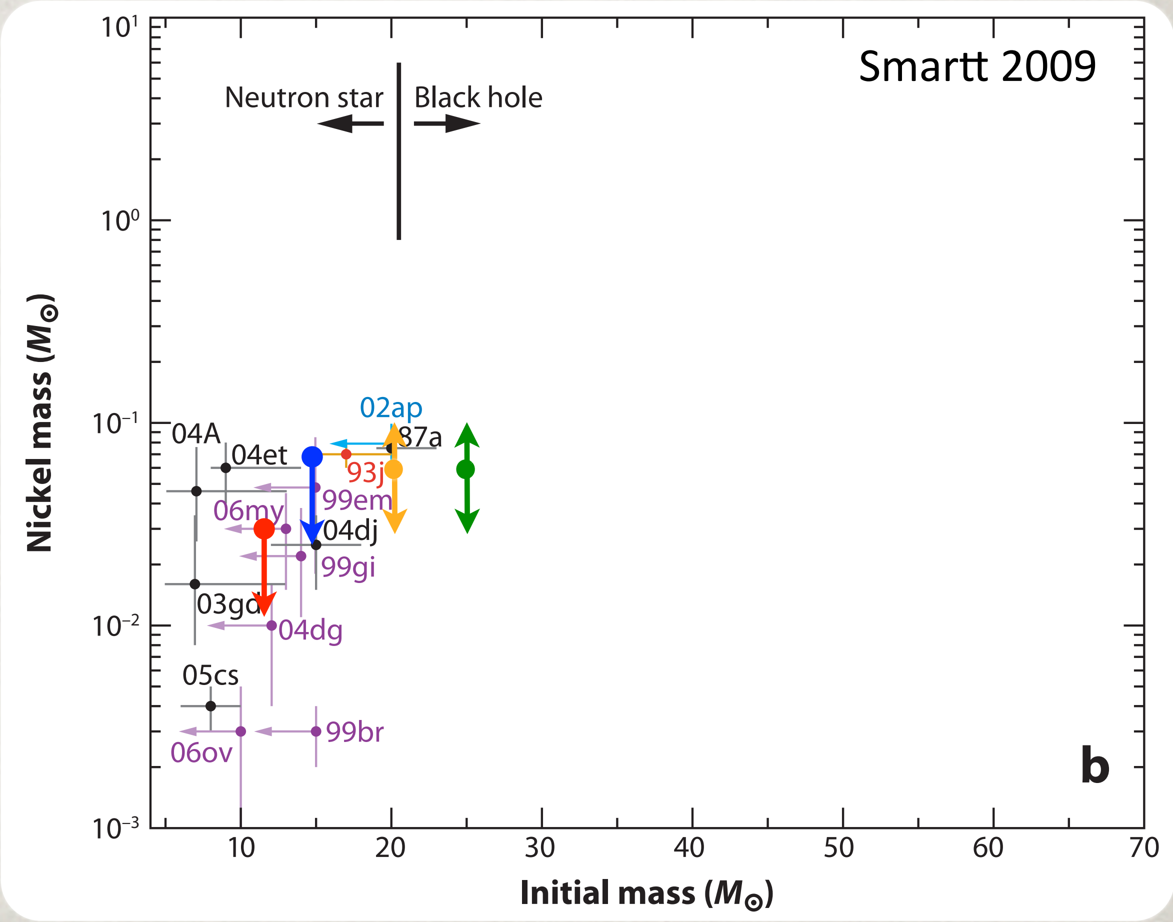

Only in the 12 $M_\odot$ case is the ^{56}Ni mass saturated.

Mass of other iron-peak species is comparable to ^{56}Ni.

Results are reasonable, though fallback over longer timescales is uncertain. Recent studies are finding differing results on fallback.

Our First 3D simulations

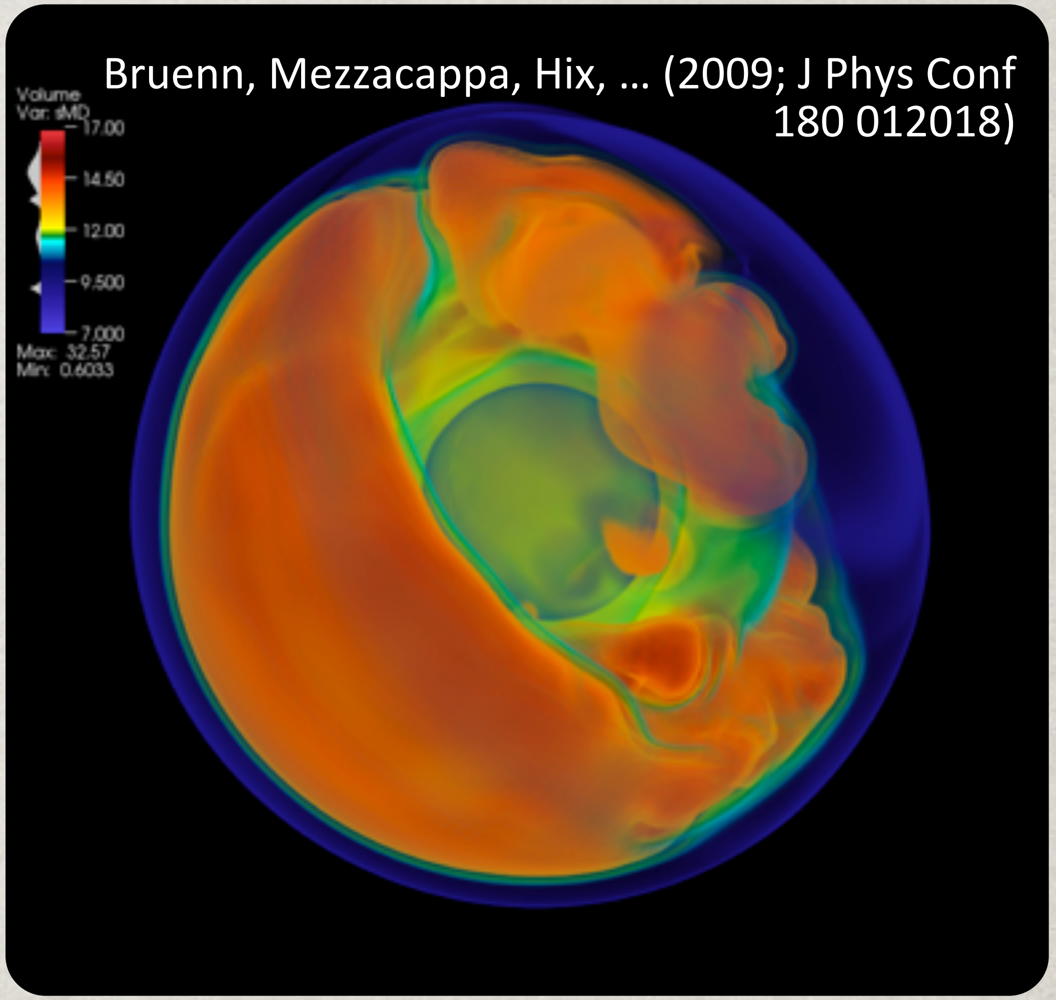

Our First 3D simulations

CHIMERA3D Maiden voyage (2009)

304 adaptive radial zones, 2.4° in latitude and longitude, on 11552 processors consumed 12M cpu-hours to cover 150 ms.

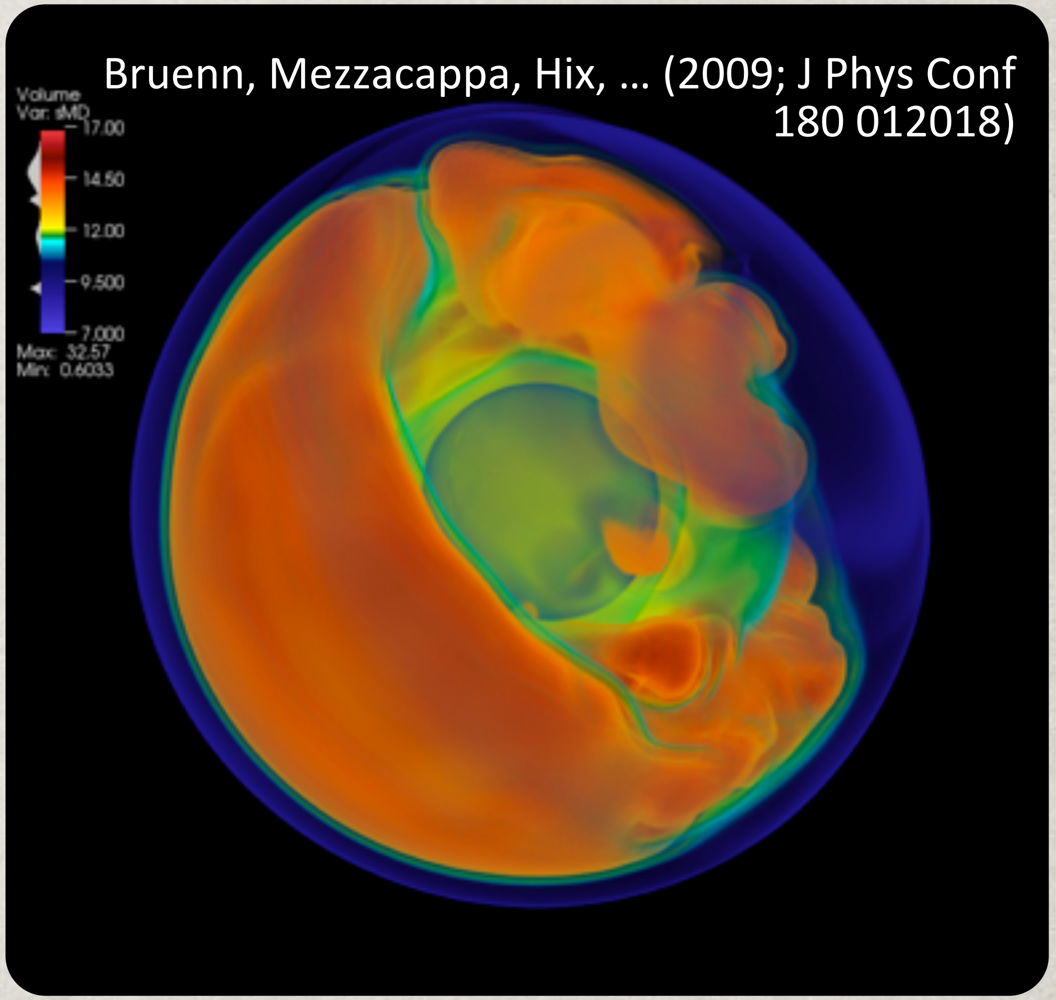

Our First 3D simulations

CHIMERA3D Maiden voyage (2009)

- 304 adaptive radial zones, 2.4° in latitude and longitude, on 11552 processors consumed 12M cpu-hours to cover 150 ms.

CHIMERA3D was tested to

- 512 adaptive radial zones, 0.7° in latitude and longitude on 131072 processors.

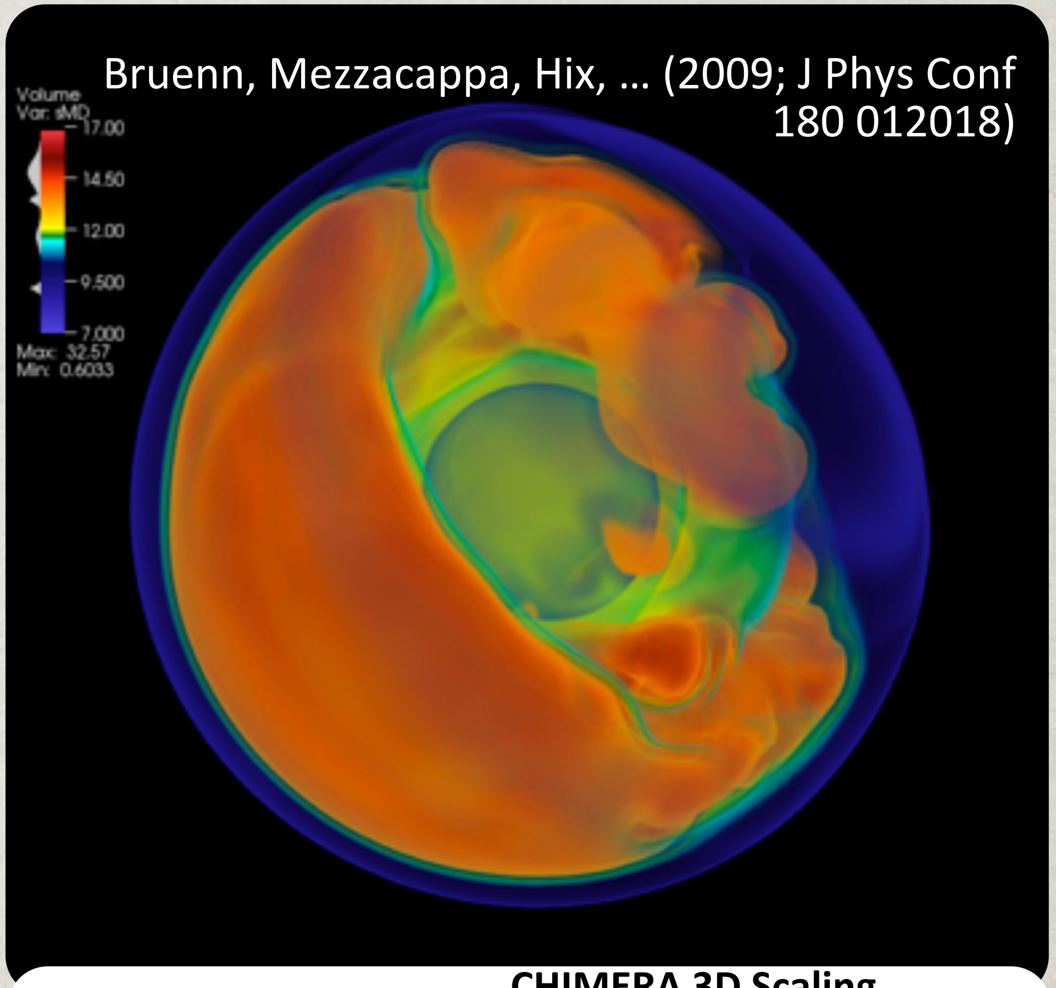

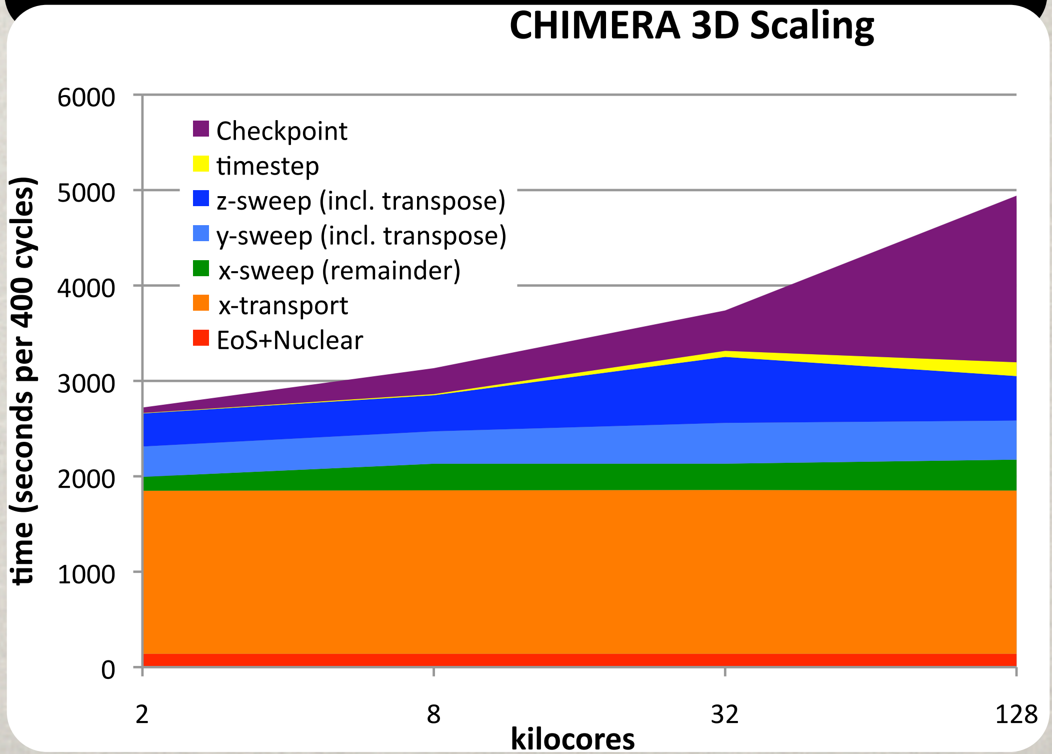

Our First 3D simulations

CHIMERA3D Maiden voyage (2009)

304 adaptive radial zones, 2.4° in latitude and longitude, on 11552 processors consumed 12M cpu-hours to cover 150 ms.

CHIMERA3D was tested to

512 adaptive radial zones, 0.7° in latitude and longitude on 131072 processors.

Second CHIMERA3D run (2011)

512 adaptive radial zones, 2.8° in latitude and longitude, on 8096 processors, reached 20 ms after bounce, limited by Courant timestep of 38 nanosecond at the pole.

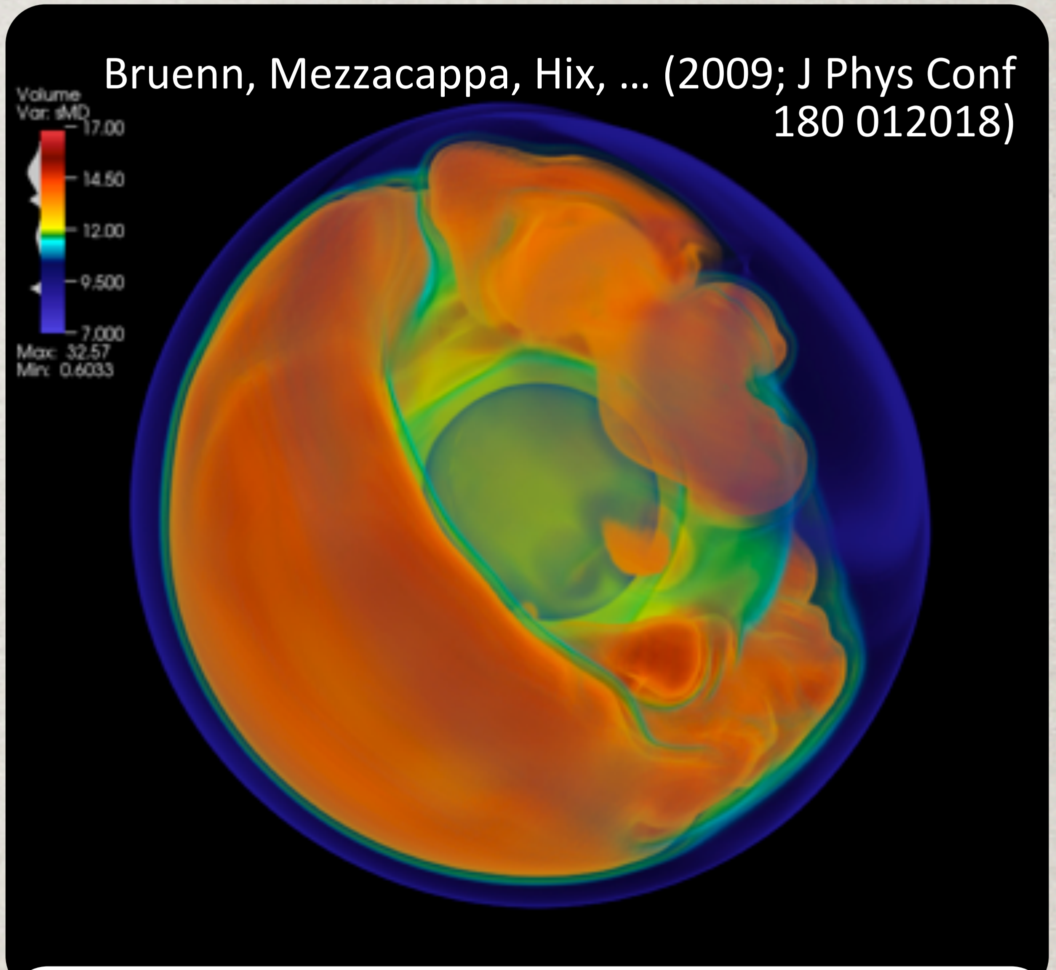

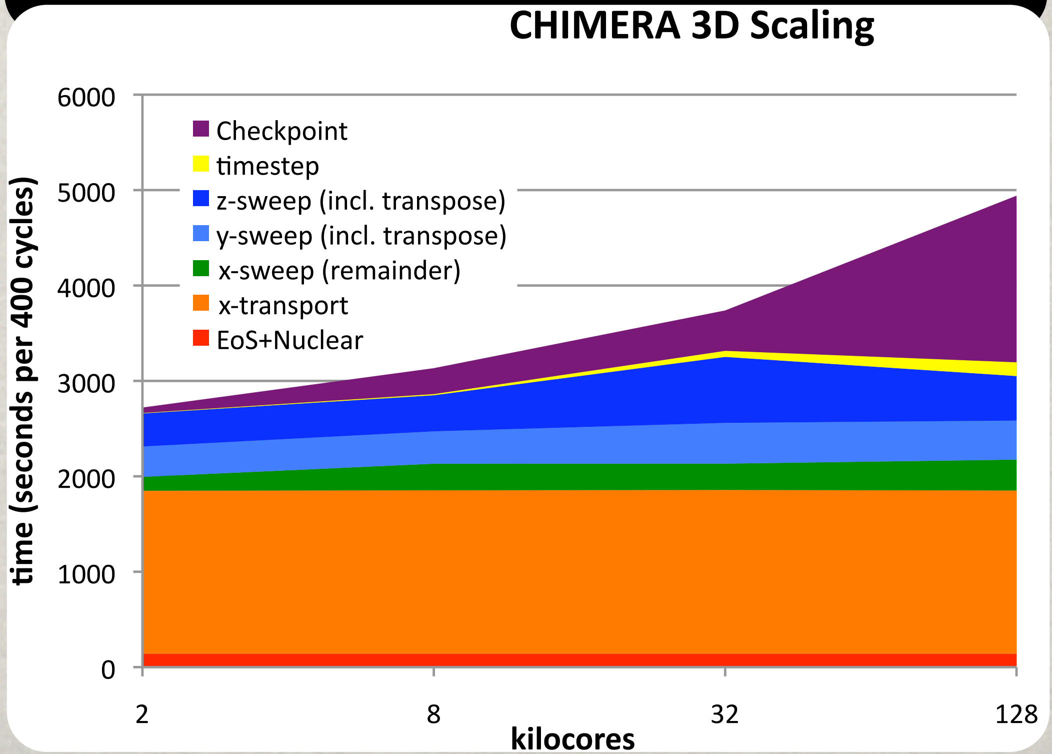

Comparing 2D & 3D

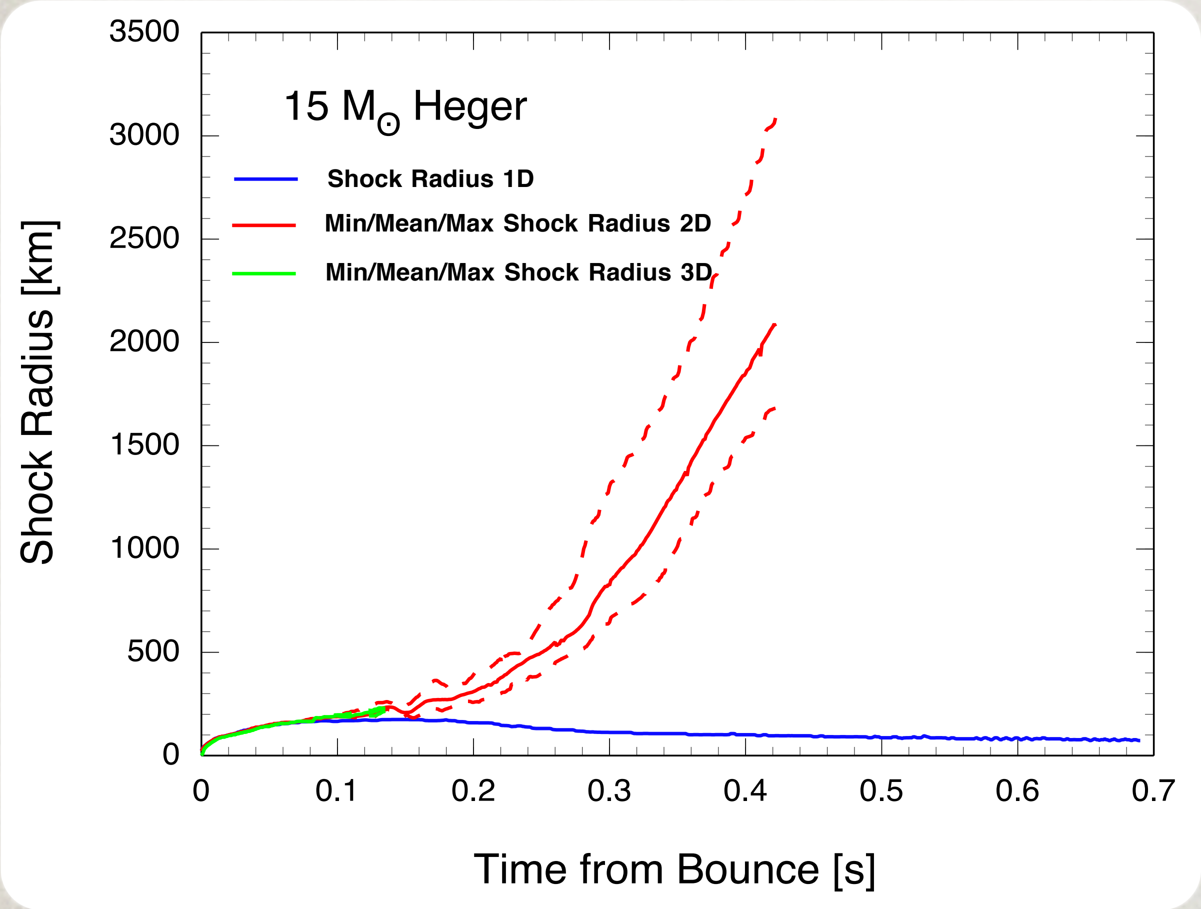

2009 CHIMERA 3D model shows similar behavior to 2D at 150 ms after bounce.

Comparing 2D & 3D

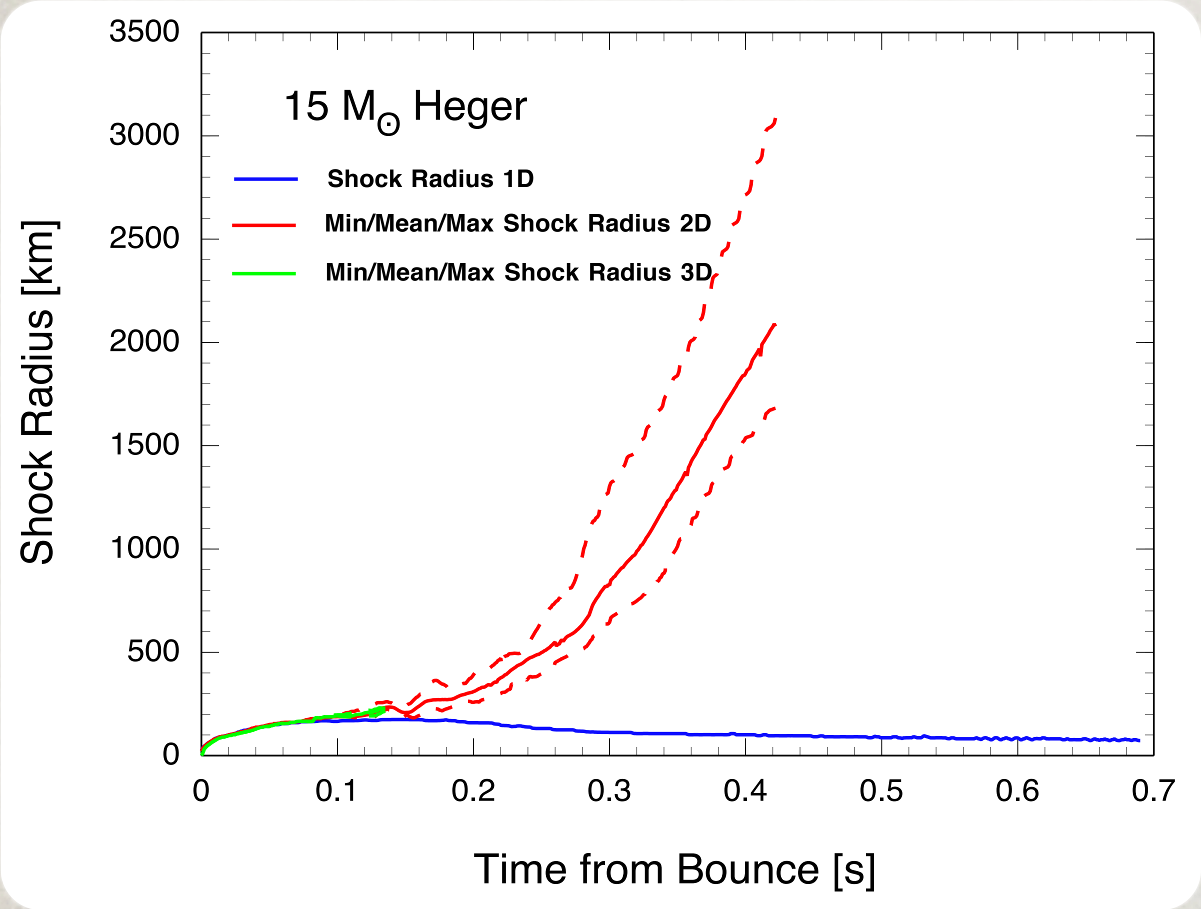

2009 CHIMERA 3D model shows similar behavior to 2D at 150 ms after bounce.

But it was just getting to the interesting point when it was stopped.

Comparing 2D & 3D

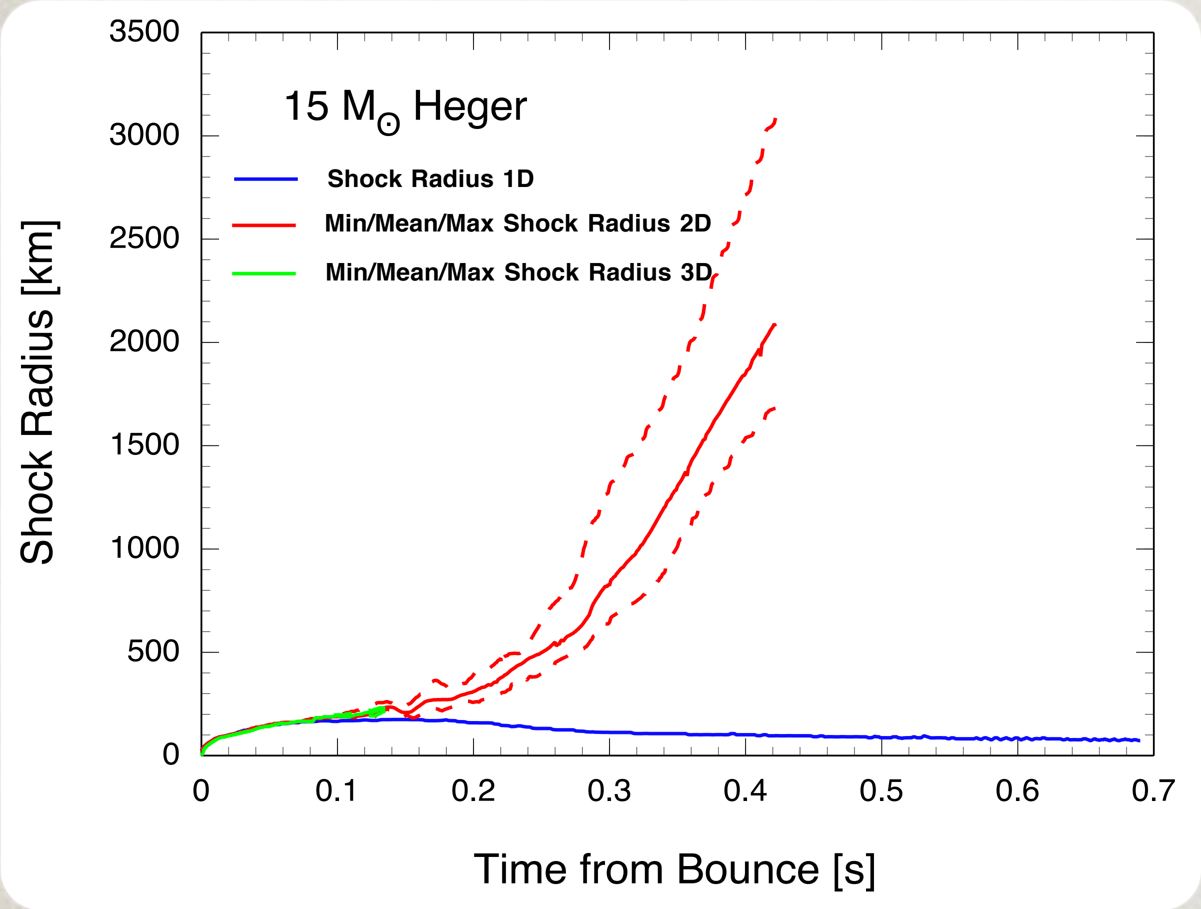

2009 CHIMERA 3D model shows similar behavior to 2D at 150 ms after bounce.

But it was just getting to the interesting point when it was stopped.

Recent self-consistent VERTEX 3D simulations also exhibit similarity between 2D and 3D for the first 200 ms.

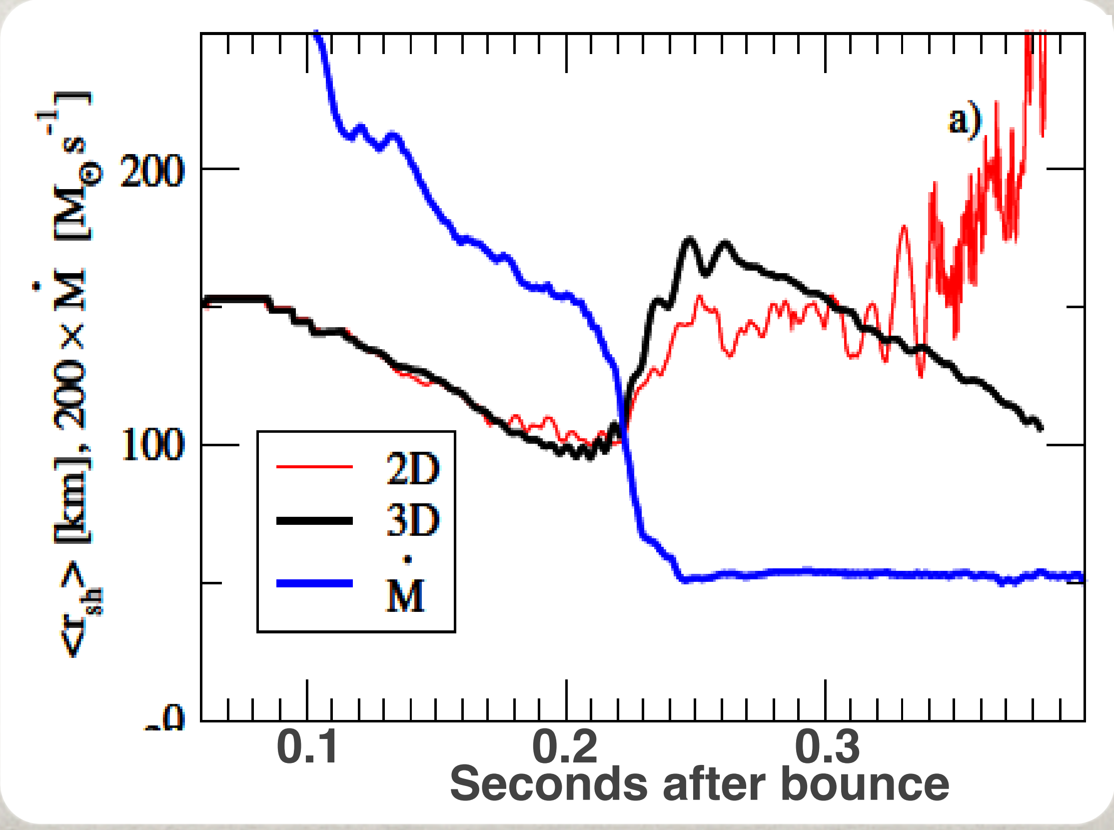

Comparing 2D & 3D

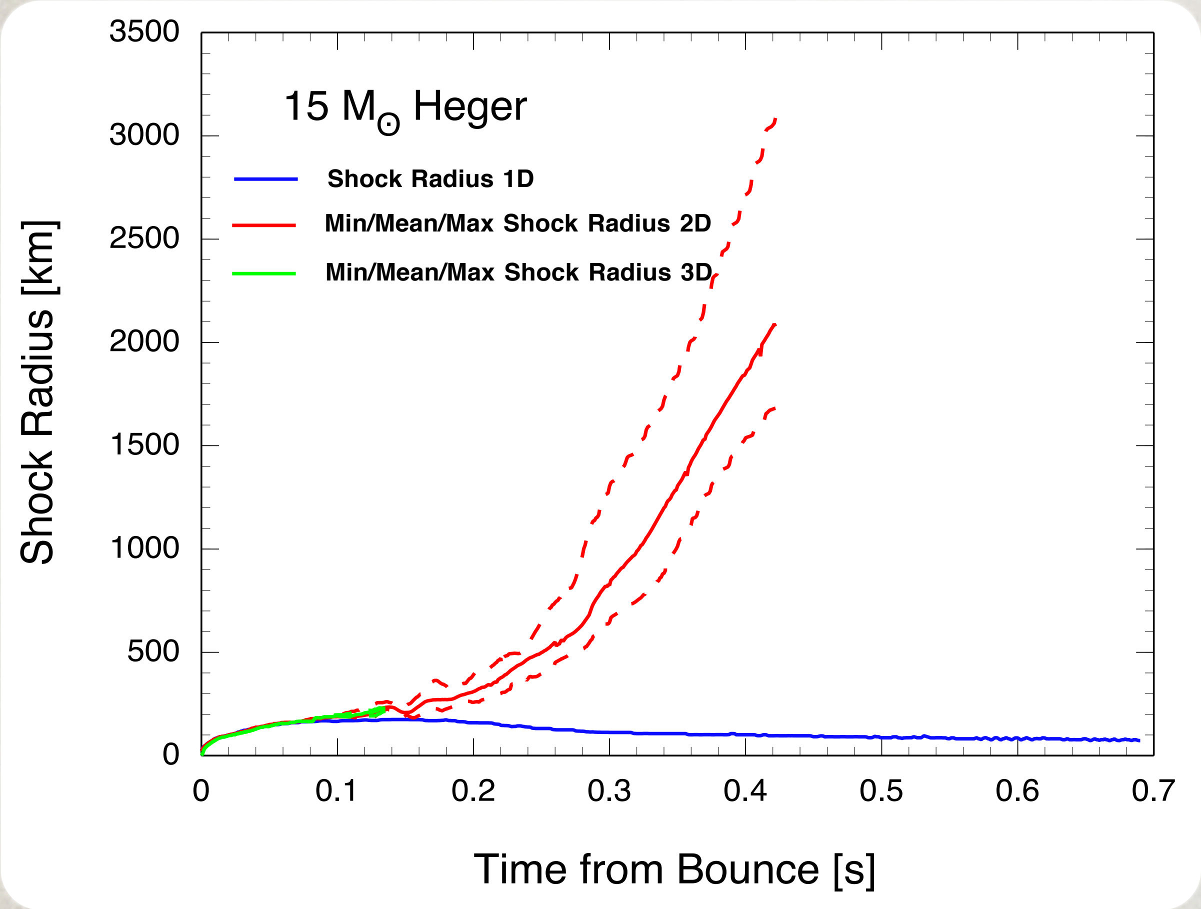

2009 CHIMERA 3D model shows similar behavior to 2D at 150 ms after bounce.

But it was just getting to the interesting point when it was stopped.

Recent self-consistent VERTEX 3D simulations also exhibit similarity between 2D and 3D for the first 200 ms.

After this point 3D seems pessimistic compared to 2D.

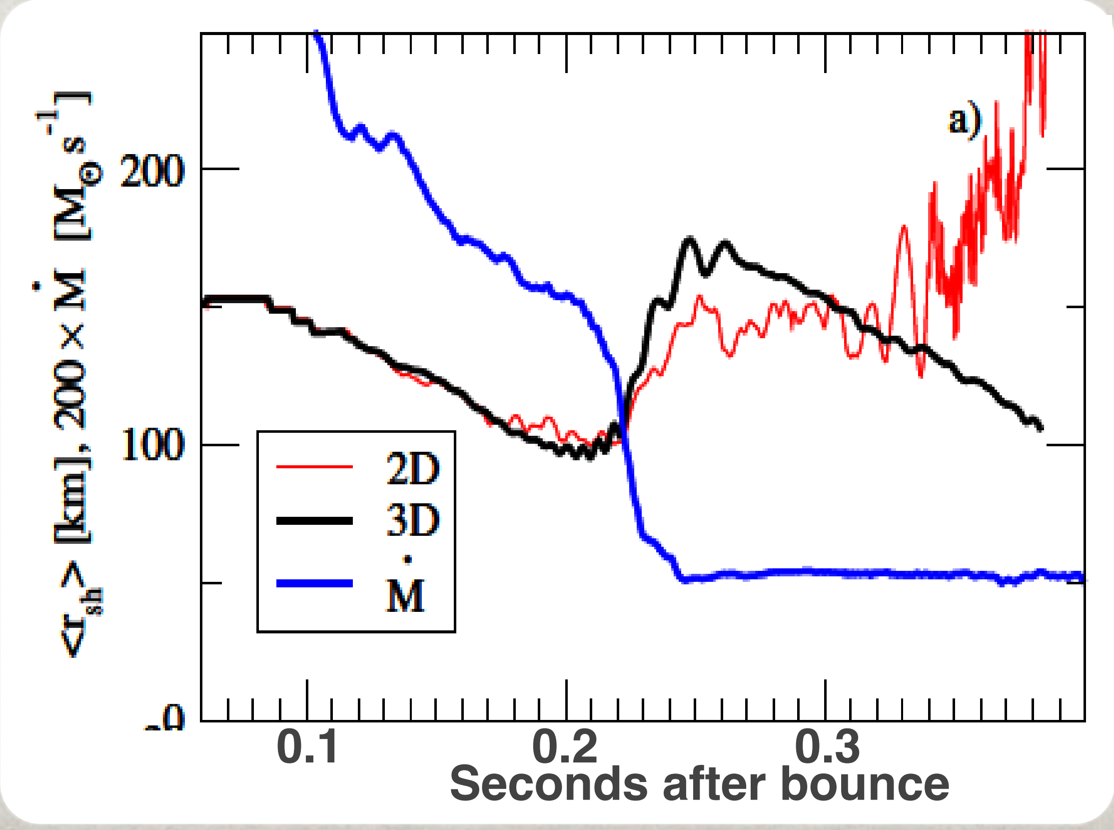

Yin-Yang

To defeat the Courant condition at the pole and allow timesteps similar to the 2D models, we have adopted 2 section overset grid, the Yin-Yang grid of Kageyama & Sato (2004).

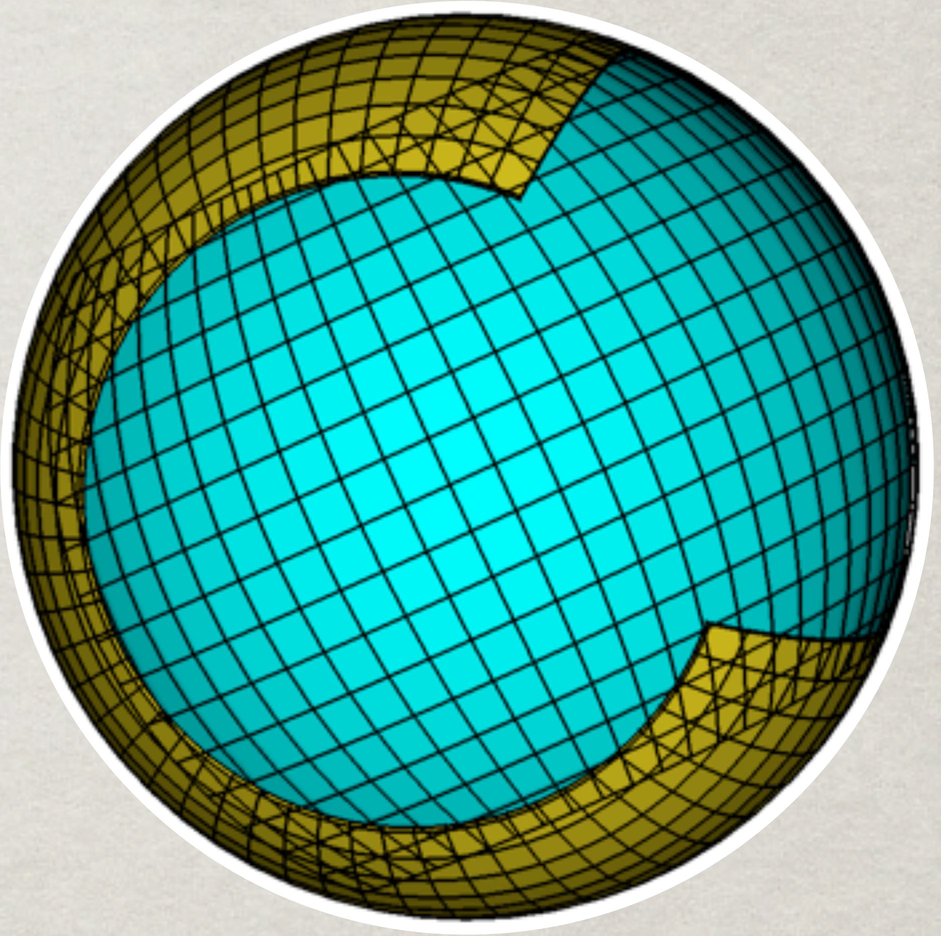

Yin-Yang

To defeat the Courant condition at the pole and allow timesteps similar to the 2D models, we have adopted 2 section overset grid, the Yin-Yang grid of Kageyama & Sato (2004).

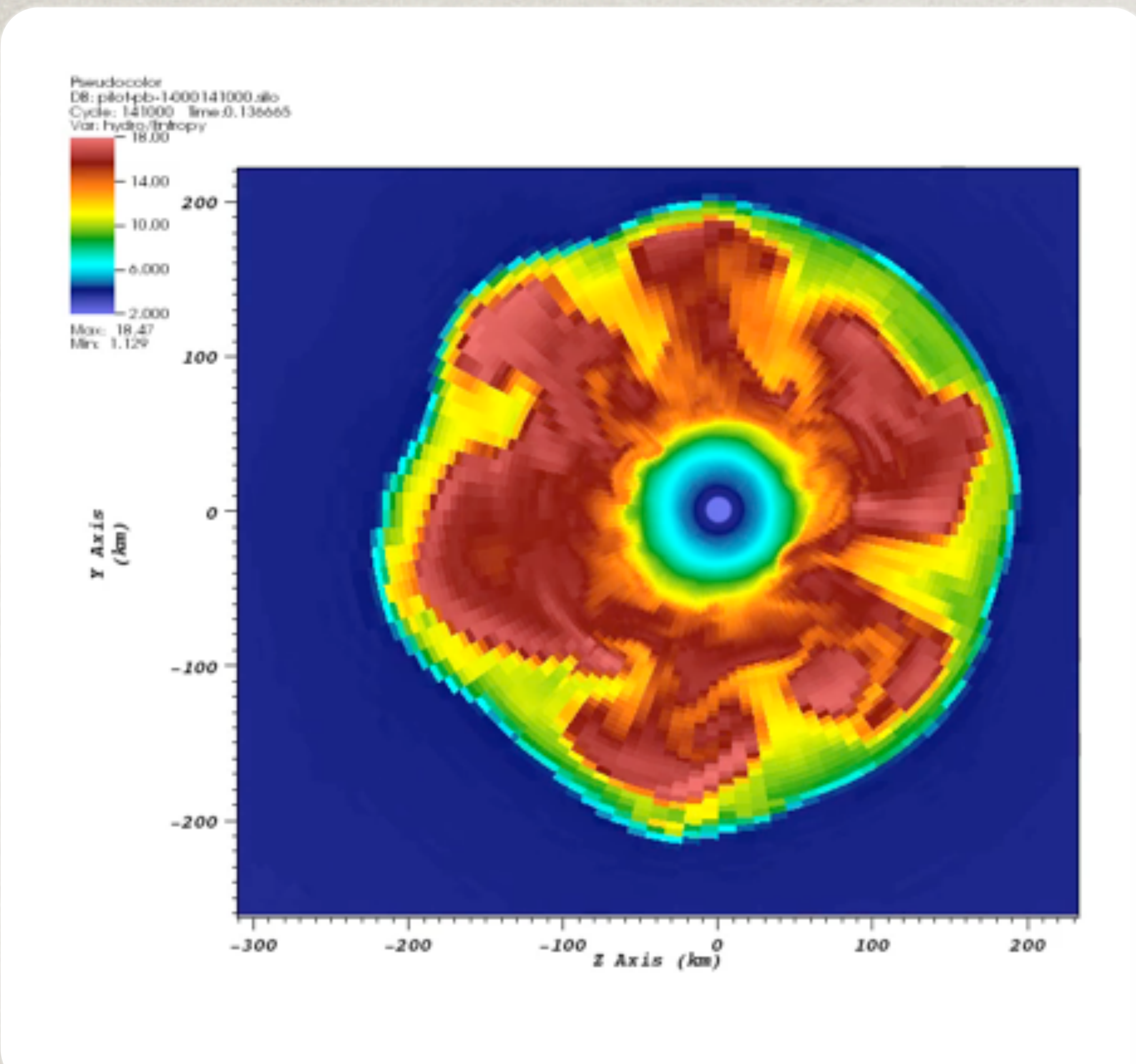

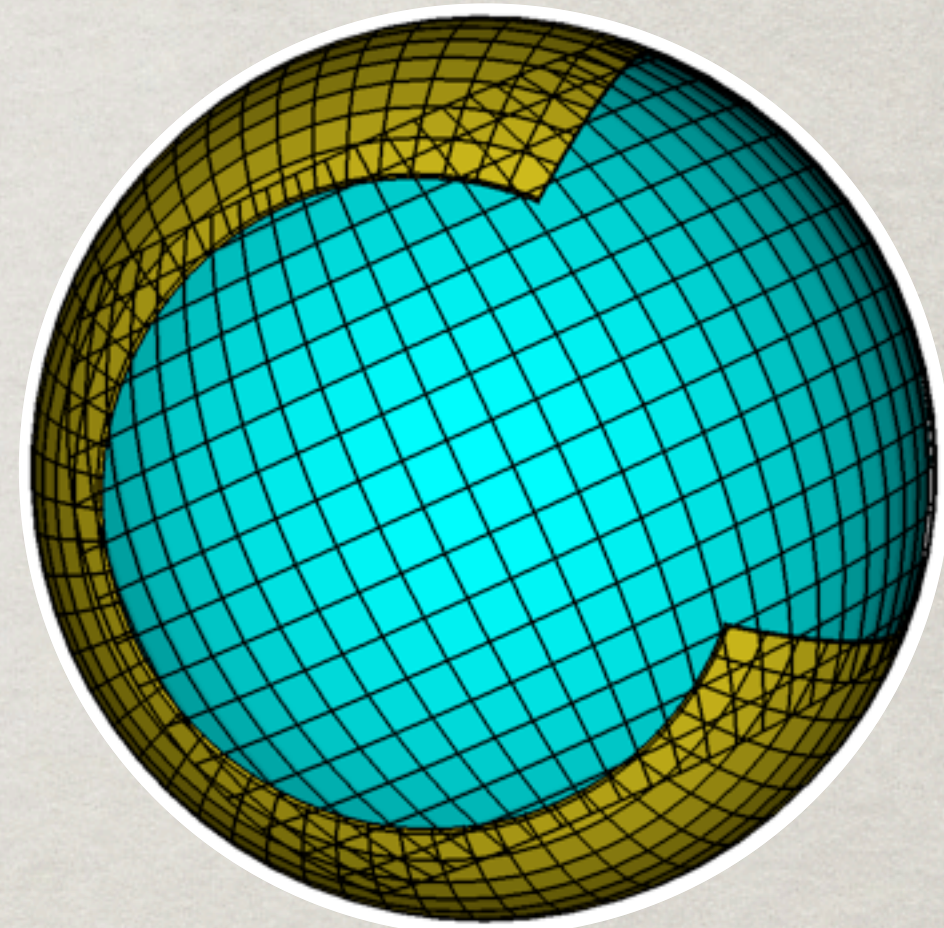

A test run with 480 radial zones & 3.3° resolution in latitude and longitude is underway. Larger model with 1.3° resolution in latitude and longitude should start shortly.

Supernova Nucleosynthesis

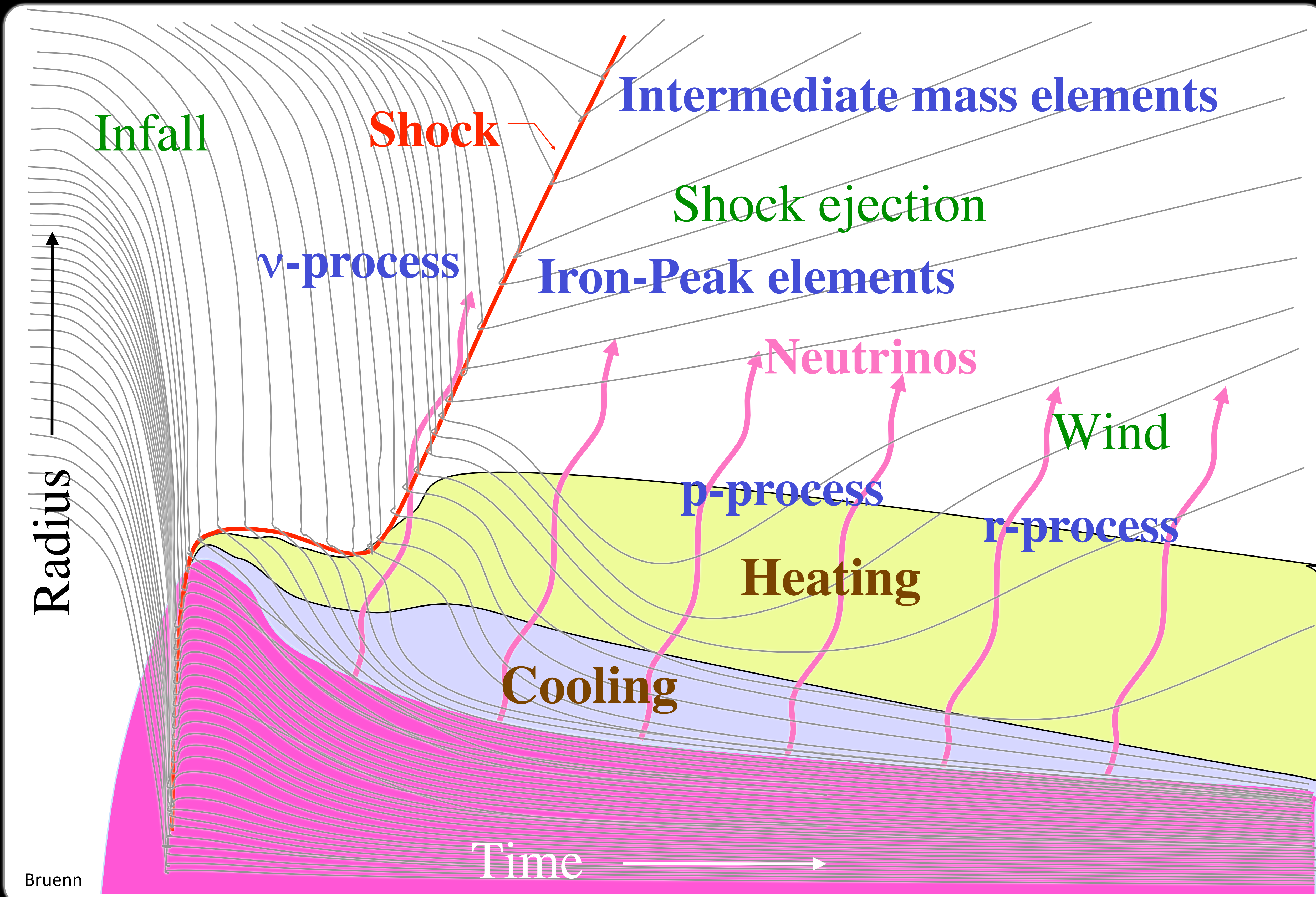

Parameterized Supernovae

Since the mid-1990s, we have had this appreciation that the supernova mechanism is intrinsically multi-dimensional and driven by neutrino-matter interactions.

Parameterized Supernovae

Since the mid-1990s, we have had this appreciation that the supernova mechanism is intrinsically multi-dimensional and driven by neutrino-matter interactions.

However, much of our understanding of the impact of the central CCSN engine neglects these facts.

Parameterized Supernovae

Since the mid-1990s, we have had this appreciation that the supernova mechanism is intrinsically multi-dimensional and driven by neutrino-matter interactions.

However, much of our understanding of the impact of the central CCSN engine neglects these facts.

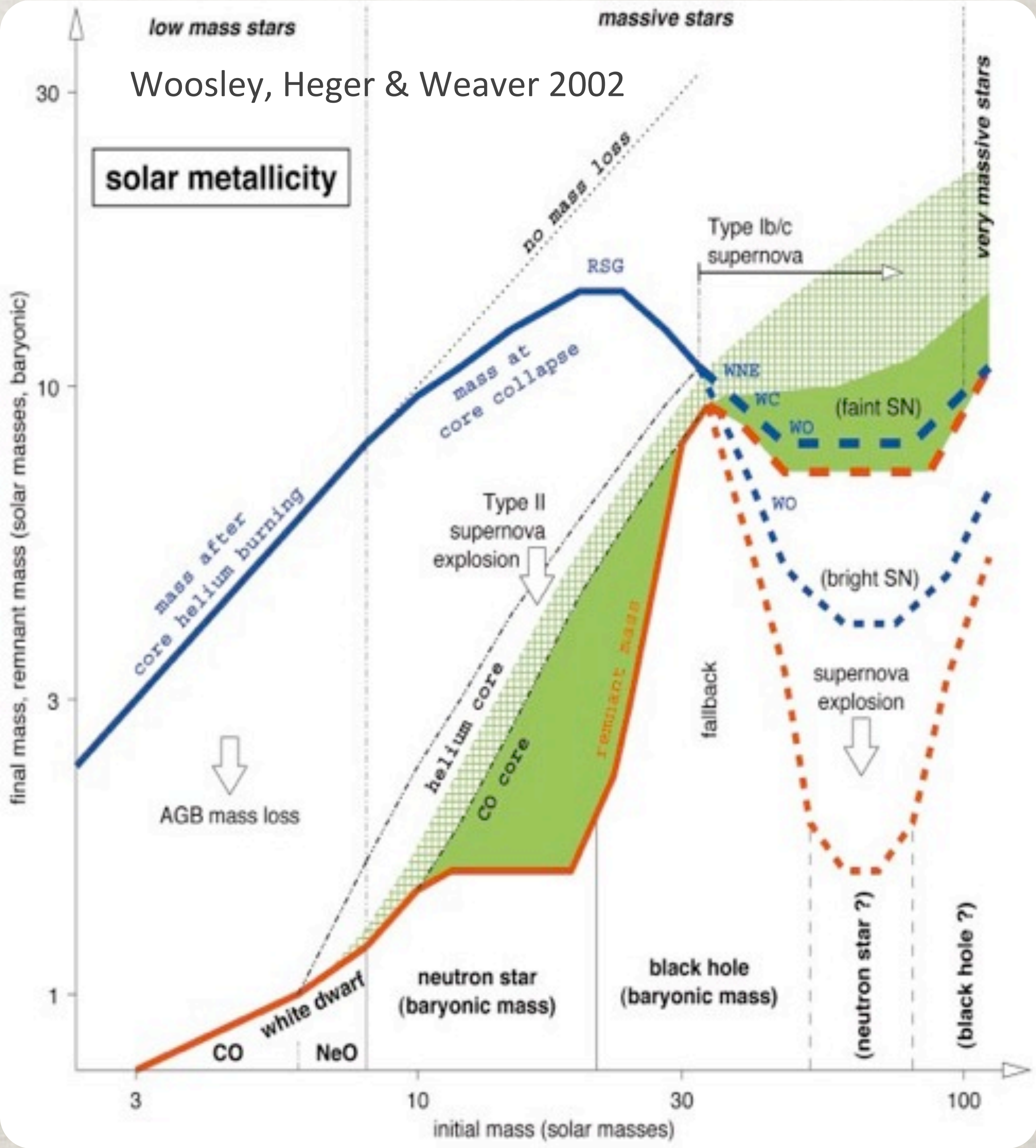

For example, discussions of supernova nucleosynthesis or maximum stellar mass that can successfully produce a supernova, are based on spherically-symmetric (1D) models and a parameterized explosion.

Tuning the Explosion

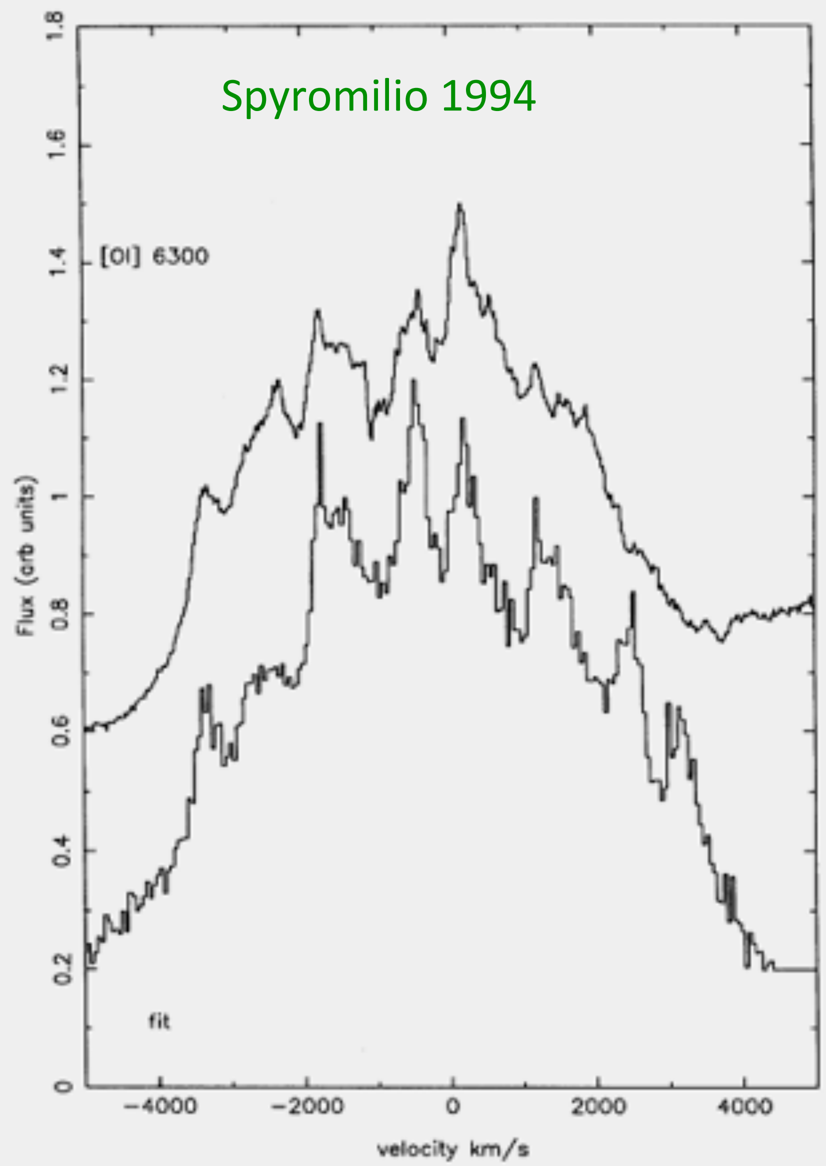

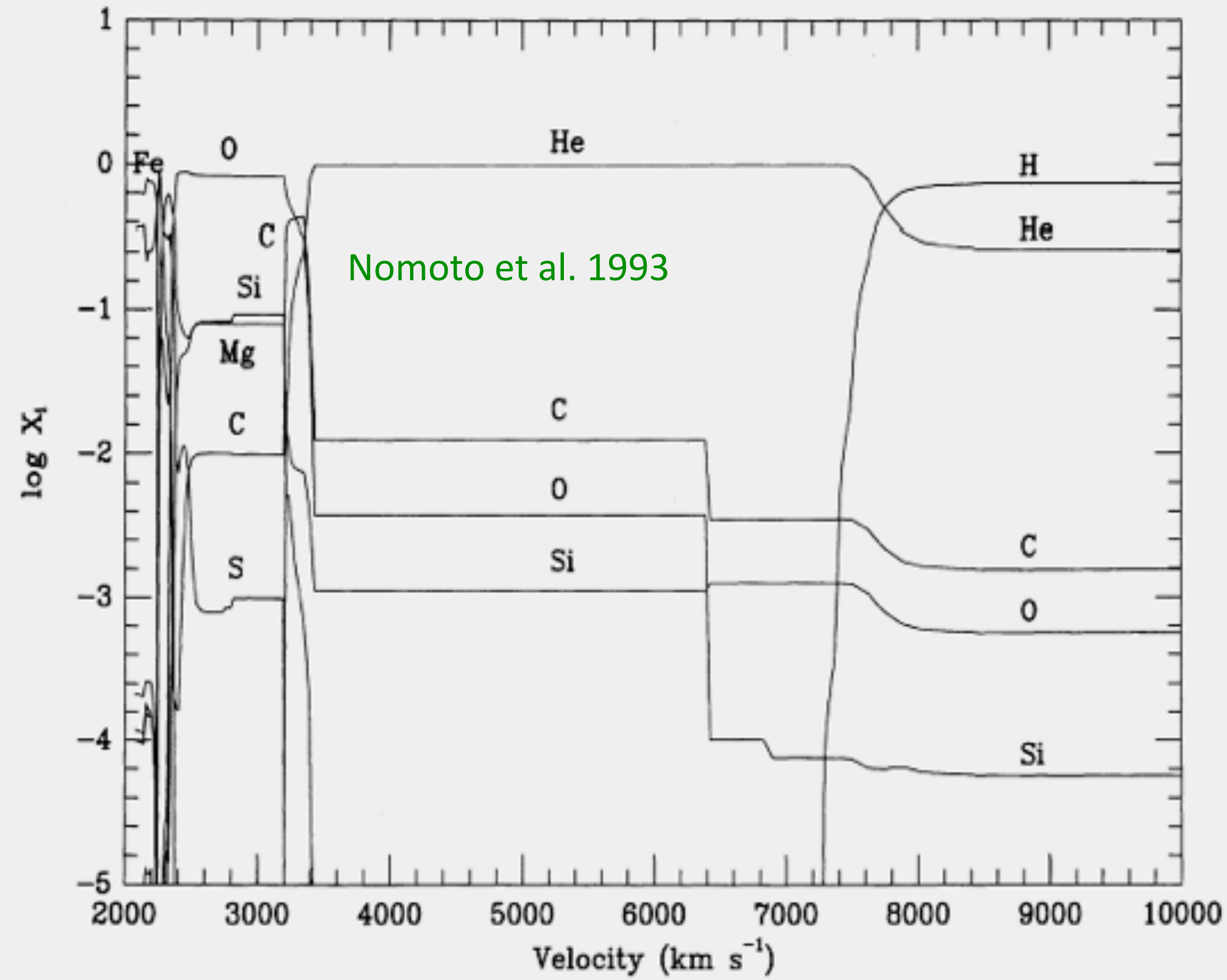

In current nucleosynthesis models, 2 parameters, the Bomb/Piston energy and the mass cut, are constrained by observations of explosion energy and mass of ^{56}Ni ejected.

Tuning the Explosion

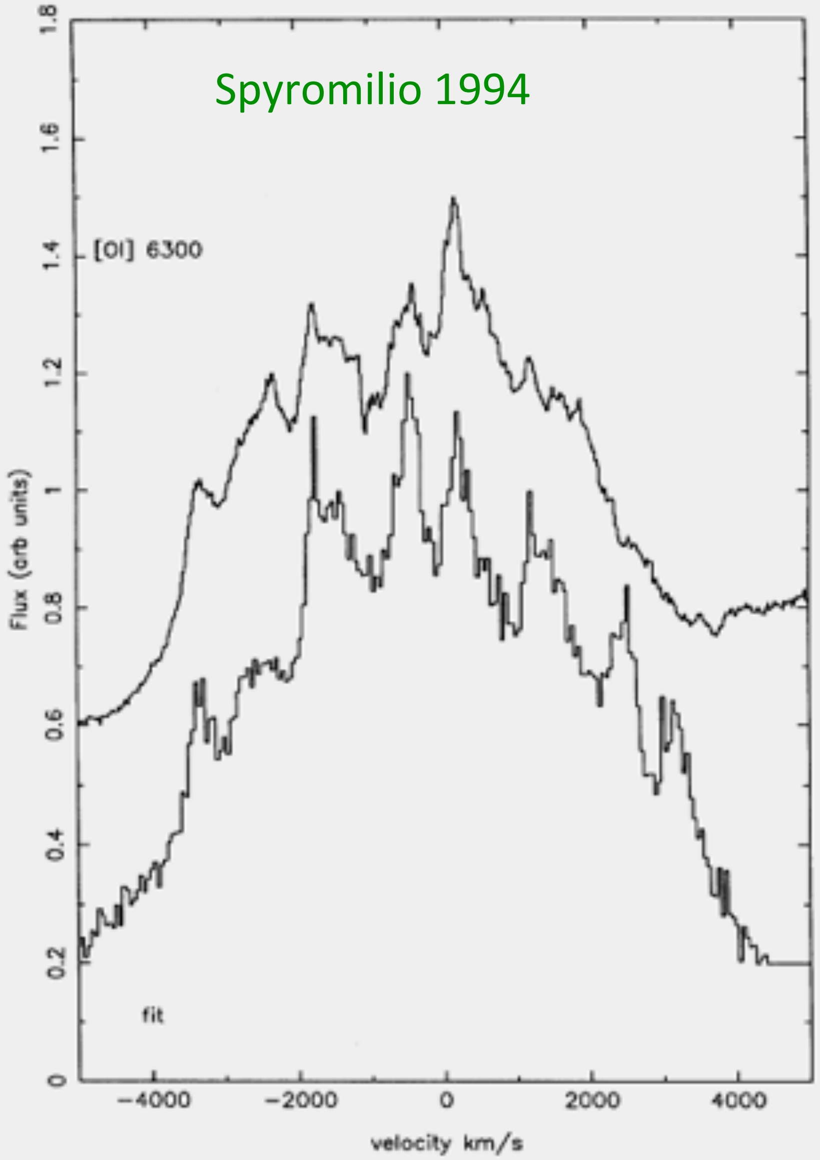

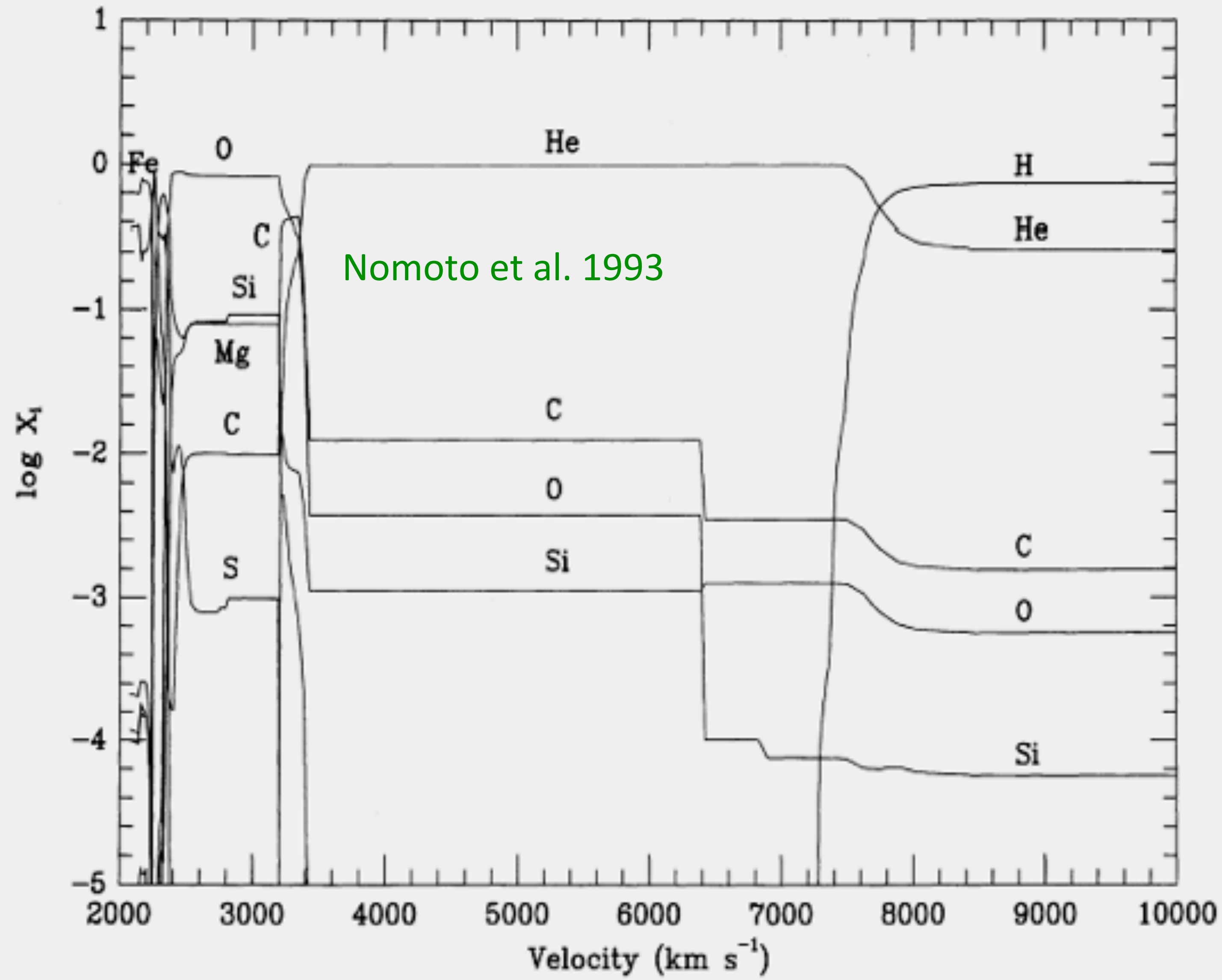

In current nucleosynthesis models, 2 parameters, the Bomb/Piston energy and the mass cut, are constrained by observations of explosion energy and mass of ^{56}Ni ejected.

On the positive side, such models include 100s-1000s of species.

Nucleosynthesis Update

In time, as the accretion onto the PNS $\Rightarrow 0$ and the explosion energy reaches its full value, we will be able to examine the nucleosynthesis of these models.

Models are however limited by the α-network included within CHIMERA (and similar codes).

Nucleosynthesis Update

In time, as the accretion onto the PNS $\Rightarrow 0$ and the explosion energy reaches its full value, we will be able to examine the nucleosynthesis of these models.

Models are however limited by the α-network included within CHIMERA (and similar codes).

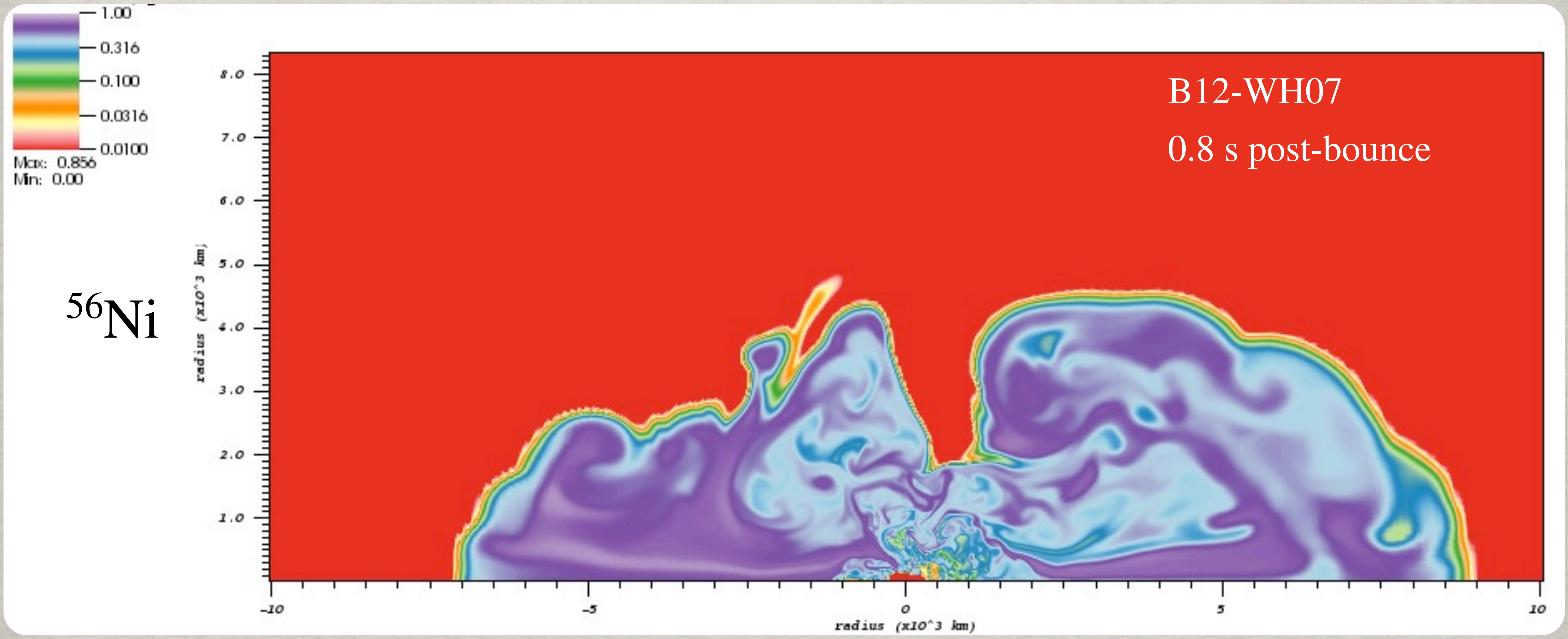

Nucleosynthesis Update

In time, as the accretion onto the PNS $\Rightarrow 0$ and the explosion energy reaches its full value, we will be able to examine the nucleosynthesis of these models.

Models are however limited by the α-network included within CHIMERA (and similar codes).

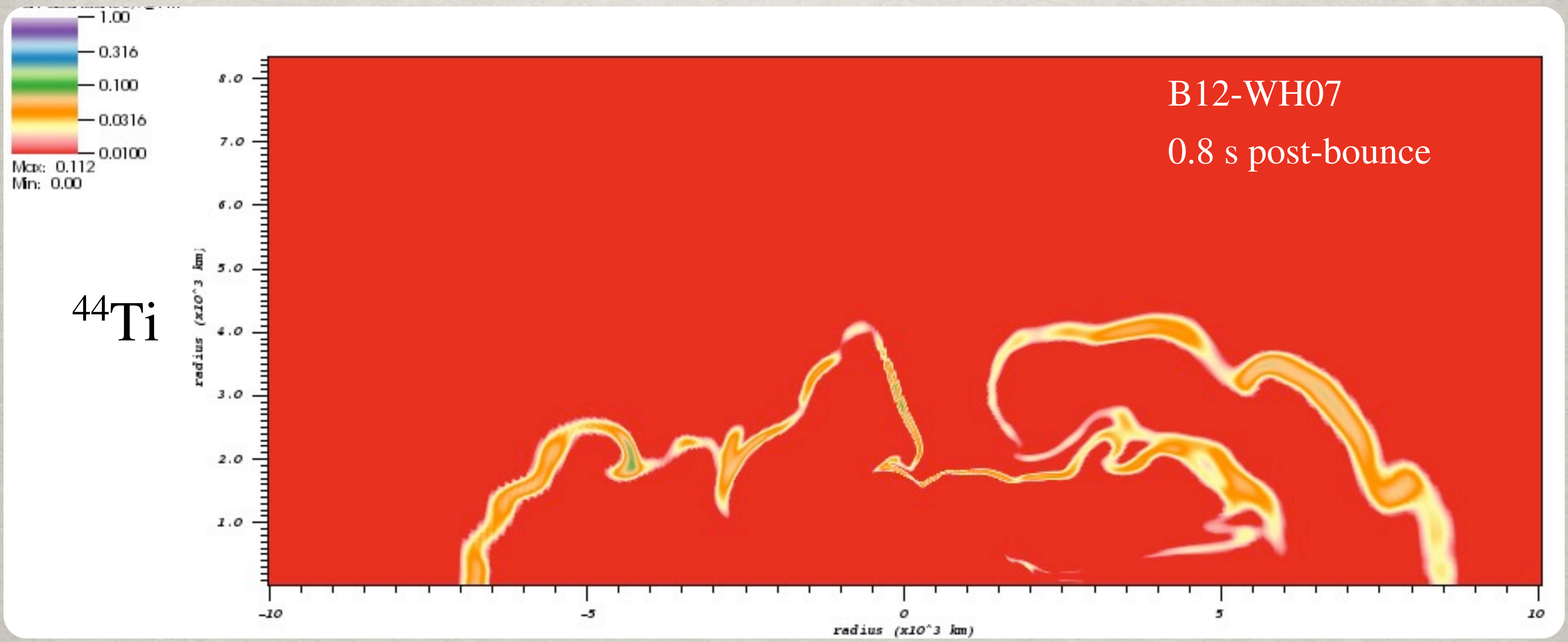

Nucleosynthesis Update

In time, as the accretion onto the PNS $\Rightarrow 0$ and the explosion energy reaches its full value, we will be able to examine the nucleosynthesis of these models.

Models are however limited by the α-network included within CHIMERA (and similar codes).

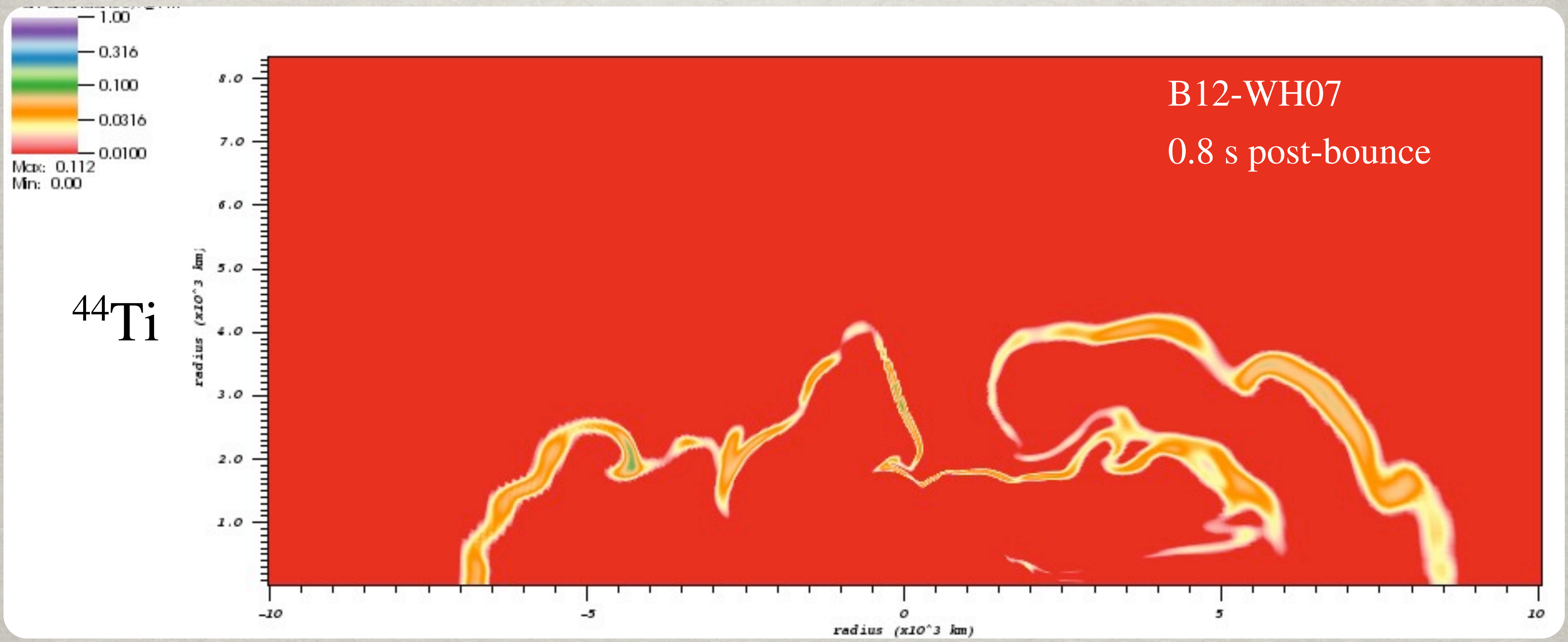

CHIMERA Shock Burning

By 800 ms after bounce, shock burning in the 12 $M_\odot$ model is nearly complete with a shock temperature of ~2 GK.

However, placement of the mass cut continues to evolve, with the fate of ~0.01 $M_\odot$ uncertain.

CHIMERA Shock Burning

By 800 ms after bounce, shock burning in the 12 $M_\odot$ model is nearly complete with a shock temperature of ~2 GK.

However, placement of the mass cut continues to evolve, with the fate of ~0.01 $M_\odot$ uncertain.

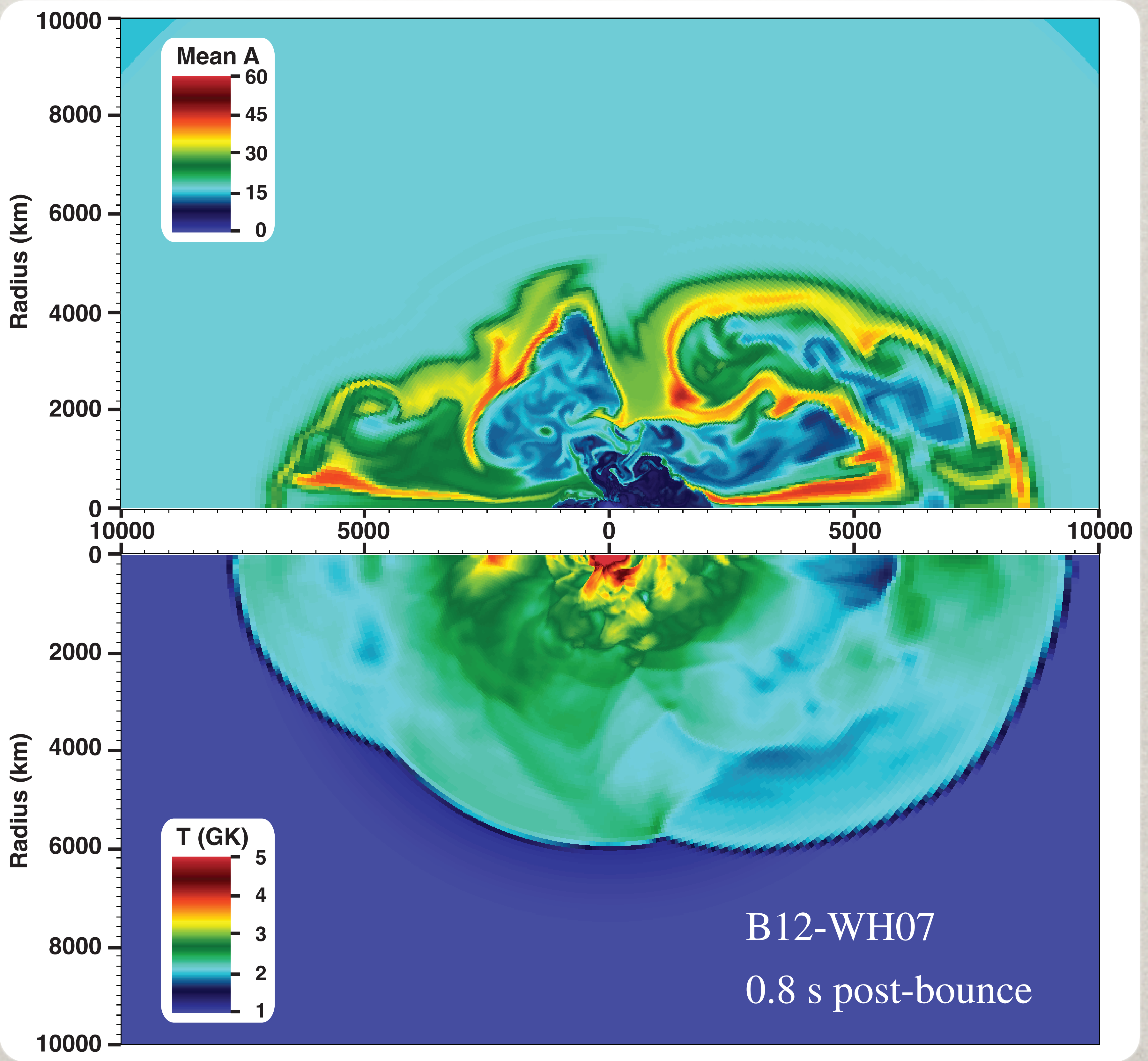

CHIMERA Shock Burning

By 800 ms after bounce, shock burning in the 12 $M_\odot$ model is nearly complete with a shock temperature of ~2 GK.

However, placement of the mass cut continues to evolve, with the fate of ~0.01 $M_\odot$ uncertain.

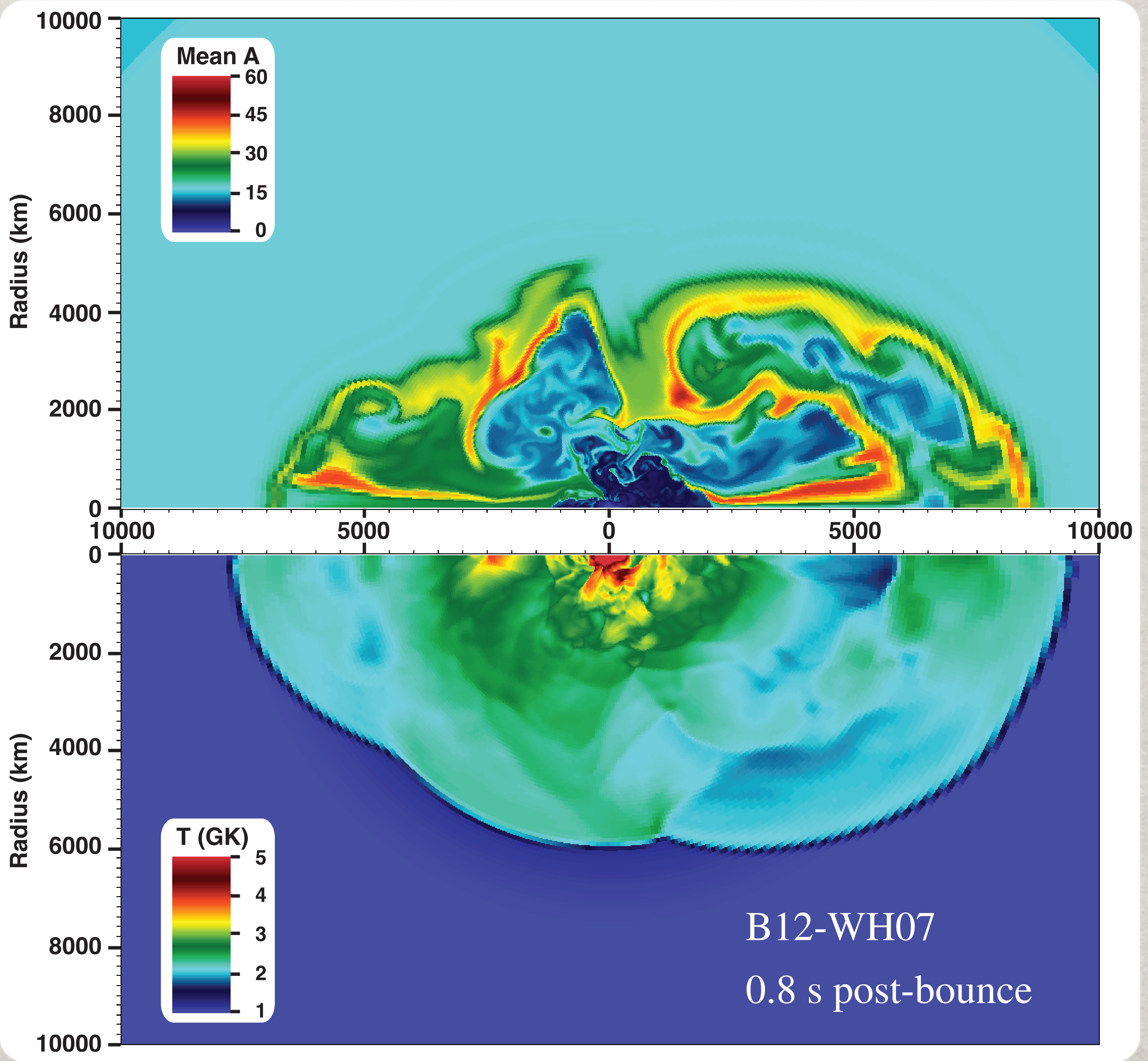

Neutrinos & Nucleosynthesis

Despite the perceived importance of neutrinos to the core collapse mechanism, models of the nucleosynthesis have largely ignored this important effect.

Neutrinos & Nucleosynthesis

Despite the perceived importance of neutrinos to the core collapse mechanism, models of the nucleosynthesis have largely ignored this important effect.

Nucleosynthesis from ν-powered supernova models shows several notable improvements.

Neutrinos & Nucleosynthesis

Despite the perceived importance of neutrinos to the core collapse mechanism, models of the nucleosynthesis have largely ignored this important effect.

Nucleosynthesis from ν-powered supernova models shows several notable improvements.

1. Over production of neutron-rich iron and nickel reduced.

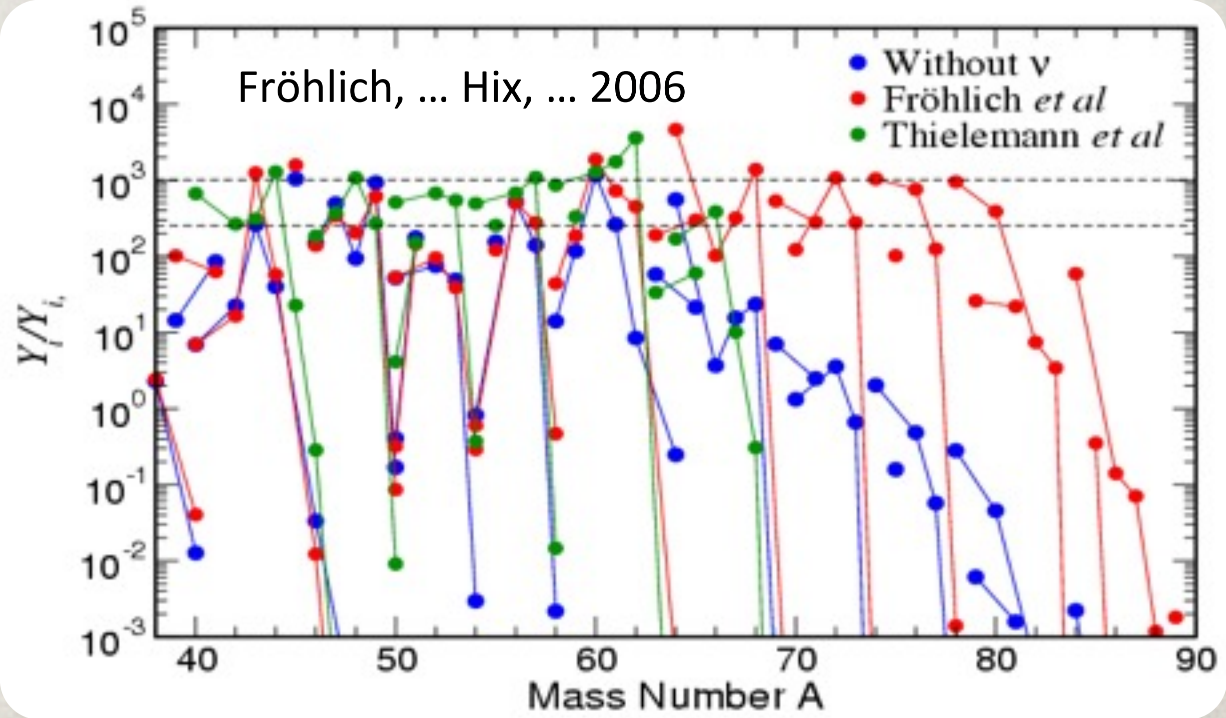

Neutrinos & Nucleosynthesis

Despite the perceived importance of neutrinos to the core collapse mechanism, models of the nucleosynthesis have largely ignored this important effect.

Nucleosynthesis from ν-powered supernova models shows several notable improvements.

1. Over production of neutron-rich iron and nickel reduced.
2. Elemental abundances of Sc, Cu & Zn closer to those observed in metal-poor stars.

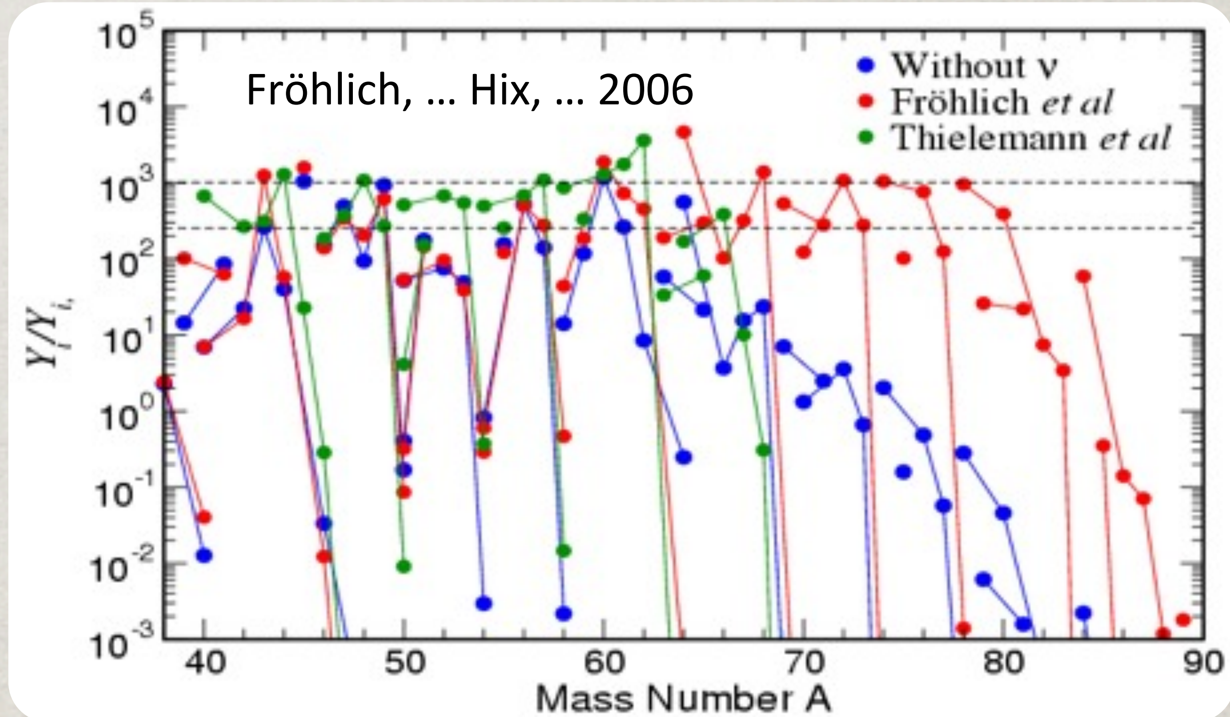

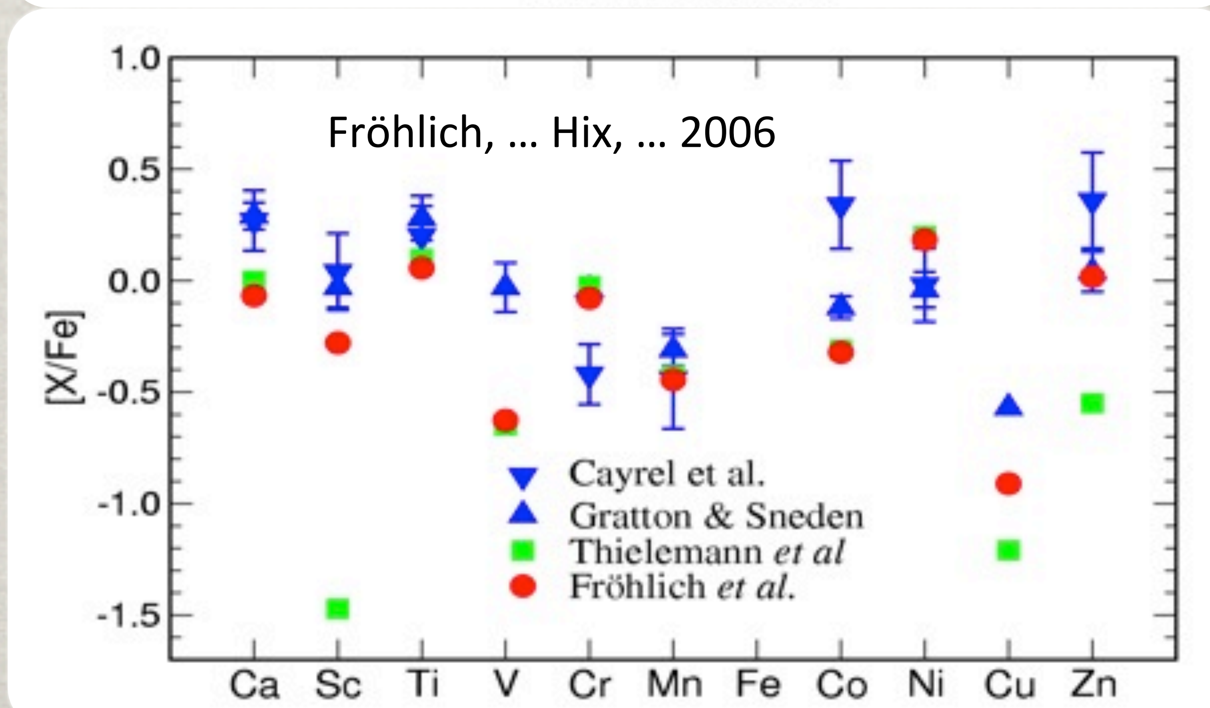

Neutrinos & Nucleosynthesis

Despite the perceived importance of neutrinos to the core collapse mechanism, models of the nucleosynthesis have largely ignored this important effect.

Nucleosynthesis from ν-powered supernova models shows several notable improvements.

1. Over production of neutron-rich iron and nickel reduced.
2. Elemental abundances of Sc, Cu & Zn closer to those observed in metal-poor stars.
3. Potential source of light p-process nuclei (^{76}Se, ^{80}Kr, ^{84}Sr, ^{92,94}Mo, ^{96,98}Ru).

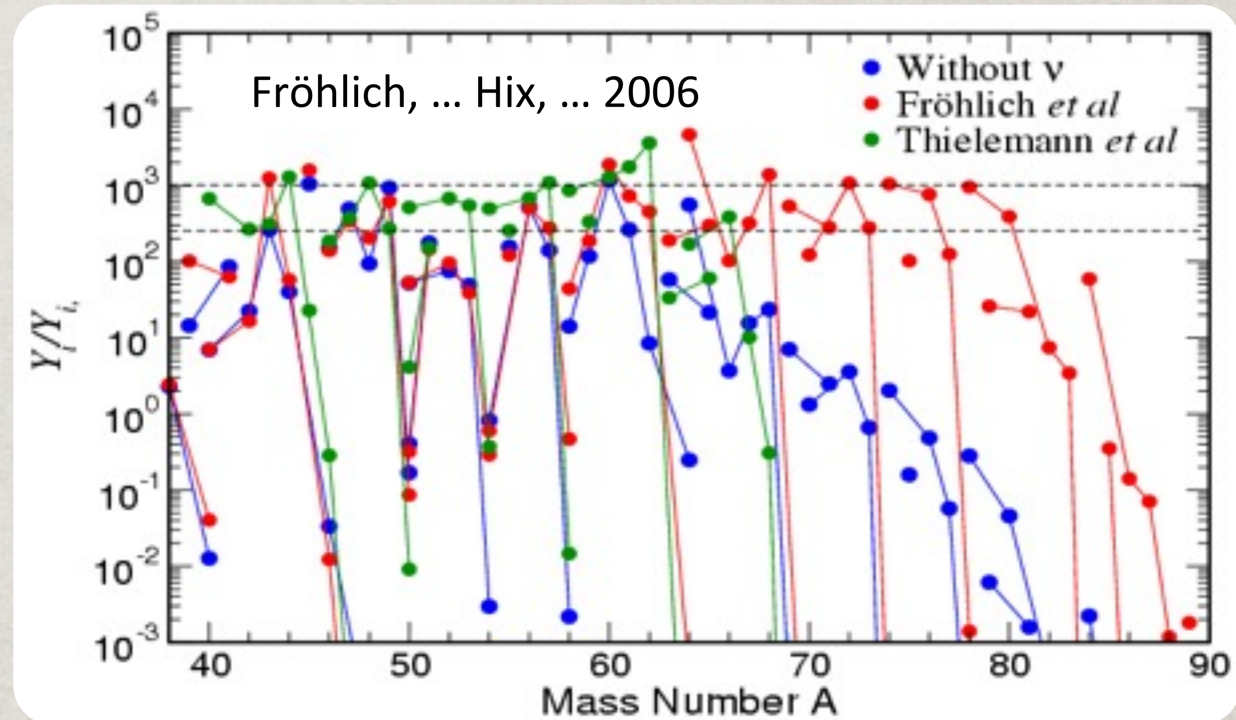

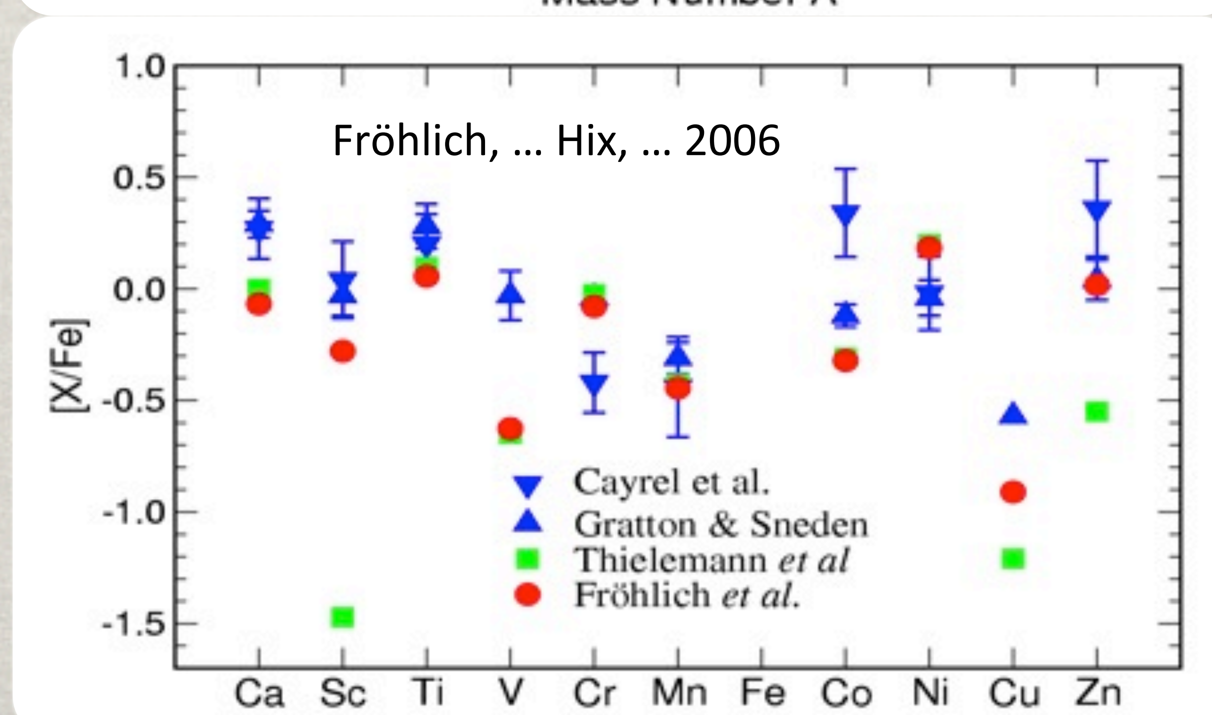

Putting the ν in νp

The *νp*-process occurs because the supernova ejects proton-rich ($Y_e > 0.5$) gas at high temperature (~10 GK), composed of free neutrons and protons.

PUTTING THE ν IN νP

The *νp*-process occurs because the supernova ejects proton-rich ($Y_e > 0.5$) gas at high temperature (~10 GK), composed of free neutrons and protons.

Cooling produces a p-rich and α-rich freeze-out. Once temperature drops below 3 GK, free protons can capture on iron-peak species.

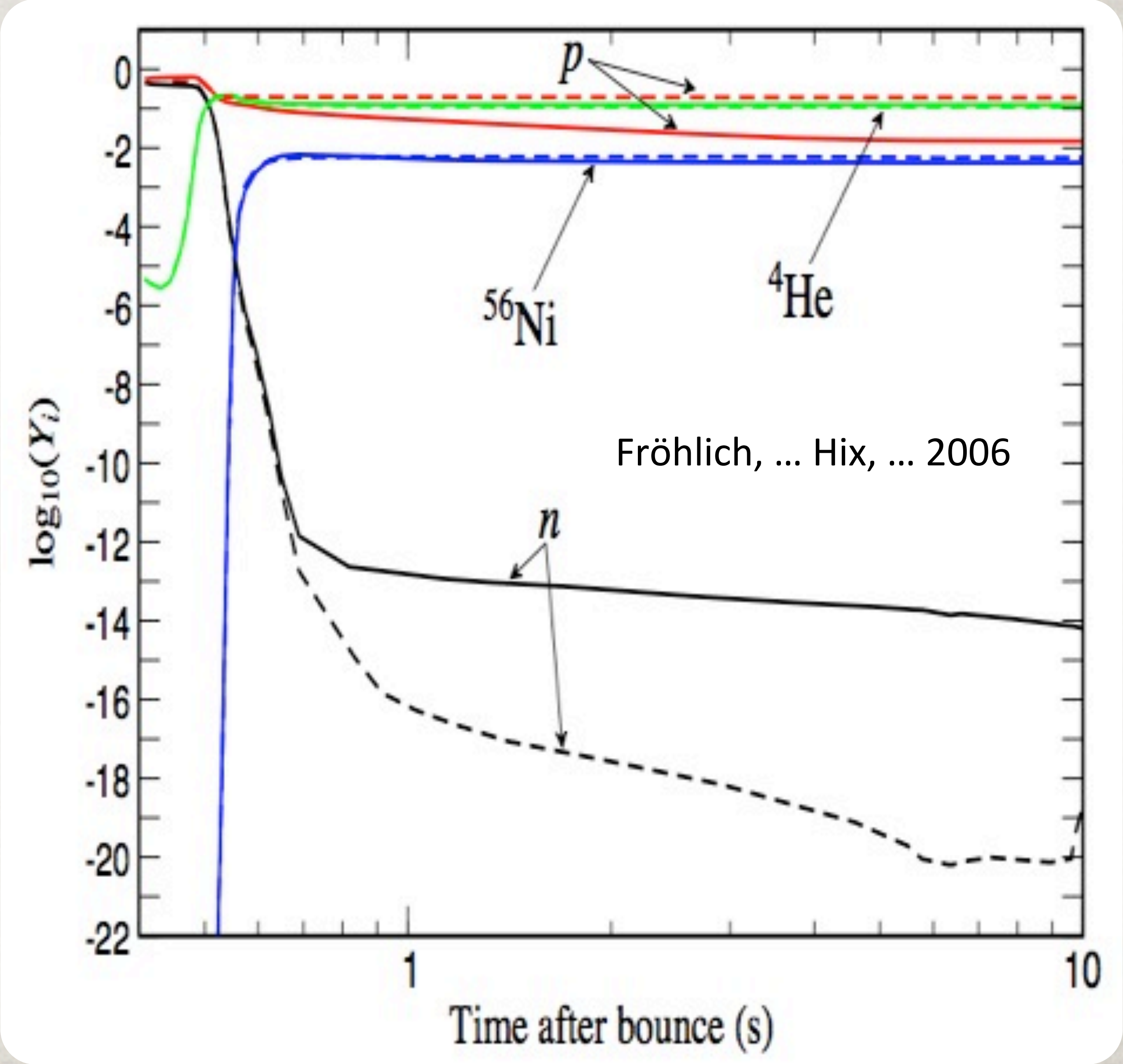

Putting the ν in νp

The νp-process occurs because the supernova ejects proton-rich ($Y_e > 0.5$) gas at high temperature (~10 GK), composed of free neutrons and protons.

Cooling produces a p-rich and α-rich freeze-out. Once temperature drops below 3 GK, free protons can capture on iron-peak species.

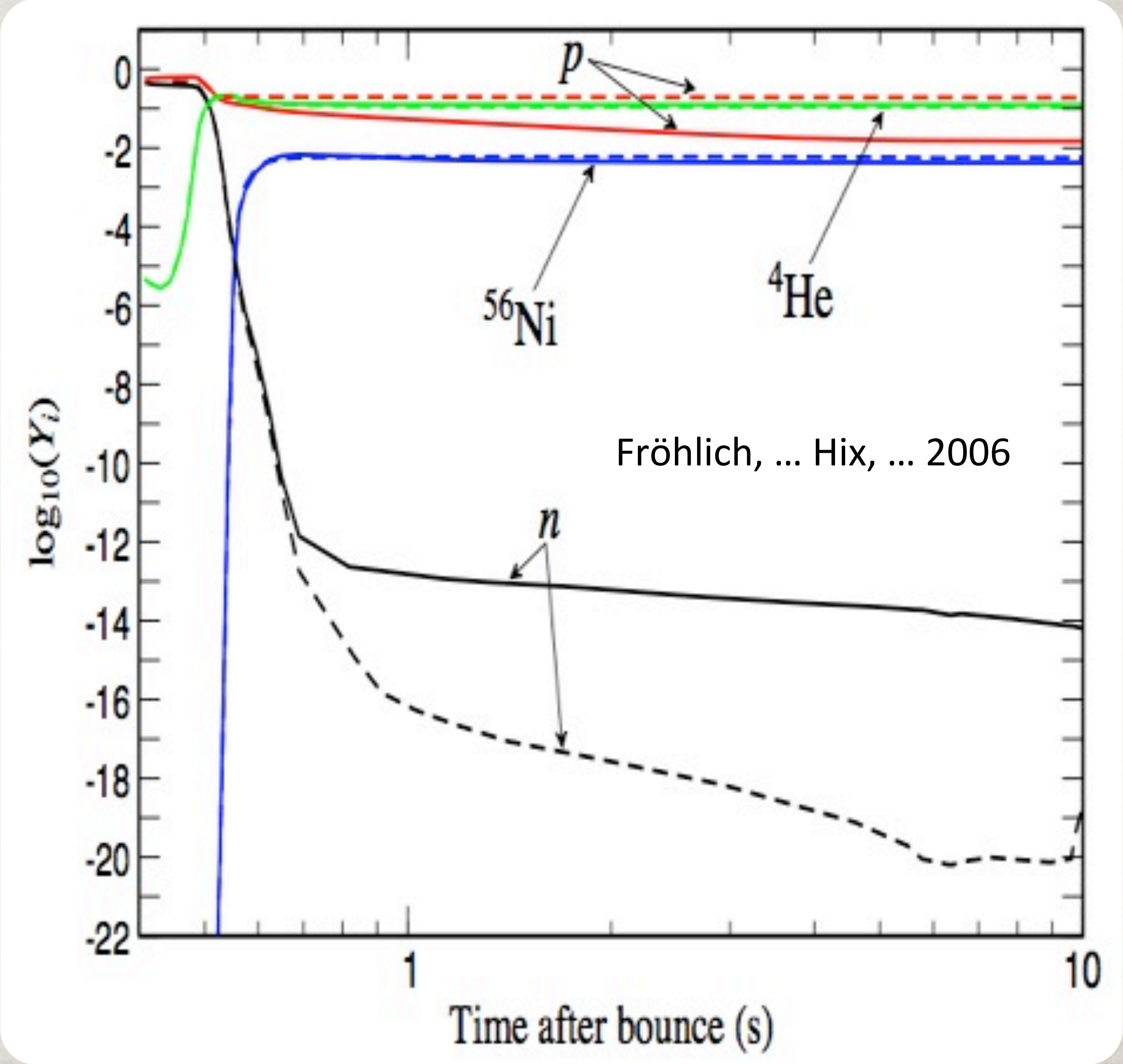

Slow β decays (e.g. ^{64}Ge, $\tau_\beta = 64$ s) would stop this process but (n,p) and (n,γ) reactions effectively "accelerate" β decays.

Putting the ν in νp

The νp-process occurs because the supernova ejects proton-rich ($Y_e > 0.5$) gas at high temperature (~10 GK), composed of free neutrons and protons.

Cooling produces a p-rich and α-rich freeze-out. Once temperature drops below 3 GK, free protons can capture on iron-peak species.

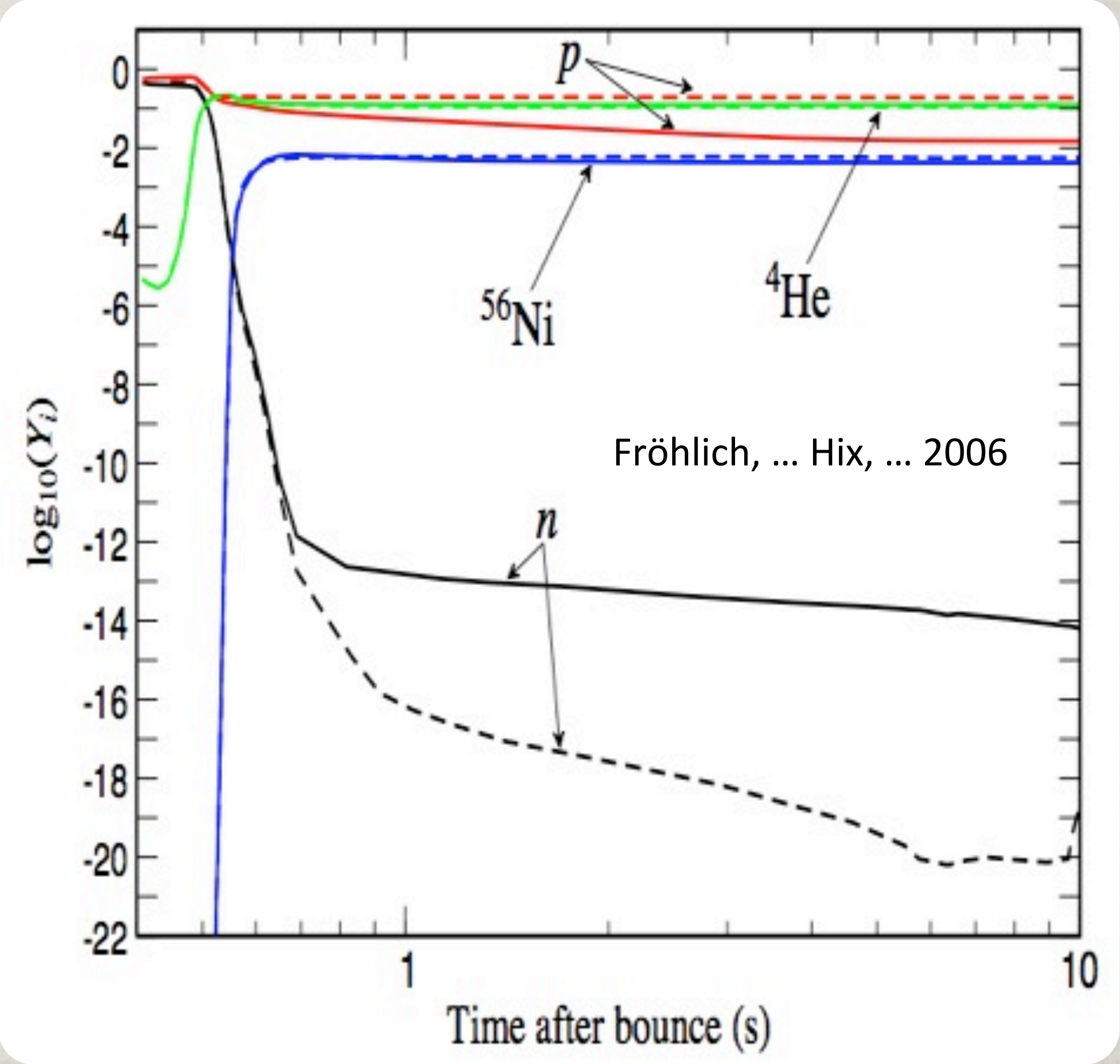

Slow β decays (e.g. ^{64}Ge, $\tau_\beta = 64$ s) would stop this process but (n,p) and (n,γ) reactions effectively "accelerate" β decays.

The needed neutrons are generated from protons converted via anti-neutrino capture.

Multi-D νp-process?

The open question is will the results of self-consistent multi-dimensional simulations match those of the parameterized neutrino-driven models that discovered the νp-process?

Multi-D νp-process?

The open question is will the results of self-consistent multi-dimensional simulations match those of the parameterized neutrino-driven models that discovered the νp-process?

Our final answer must await the completion of our models, but we can get an early indication by examining the neutronization.

There is a clear trend in the Y_e distribution, with more massive models having more proton-rich material.

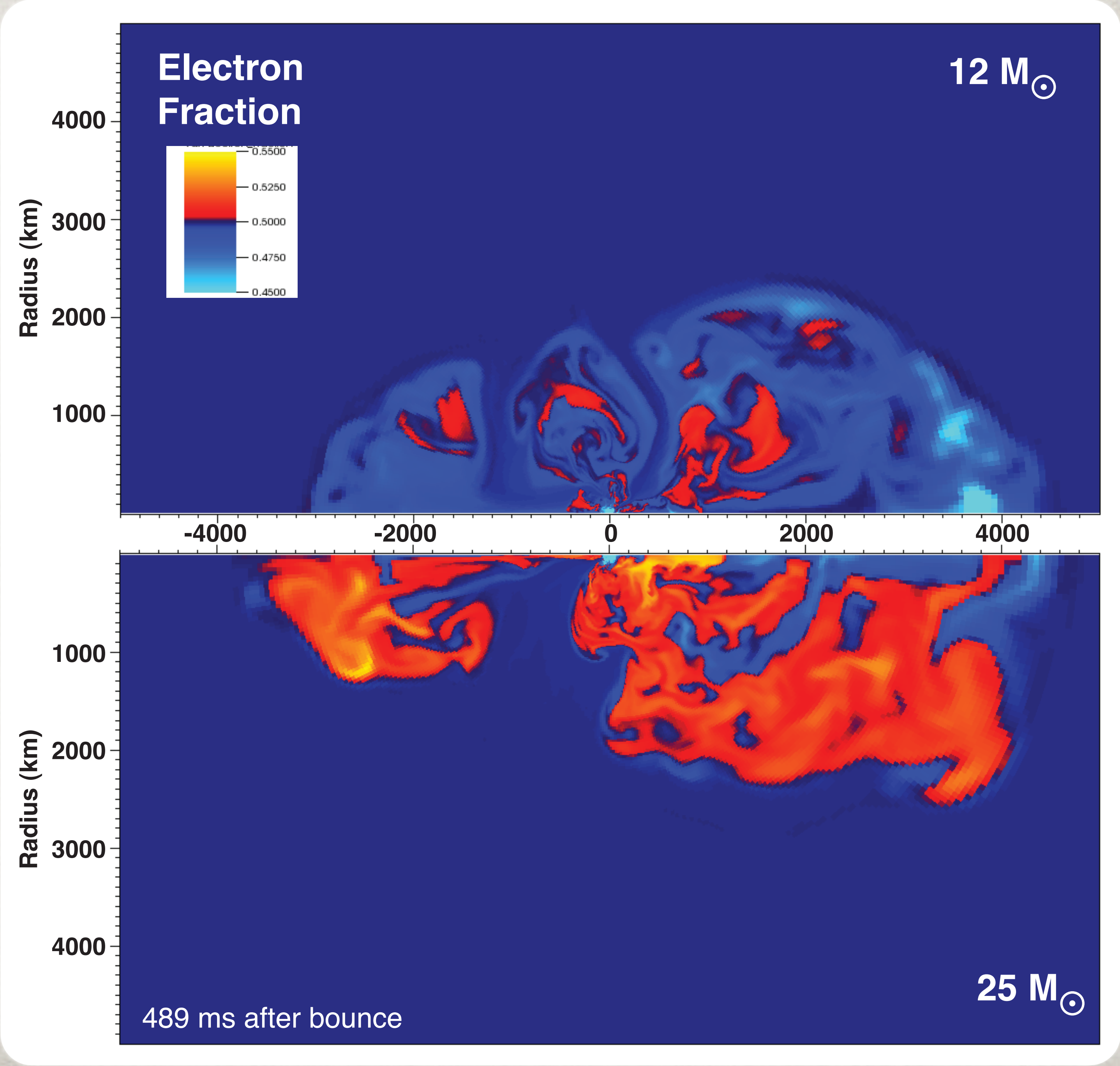

Tracing the Mass Cut

Tracing the Mass Cut

Post-processing of tracer particles will allow nucleosynthesis predictions that capture the multi-D effects beyond the α-network.

Tracing the Mass Cut

Post-processing of tracer particles will allow nucleosynthesis predictions that capture the multi-D effects beyond the α-network.

However the coupling (energy generation, neutronization, mixing, etc.) between the nucleosynthesis and the multi-D effects is lost and unrecoverable.

Tracing the Mass Cut

Post-processing of tracer particles will allow nucleosynthesis predictions that capture the multi-D effects beyond the α-network.

However the coupling (energy generation, neutronization, mixing, etc.) between the nucleosynthesis and the multi-D effects is lost and unrecoverable.

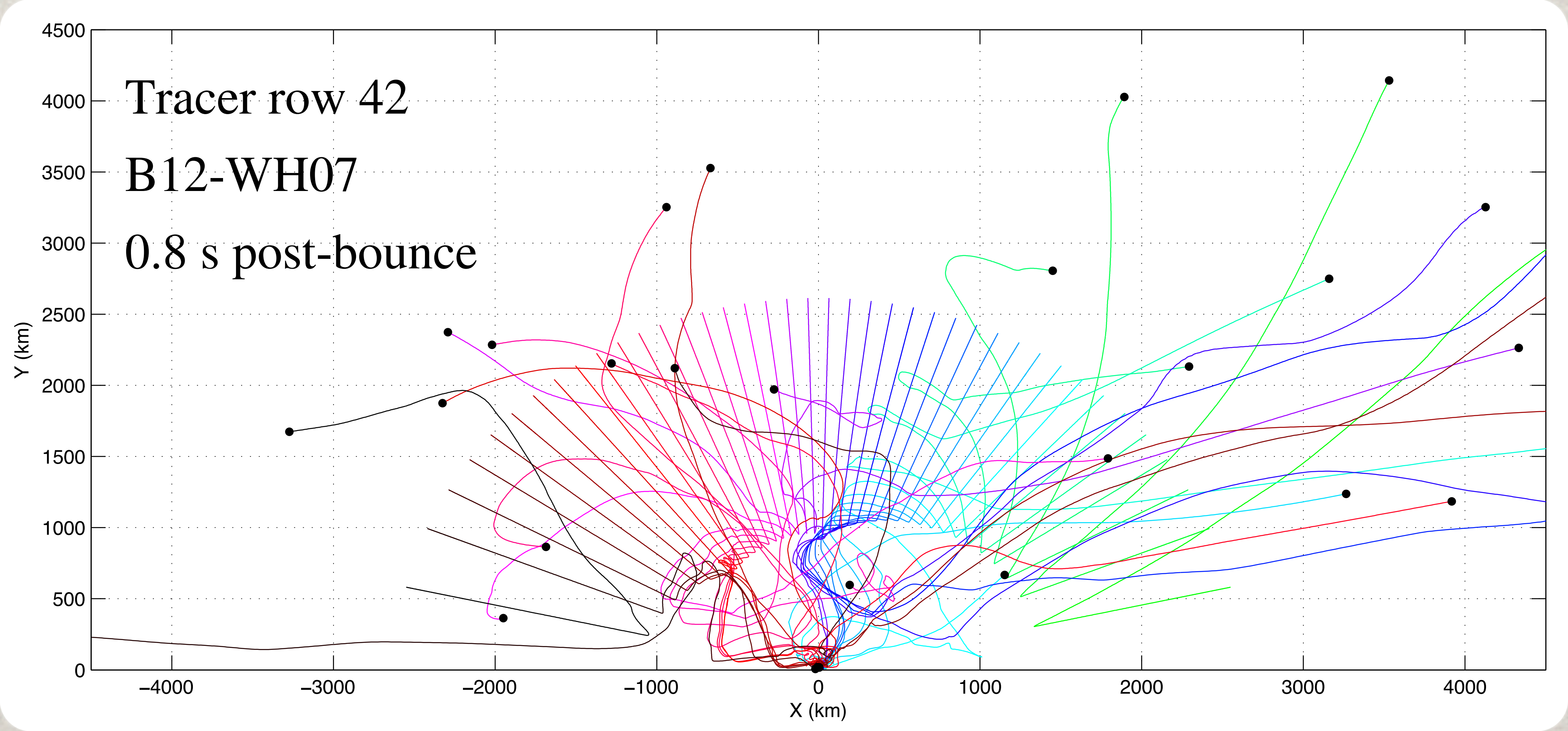

They reveal the complexity of defining the mass cut.

Tracing the Mass Cut

Post-processing of tracer particles will allow nucleosynthesis predictions that capture the multi-D effects beyond the α-network.

However the coupling (energy generation, neutronization, mixing, etc.) between the nucleosynthesis and the multi-D effects is lost and unrecoverable.

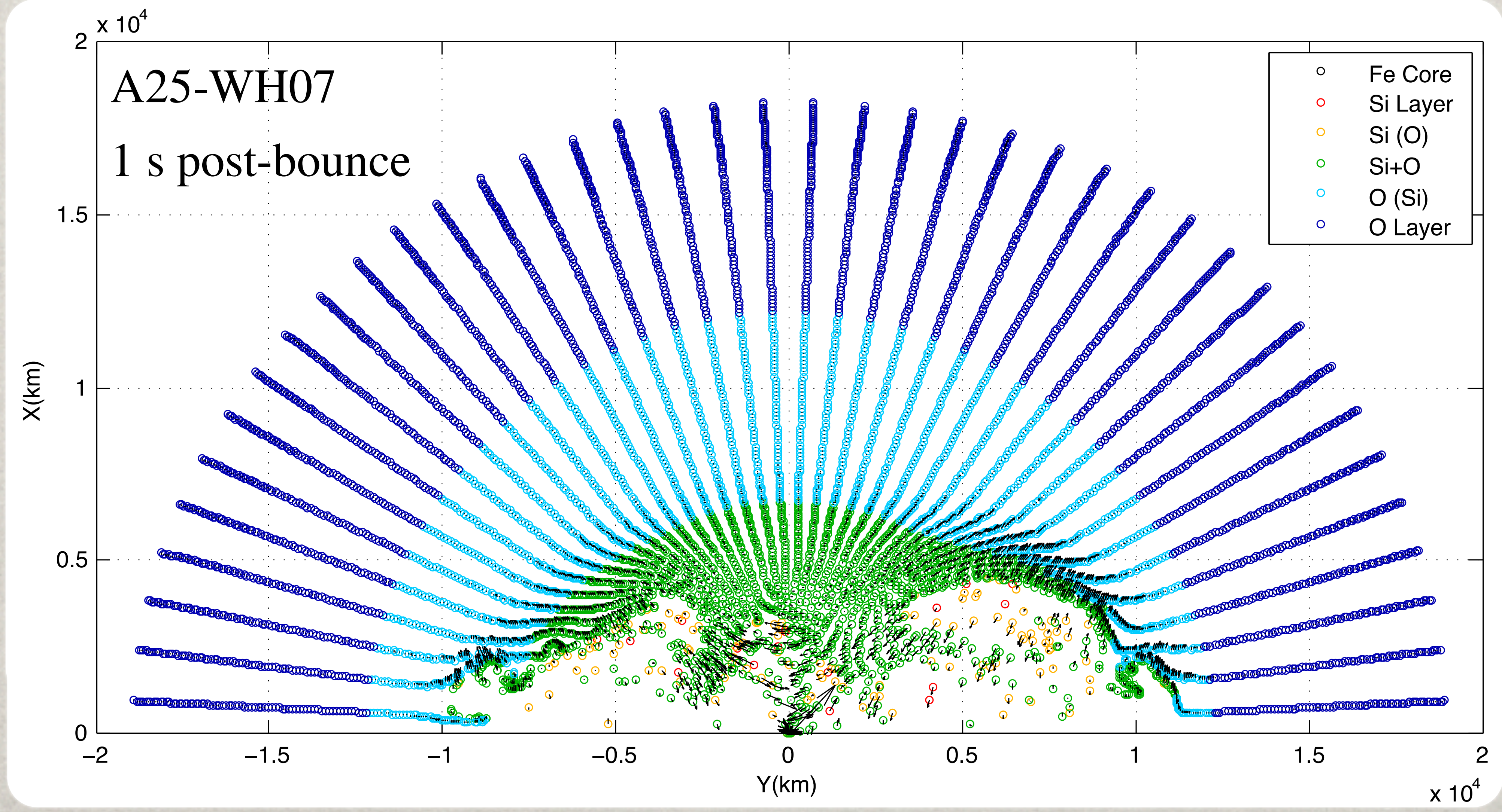

νp-PROCESS

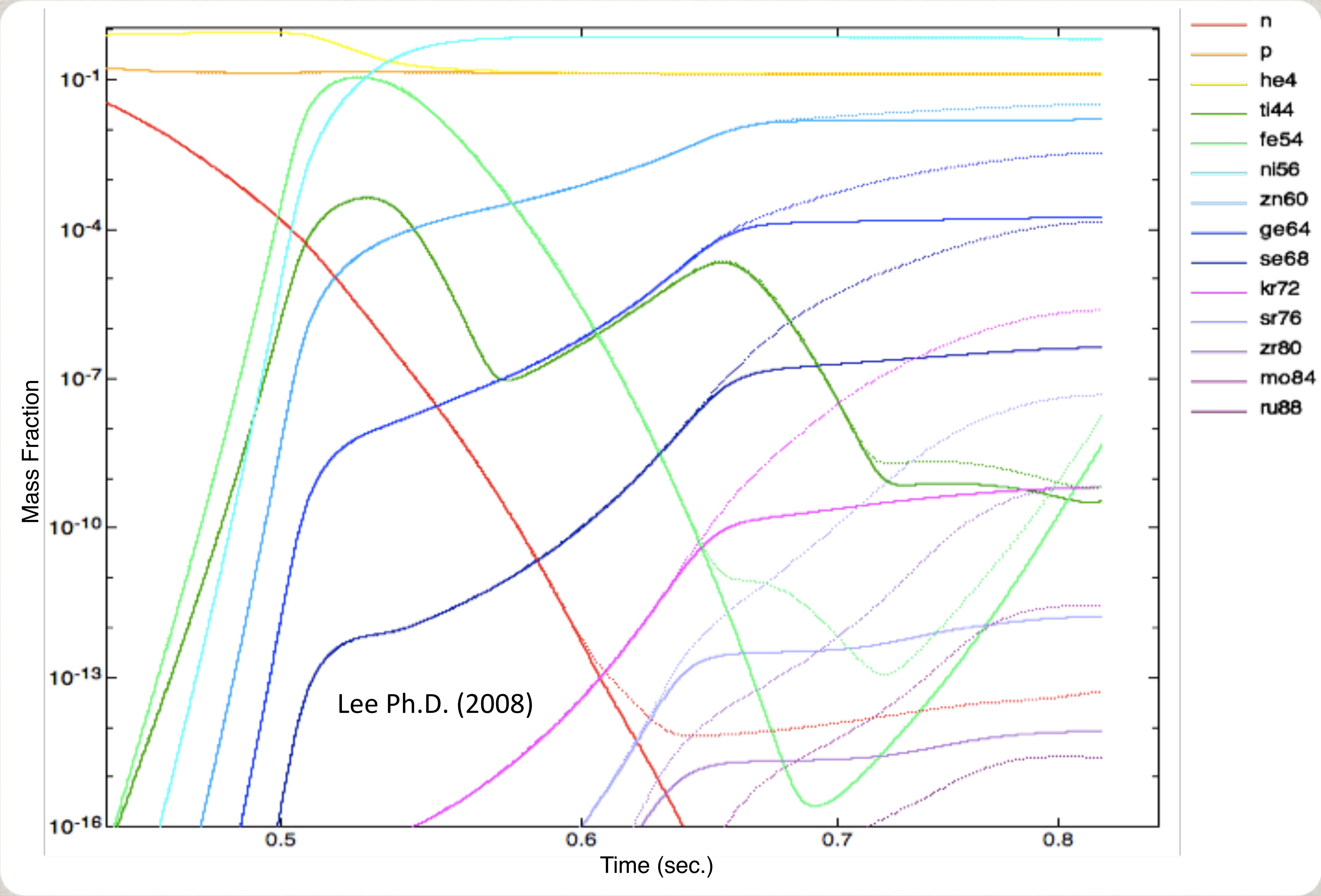

Our preliminary results show proton-rich ejecta and νp-process (dotted lines), but more weakly than previous results.

νp-process

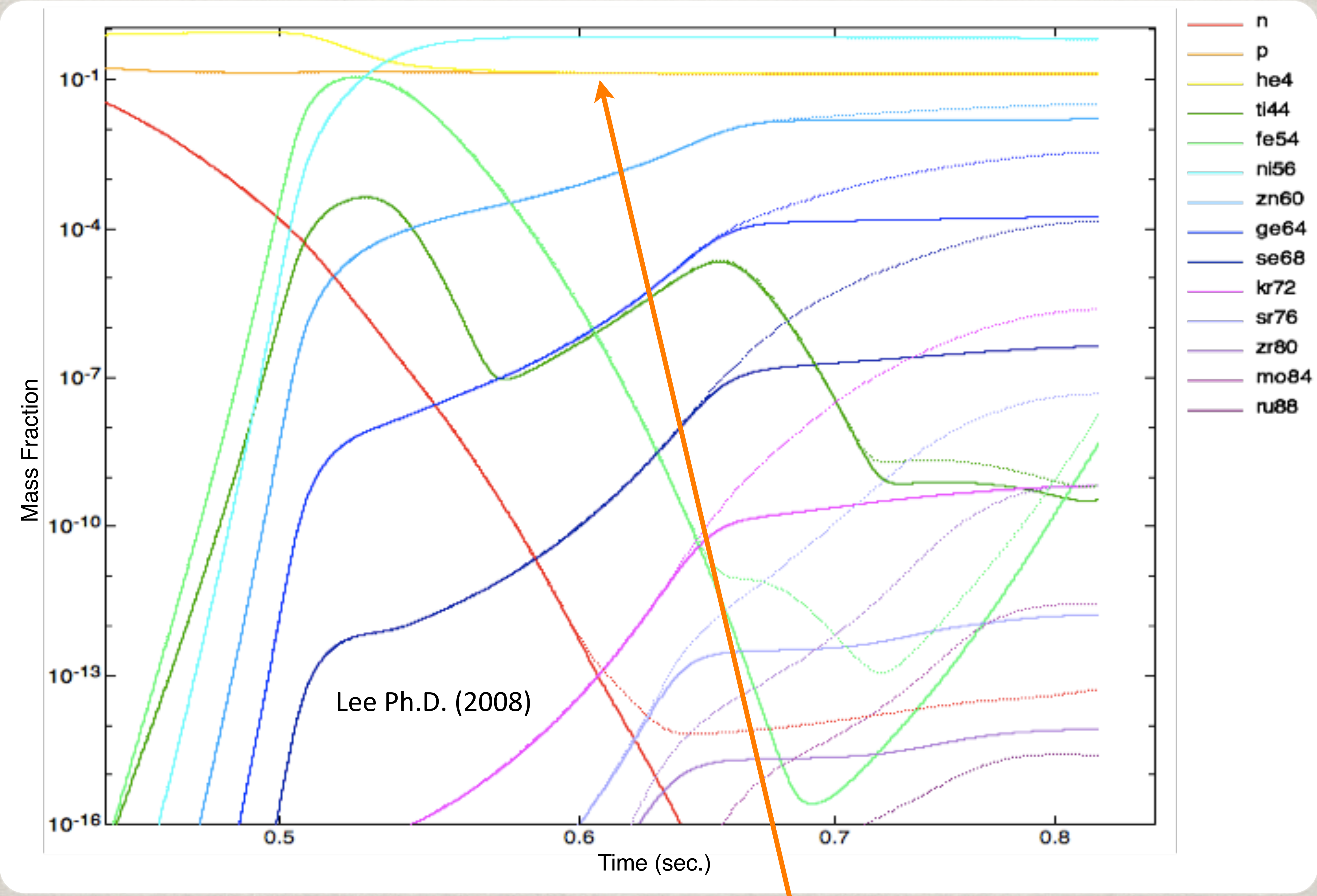

Our preliminary results show proton-rich ejecta and νp-process (dotted lines), but more weakly than previous results.

νp-process

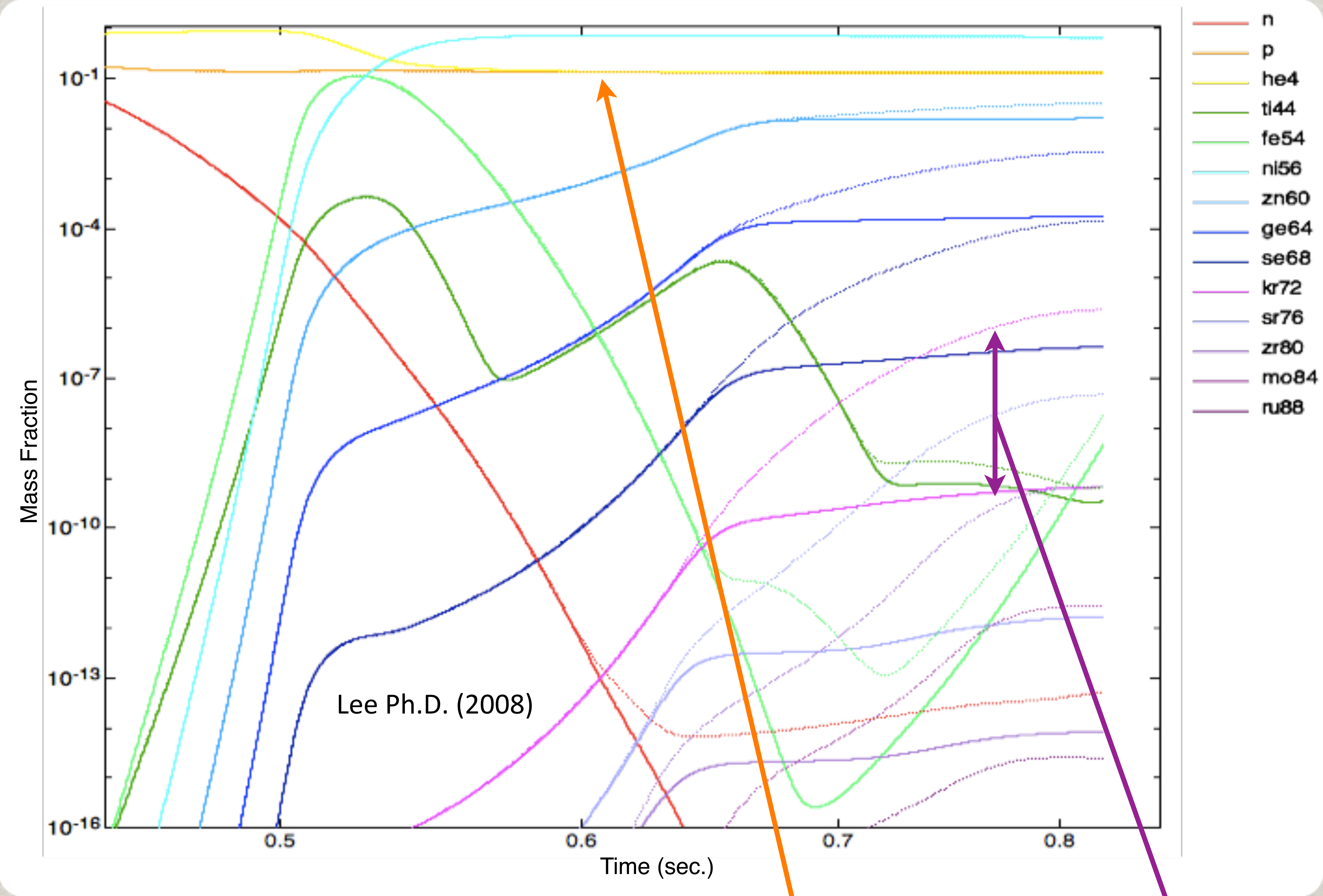

Our preliminary results show proton-rich ejecta and νp-process (dotted lines), but more weakly than previous results.

Detailed Composition

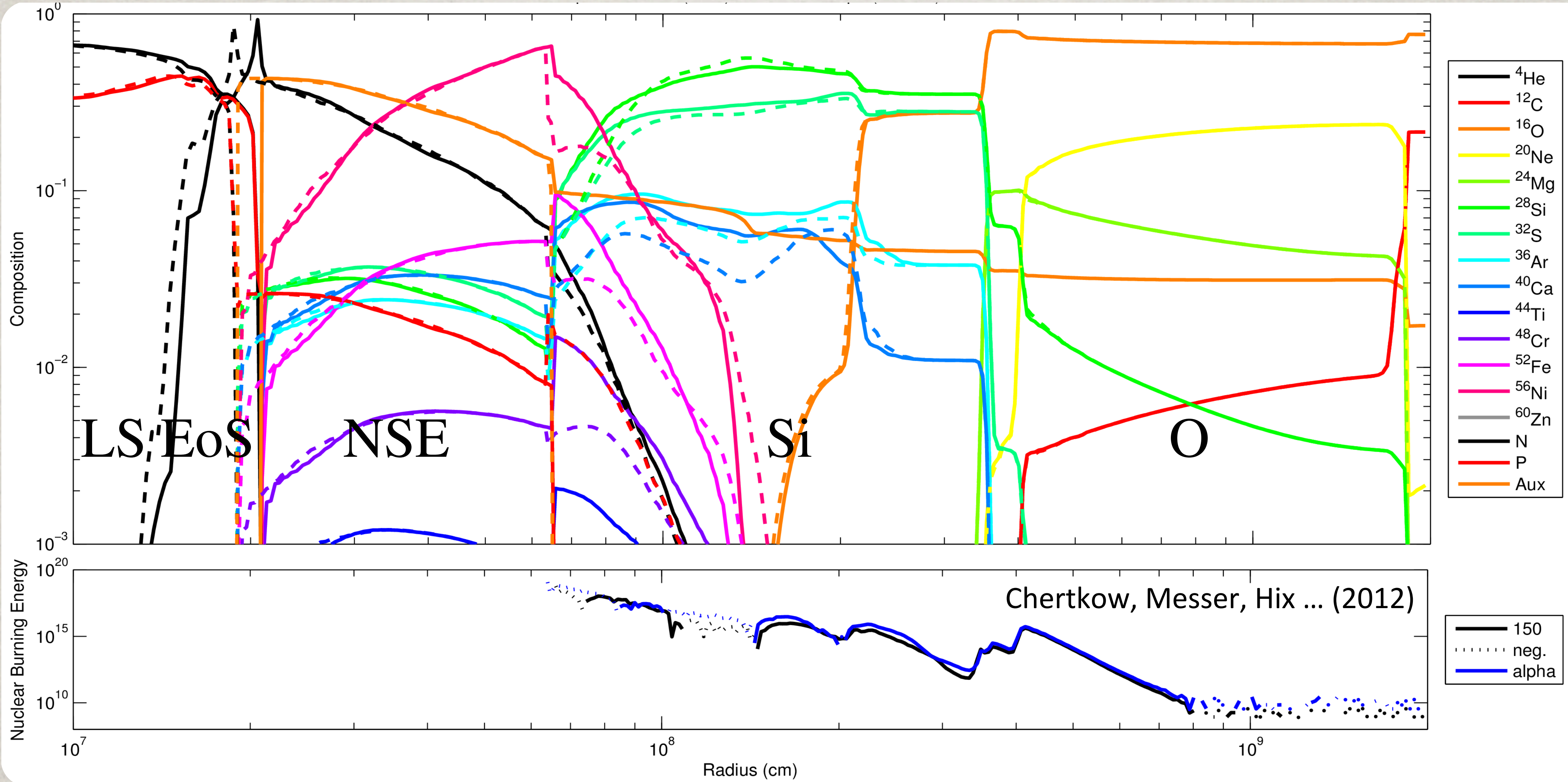

As a first step toward large networks, we've replaced the α-network in CHIMERA with 150 species (in 1D only so far).

The network cost grows from 3-5% of the simulation to 200%-400%, making the total simulation 3-5× as expensive.

Detailed Composition

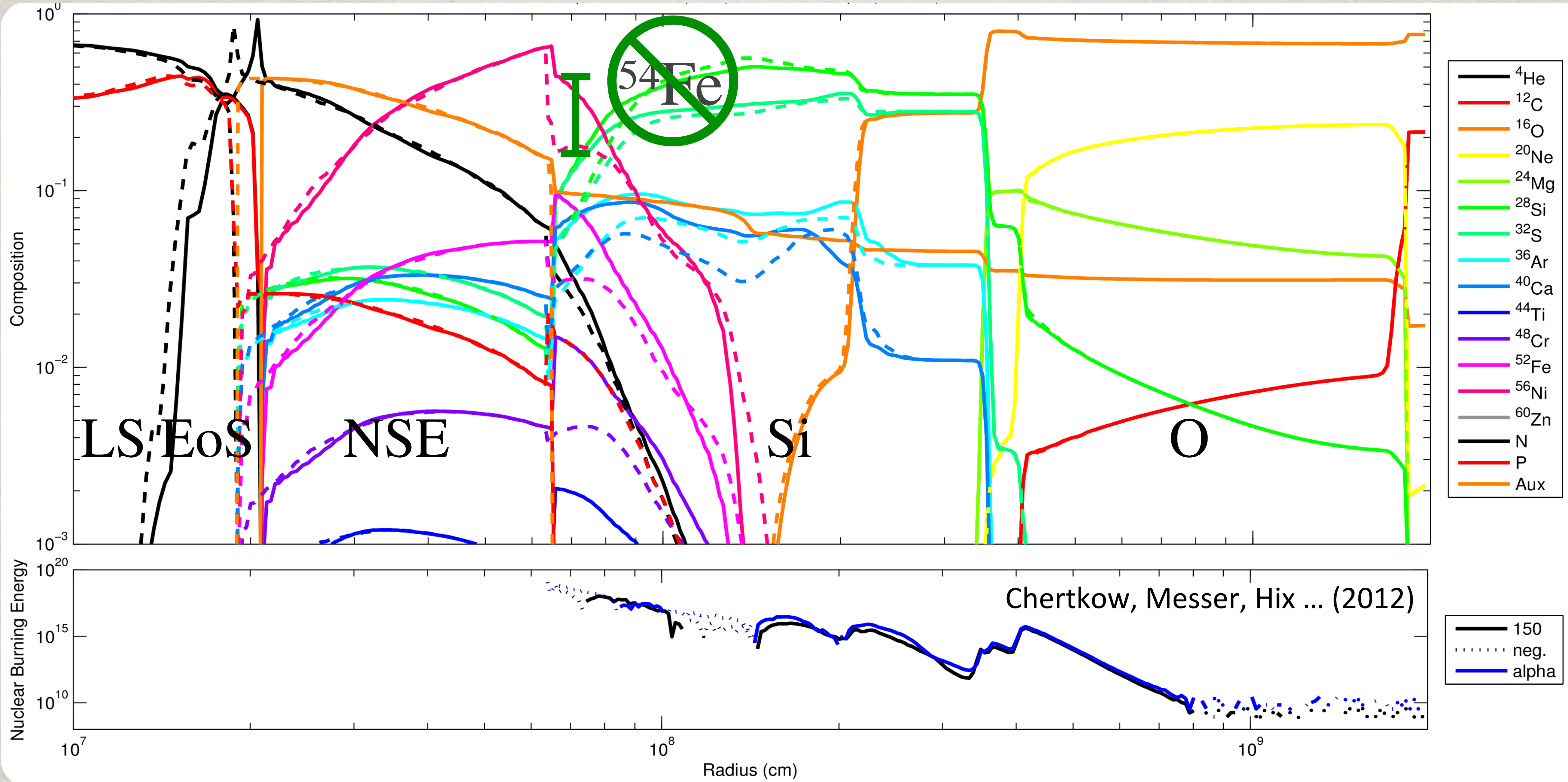

As a first step toward large networks, we've replaced the α-network in CHIMERA with 150 species (in 1D only so far).

The network cost grows from 3-5% of the simulation to 200%-400%, making the total simulation 3-5× as expensive.

Detailed Composition

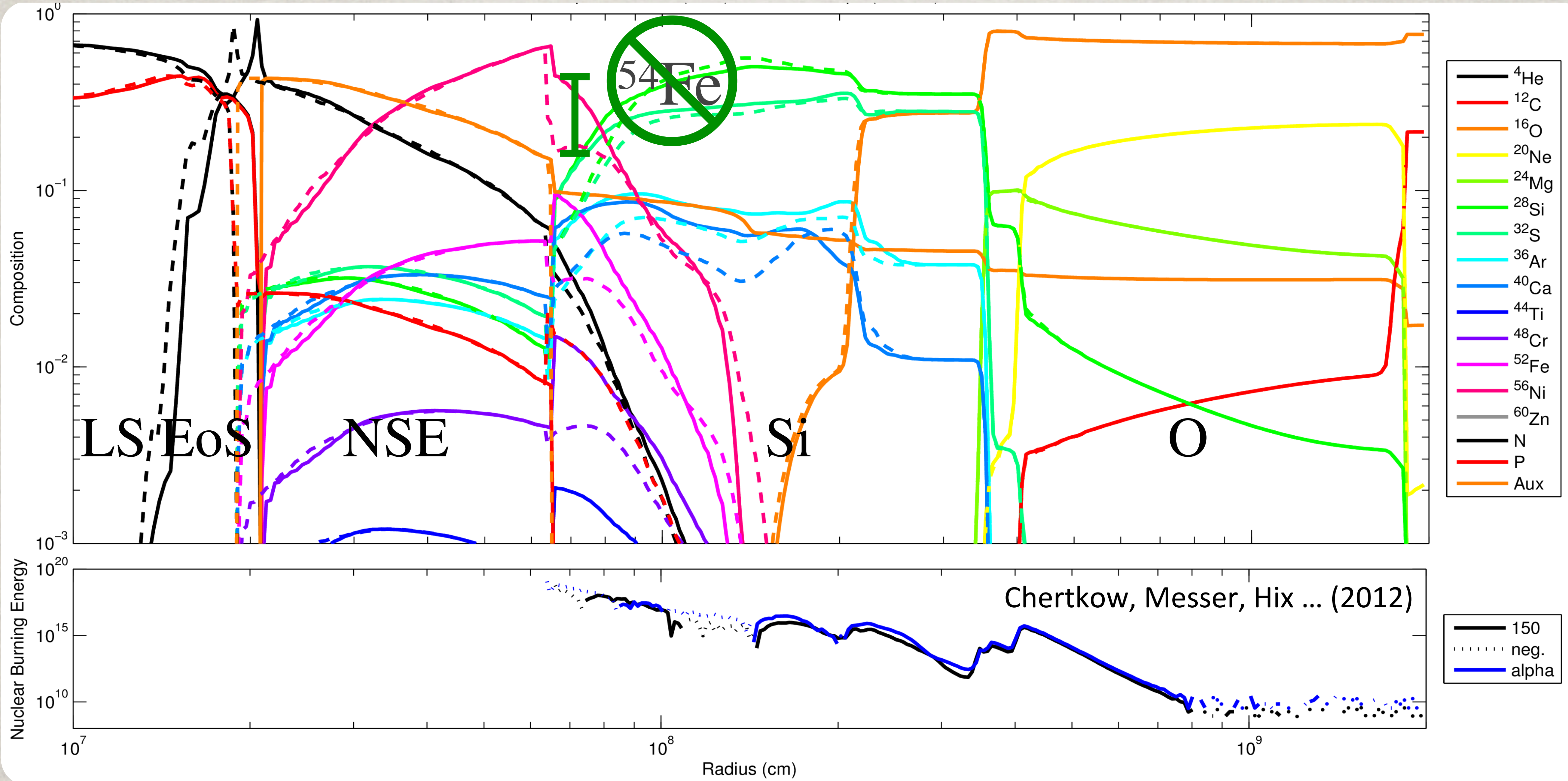

As a first step toward large networks, we've replaced the α-network in CHIMERA with 150 species (in 1D only so far).

The network cost grows from 3-5% of the simulation to 200%-400%, making the total simulation 3-5× as expensive.

Progress Report

Ongoing improved CHIMERA models confirm successful, mostly prolate, explosions across a range of progenitors from 12-25 $M_\odot$ driven by neutrino heating and SASI.

These self-consistent CHIMERA simulations, together with similar VERTEX simulations from Janka and collaborators, point to a successful neutrino-reheating mechanism, with the explosion delayed by 300 ms or more after bounce, at least in axisymmetry (2D).

Self-consistent 3D simulations, while very expensive, are possible. They are critical to teach us the value of our 2D simulations. Early indications are that 3D is somewhat more pessimistic than 2D, but this view may be colored by relatively low resolution in 3D.

Future Nucleosynthesis

Future Nucleosynthesis

We expect large differences in nucleosynthesis from parameterized 1D and older 2D models because of neutrinos, increased delay time and convoluted mass cut.

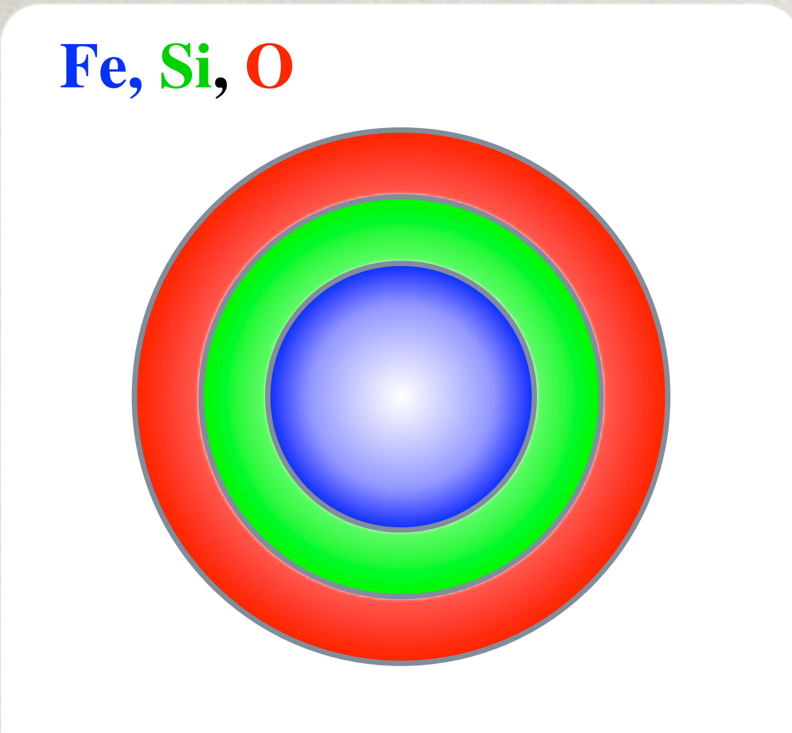

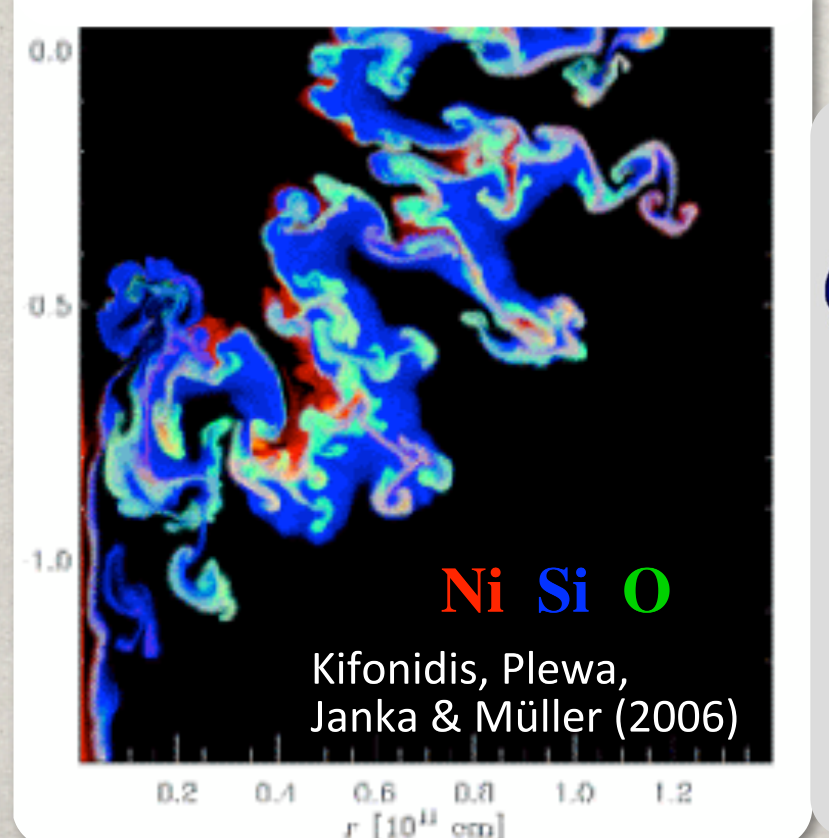

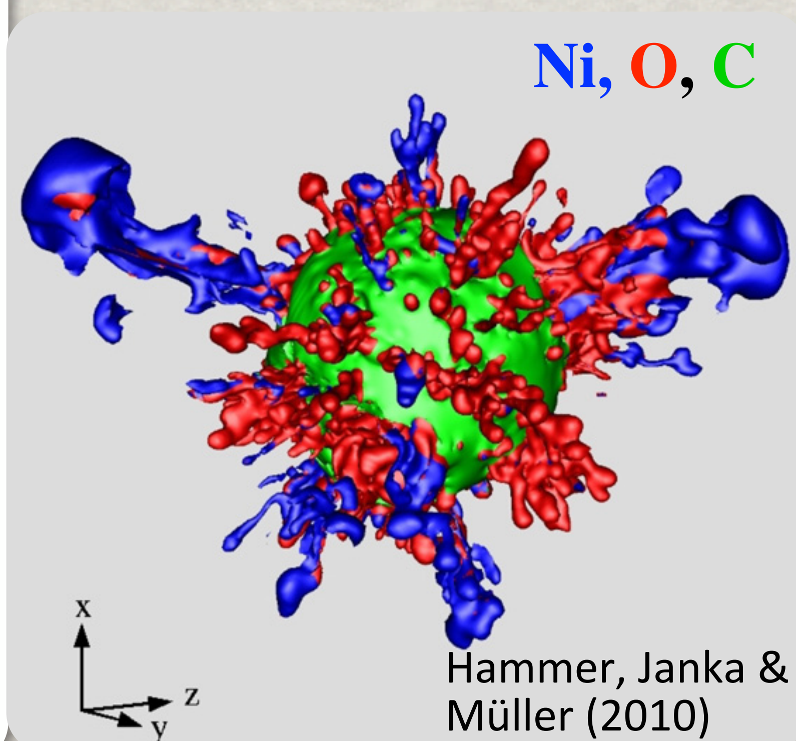

Future Nucleosynthesis

We expect large differences in nucleosynthesis from parameterized 1D and older 2D models because of neutrinos, increased delay time and convoluted mass cut.

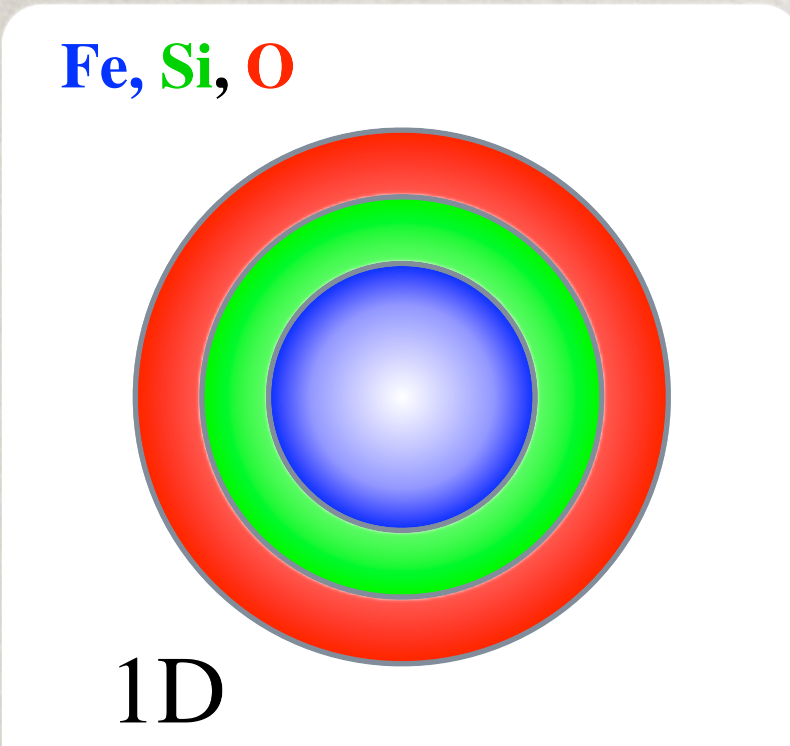

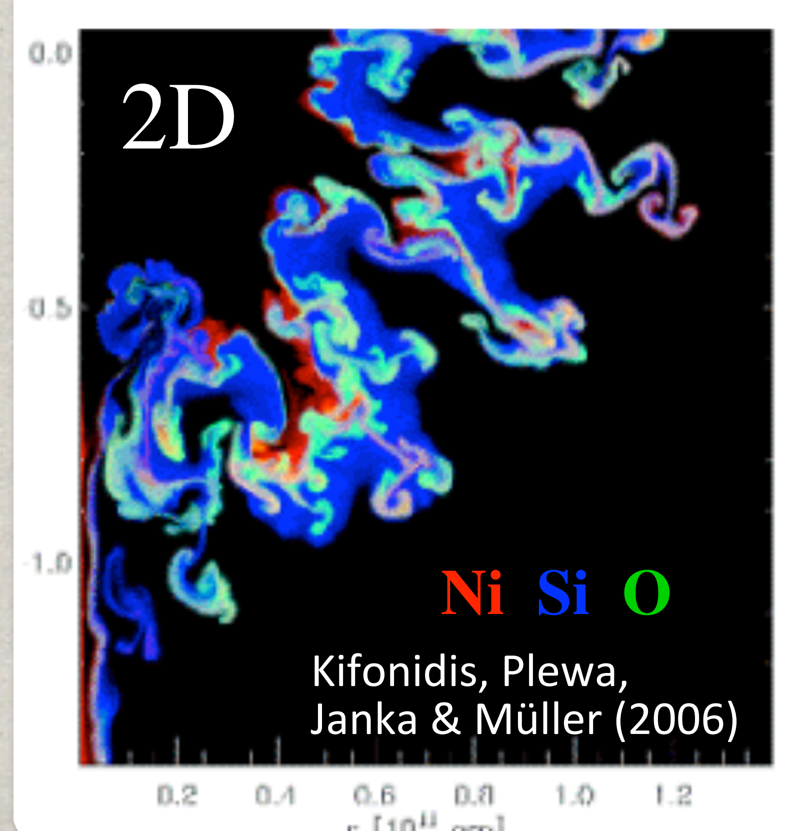

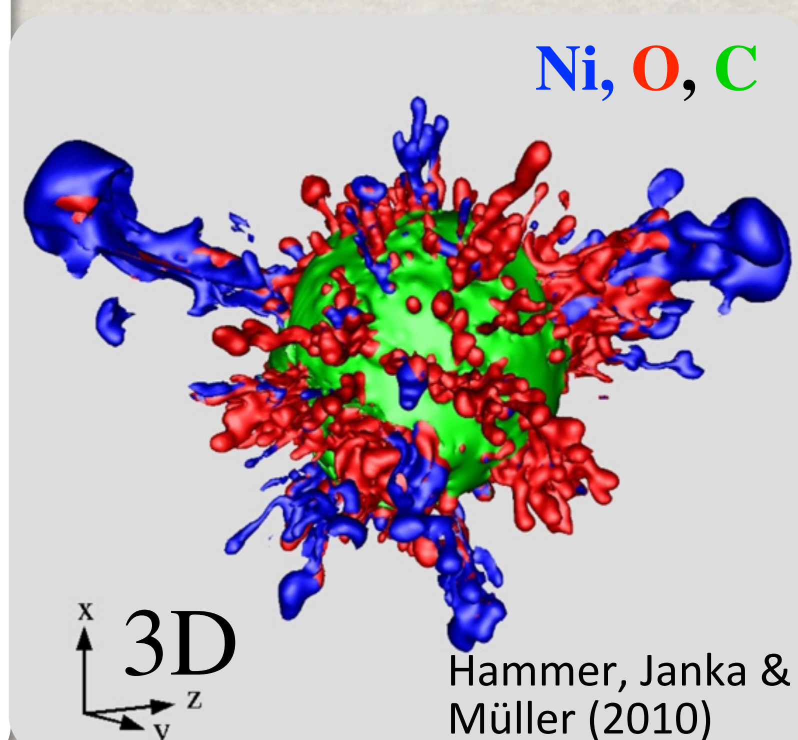

Future Nucleosynthesis

We expect large differences in nucleosynthesis from parameterized 1D and older 2D models because of neutrinos, increased delay time and convoluted mass cut.

Must simulate with large networks, neutrino transport and multi-D hydro.